(12) INTERNATIONAL APPLICATION PUBLISHED UNDER THE PATENT COOPERATION TREATY (PCT)

(19) World Intellectual Property Organization
International Bureau

(43) International Publication Date
26 September 2024 (26.09.2024)

WIPO | PCT

(10) International Publication Number
WO 2024/197304 A2

(51) International Patent Classification:
*A61F 2/02* (2006.01)

(21) International Application Number:
PCT/US2024/021334

(22) International Filing Date:
25 March 2024 (25.03.2024)

(25) Filing Language: English

(26) Publication Language: English

(30) Priority Data:
63/491,764 23 March 2023 (23.03.2023) US

(71) Applicant: **THE REGENTS OF THE UNIVERSITY OF CALIFORNIA** [US/US]; 1111 Franklin Street, Twelfth Floor, Oakland, CA 94607 (US).

(72) Inventors: **MORALES, Jose**; 10833 Wilshire Blvd, Apt 528, Los Angeles, CA 90024 (US). **LU, Haotian**; C/o The Regents Of The University Of California, 1111 Franklin Street, Twelfth Floor, Oakland, CA 94607 (US). **CUI, Huachen**; C/o The Regents Of The University Of California, 1111 Franklin Street, Twelfth Floor, Oakland, CA 94607 (US). **ZHENG, Xiaoyu**; C/o The Regents Of The University Of California, 1111 Franklin Street, Twelfth Floor, Oakland, CA 94607 (US).

(74) Agent: **ABDULHAY, Ali, G.** et al.; Riverside Law, LLP, 175 Strafford Ave Ste 100, Wayne, PA 19087 (US).

(81) Designated States *(unless otherwise indicated, for every kind of national protection available)*: AE, AG, AL, AM, AO, AT, AU, AZ, BA, BB, BG, BH, BN, BR, BW, BY, BZ, CA, CH, CL, CN, CO, CR, CU, CV, CZ, DE, DJ, DK, DM, DO, DZ, EC, EE, EG, ES, FI, GB, GD, GE, GH, GM, GT, HN, HR, HU, ID, IL, IN, IQ, IR, IS, IT, JM, JO, JP, KE, KG, KH, KN, KP, KR, KW, KZ, LA, LC, LK, LR, LS, LU, LY, MA, MD, MG, MK, MN, MU, MW, MX, MY, MZ, NA, NG, NI, NO, NZ, OM, PA, PE, PG, PH, PL, PT, QA, RO, RS, RU, RW, SA, SC, SD, SE, SG, SK, SL, ST, SV, SY, TH, TJ, TM, TN, TR, TT, TZ, UA, UG, US, UZ, VC, VN, WS, ZA, ZM, ZW.

(84) Designated States *(unless otherwise indicated, for every kind of regional protection available)*: ARIPO (BW, CV, GH, GM, KE, LR, LS, MW, MZ, NA, RW, SC, SD, SL, ST, SZ, TZ, UG, ZM, ZW), Eurasian (AM, AZ, BY, KG, KZ, RU, TJ, TM), European (AL, AT, BE, BG, CH, CY, CZ, DE, DK, EE, ES, FI, FR, GB, GR, HR, HU, IE, IS, IT, LT, LU, LV, MC, ME, MK, MT, NL, NO, PL, PT, RO, RS, SE,

(54) Title: ADVANCED FUNCTION STENT SYSTEM FOR CHRONIC ON-DEMAND DRUG DELIVERY, SONOGENETIC CONTROL OF CELLS, AND ACOUSTIC MODULATION OF CELL FUNCTION

(57) Abstract: In some aspects, a stent system including a support structure having first and second ends, comprising one or more members defining interior and peripheral regions for the structure, a lattice interfaced with the support structure, at least one transducer attached to the lattice, one or more leads electrically connected to the at least one transducer, and a power source connected to the one or more lead wires. In other aspects, a method for spatiotemporal control or expression of genes of one or more cells.

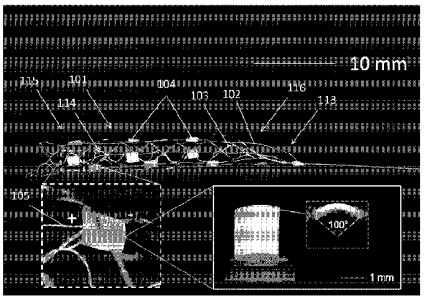


Fig. 1A

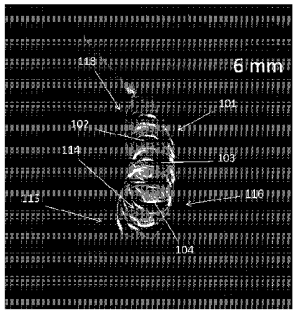


Fig. 1B

WO 2024/197304 A2

*[Continued on next page]*

SI, SK, SM, TR), OAPI (BF, BJ, CF, CG, CI, CM, GA, GN, GQ, GW, KM, ML, MR, NE, SN, TD, TG).

**Published:**

— *without international search report and to be republished upon receipt of that report (Rule 48.2(g))*

TITLE

# Advanced Function Stent System for Chronic On-Demand Drug Delivery, Sonogenetic Control of Cells, and Acoustic Modulation of Cell Function

## CROSS-REFERENCE TO RELATED APPLICATIONS

This application claims priority to U.S. Provisional Application No. 63/491,764 filed on March 23, 2023, incorporated herein by reference in its entirety.

## STATEMENT REGARDING FEDERALLY SPONSORED RESEARCH OR DEVELOPMENT

This invention was made with government support under N00014-19-1-2723 awarded by U.S. Navy, Office of Naval Research. The government has certain rights in the invention.

## BACKGROUND OF THE INVENTION

The global implantable drug delivery devices market size was estimated at USD 16.6 billion in 2016 and is anticipated to exhibit a lucrative CAGR of 7.5% over the coming years. A rise in the incidence of chronic neurological conditions, such as neurodegenerative, neurooncological, and neuroinflammatory diseases, is creating a need for efficient medication delivery. For neurological disorders, the blood brain barrier significantly reduces the concentration of cytoactive drugs that penetrate into the central nervous system to affect its action on target cells. In some cases, drugs like Nusinersen (and other such gene therapies) that are used to treat spinal muscular atrophy and other such neurogenetic diseases require discomforting lumbar and/or cervical punctures in patients who often have skeletal deformities and poorly tolerate this procedure without significant discomfort. Neuro-oncological, neurogenerative (Alzheimer's disease, Parkinson's Disease, etc.), and the wide variety of difficult to control neurologic diseases require frequent and poorly penetrating drugs to be systemically administered. Additionally, the surgical insertion of electrodes for deep brain and /or cortical neuromodulation often results in damage to normal brain parenchyma, as well as progressive scarring/gliosis at the tissue interface directly contacting the neuroanatomical target leading to waning efficacy over time. Furthermore, the volume of tissue activated by the electrically conducting electrode is constrained by the Euclidean distance to the neuroanatomical target of

interest. Lastly, the spatiotemporal expression or control of intrinsic or exogenous genes can be performed with targeted acoustic stimulation of cells transfected with select Transient Receptor Potential channels, which also have the potential to enhance precision treatment of neurologic diseases and disorders by activating, silencing, or modulating gene function. A minimally invasive, chronically implantable solution harnessing ultrasound opens up vast possibilities for the efficacious treatment of neurological disease.

Thus, there is a need in the art to develop minimally invasive implantable treatment systems for the efficacious treatment of neurological disease. The present invention meets this need.

## SUMMARY OF THE INVENTION

Aspects of the present invention relate to a stent system including a support structure having first and second ends having one or more members defining interior and peripheral regions for the structure, a lattice interfaced with the support structure, at least one transducer attached to the lattice, one or more leads electrically connected to the at least one transducer, and a power source connected to the one or more lead wires.

In some embodiments, the at least one transducer is at least partially formed in one or more shapes selected from the group consisting of: non-planar, curved, cylindrical, concentrical circles, concentric circles with struts, hemispherical, annular, ring, half-ring, spherical, rectangular, prism, pyramidal, helical and polyhedral. In some embodiments, the at least one transducer is arranged in one or more patterns or configurations selected from: radial, radially outward, radially inward, focused inward, focused outward, circumferential, peripheral, helical, double-helical, triplicate, staggered, eccentric, biased, symmetrical, asymmetrical, or grouped.

In some embodiments, the at least one transducer has length of 5 μm to 50 mm, a width or diameter of 5 μm to 50 mm, and a height of 5 μm to 50 mm. In some embodiments, the at least one transducer has a curvature ranging from 0 degrees to 180 degrees, a focal depth ranging between 0.1 mm and 25 mm, or an arc length ranging from 0.1 μm to 10 mm.

In some embodiments, the support structure has a length of 10 mm to 60 mm, and a width or diameter of 0.5 mm to 20 mm. In some embodiments, the one or more members of the support structure have a width or diameter between 0.01 mm and 2 mm. In some

embodiments, the openings of the lattice range between 0.1 mm and 5 mm.

In some embodiments, the one or more members of the support structure are formed of one or more materials selected from the group consisting of: elastic material, superelastic material, sputtered superelastic material, resilient material, nonconductive metal or alloy, poorly conductive metal or alloy, platinum, magnesium, stainless steel, nickel-titanium alloy/nitinol, nitinol thin film (i.e., NiTi thin film), cobalt-nickel alloys, tantalum alloys, cobalt-chromium alloys, platinum-tungsten metal, cobalt alloy, platinum-iridium alloy, cobalt, chromium, conductive metal, gold, copper, silver, titanium, titanium alloys, or any combination thereof.

In some embodiments, the lattice is formed of one or more materials selected from the group consisting of: elastic material, superelastic material, sputtered superelastic material, resilient material, nonconductive metal or alloy, poorly conductive metal or alloy, platinum, magnesium, stainless steel, nickel-titanium alloy/nitinol, nitinol thin film (i.e., NiTi thin film), cobalt-nickel alloys, tantalum alloys, cobalt-chromium alloys, platinum-tungsten metal, cobalt alloy, platinum-iridium alloy, cobalt, chromium, conductive metal, gold, copper, silver, titanium, titanium alloys, or any combination thereof.

In some embodiments, the lead wires are formed of one or more materials selected from the group consisting of: conductive metal, conductive metal allow, gold, copper, aluminum, silver, insulating material, biocompatible material, polymer material, synthetic material, plastic, or any combination thereof.

In some embodiments, at least one of the support structure, lattice, at least one transducer and one or more lead wires are at least partially coated with one or more coatings selected from the group consisting of: biocompatible coating, conductive coating, non-conductive coating, insulating coating, oxide-film, titanium-nitride-oxide, organic polymer, polyurethane, polyimide, bioactive/covalently bonded coating, covalently-linked heparin, polymerized allylamine, poly(dimethylsiloxane), phosphorylcholine, 2-methylacryloyloxyethyl phosphorylcholine, poly(2-methoxyethyl acrylate), enzyme-loaded inducible nitric acid oxide, synthase oxygenase on polyethylenimine, chromium, platinum, gold, silver, stealth coating, trimethylolpropane triacrylate (TMPTA), or any combination thereof.

In some embodiments, the at least one transducer is a piezoelectric device including a bipolar ceramic stack, at least one electrode, a back mass, a front mass, and at least

one biocompatible coating covering at least a portion of the at least one transducer, wherein the transducer is coated in trimethylolpropane triacrylate (TMPTA).

In some embodiments, the system further includes a computing system communicatively connected to the power source, having a processor and a non-transitory computer-readable medium with instructions stored thereon, which when executed by a processor, perform steps including providing power at one or more voltages in one or more frequencies from the power source to the at least one transducer for at least one duration. In some embodiments, the one or voltages is between 0.1 V to 500 V, the one or more frequencies are between 0.1 Hz and 10000 MHz, and the at least one duration is between 0.1 μs and 1 hour.

In some embodiments, the system further includes at least one microfluidic chamber positioned in the interior region of the support structure fluidly connected to at least one microfluidic reservoir positioned outside of the support structure with at least one conduit having at least one lumen.

In some embodiments, the at least one microfluid chamber is at least partially formed in one or more shapes selected from: cylinder, disk, toroid, annulus, capsule, pill, cube, sphere, dome, arc, spiral, helix, double helix, or any combination thereof.

In some embodiments, the at least one microfluid chamber has a volume ranging between 1 μl and 1000 μl or a diameter between 0.1 mm and 1 mm, the at least one microfluid reservoir has a volume ranging between 100 μl and 2 ml.

In some embodiments, the at least one conduit has a length ranging between 1 mm and 200 cm.

In some embodiments, the at least one microfluidic chamber includes first and second microfluidic chambers, and the at least one microfluidic chamber includes first and second microfluidic chambers.

In some embodiments, the first microfluidic chamber and first microfluidic reservoir are at least partially fluidly filled with a solution including microbubbles, and the second microfluid chamber and second microfluidic reservoir are at least partially fluidly filled with a solution including at least one therapeutic.

In some embodiments, the at least one therapeutic is selected from the group consisting of: gene therapy, Nusinersen, Levodopa, anti-seizure medication, DNA or RNA based biologic/viral-vector gene replacement therapies, CRISPR, Nusinersen for SMA, RGX-111,

RGX-112, condensed tuberin, APOE2, hTERT, GBA, SOD-1, C9orf72, HTT, antibody-based biologic therapies, Lecanemab, small molecules, proteins, or any combination thereof.

In some embodiments, the system further includes at least one port in each microfluidic reservoir configured to receive one or more fluids or solutions.

In some embodiments, the system further includes an implantable housing at least partially enclosing the power source, the first microfluidic reservoir, and the second microfluidic reservoir.

In some embodiments, the system further includes at least one tubular conduit having at least one lumen extending from the housing to a position on the first end of the support structure.

Aspects of the present invention relate to a method for spatiotemporal control of intrinsic or exogenous genes, including providing any disclosed stent system, implanting the stent system near or in a target site of a subject, providing power at one or more voltages in one or more frequencies from the power source to the at least one transducer for at least one duration.

In some embodiments, the one or voltages is between 0.1 V to 500 V, the one or more frequencies are between 0.1 Hz and 10000 MHz, and the at least one duration is between 0.1 μs and 1 hour.

Aspects of the present invention relate to a drug delivery method including providing any disclosed stent system, implanting the stent system in or near a target site of a subject, filling the at least one microfluidic chamber at least partially with a solution including at least one therapeutic and microbubbles, producing microbubble cavitation via the at least one transducer and delivering the at least one therapeutic to the target site.

Aspects of the present invention relate to a method of fabricating a stent system including fabricating a stent, fabricating at least one PZT transducer, fabricating at least one microfluidic chamber, fixing the at least one PZT transducer to the stent, disposing the at least one microfluidic chamber within the stent.

In some embodiments, the step of fabricating the PZT transducer includes 3D printing a PZT base layer on a polymer support layer, debonding the PZT base layer from the polymer support layer, sintering the PTZ base layer in a PTZ powder bed with heat to form a PTZ element, submerging the PTZ element into an isolation liquid, polarizing the dipoles within the sintered PTZ element, applying an electric field to the PTZ element and cooling the PTZ

element.

## BRIEF DESCRIPTION OF THE DRAWINGS

The following detailed description of embodiments of the invention will be better understood when read in conjunction with the appended drawings. It should be understood, however, that the invention is not limited to the precise arrangements and instrumentalities of the embodiments shown in the drawings.

Fig. 1A and Fig. 1B depict an exemplary advanced function stent having one or more transducers according to aspects of the present invention. Fig. 1A depicts a side view of an exemplary advanced function stent. Fig. 1B depicts a perspective view of an exemplary advanced function stent.

Fig. 2 depicts an exemplary Intravascular Ultrasound transducer design (IVUS).

Fig. 3 depicts an exemplary Advanced Function Stent System according to aspects of the present invention.

Fig. 4 depicts an illustrative computer architecture for a computer for practicing the various embodiments of the invention.

Fig. 5A through Fig. 5C depict an exemplary Intravascular Ultrasound (IVUS) transducer design and an exemplary 3D printed Piezoelectric transducer according to aspects of the present invention. Fig. 5A depicts an exemplary manufacturing approach comprising additive manufacturing (AM) and a liquid phase sintering. Fig. 5B depicts an exemplary fully 3D printed IVUS transducer with focusing features. Fig. 5C depicts an exemplary application for the disclosed advanced function stent system displaying ultrasound-enabled localization cavitation in a blood vessel phantom.

Fig. 6A through Fig. 6G depict an exemplary 3D printed Piezoelectric transducer according to aspects of the present invention. Shown is an exemplary miniaturized ultrasound transducer design and 3D printing of a highly loaded Lead Zirconate Titanate (PZT) composite and liquid phase sintering. Fig. 6A shows an exemplary miniaturized ultrasound transducer with curved PZT element configured to produce an acoustic beam with a focal line sized appropriately to at least partially surround a vein according to aspects of the present invention. Fig 6B shows an exemplary schematic of the liquid sintering resin components. Fig. 6C shows an exemplary novel 3D printing system for liquid phase sintering (LPS) piezoelectric composites. Fig. 6D

shows an example debonding process to burn off the supportive polymer. Fig. 6E shows an example liquid sealing process to reduce the lead loss during high-temperature sintering. Fig. 6F shows an example LPS process to form dense PZT sample. Fig. 6G shows exemplary generated acoustic pressure curves of the 3D printed 9.75-Mhz miniaturized ultrasound transducers, indicating that the values exceeded many medical thresholds.

Fig. 7A through Fig. 7J depict exemplary transducer designs, a PZT free-form fabrication and piezoelectric performance of the as-fabricated piezoelectric elements (i.e, transducers). Fig. 7A shows exemplary transducer designs comprising micro-curved stave elements with different curvatures. Fig. 7B shows exemplary transducer designs comprising hemisphere elements typically found in a general ultrasound transducer for medical imaging and nondestructive testing. Fig. 7C shows an exemplary transducer design comprising helical elements for generating spiral acoustic fields for ultrasound manipulation. Fig. 7D shows exemplary transducer designs comprising cylindrical transducer elements with multiple concentric annular layers. Fig. 7E shows an exemplary transduce design comprising lattice sensor elements for low-frequency (<100 kHz) ultrasound. Fig. 7F shows an exemplary transducer design comprising a force sensor element with ultrahigh sensitivity. Fig. 7G shows a scanning electron microscope (SEM) image comparison between samples sintered by conventional sintering and optimized sintering methods. Fig. 7H is a plot showing the results for sound speed measurements against the sample thickness. Fig. 7I is a plot showing the results for polarization-electric field (P-E) loop of an exemplary 3D printed PZT transducer. The remnant polarization $P_r$ is 32.4 $\mu C/cm^2$, which is 84% of the value of pristine materials. Fig. 7J is a plot showing the results for $d_{33}$ and coupling factor $k_t$ benchmarked with the disclosed 3D printed piezoelectric materials.

Fig. 8A through Fig. 8D show an exemplary transducer design and acoustic energy output performance of the as-fabricated miniaturized ultrasound transducer. Fig. 8A is a plot showing tunable attenuation coefficient and acoustic impedance for the exemplary of Fig. 8C. Fig. 8B is a plot showing the acoustic pressure map vs. curvature and arc length for the 3D printed miniaturized ultrasound transducer of Fig. 8C, showing that the generated acoustic pressure already exceeds many medical thresholds. Fig. 8C depicts an exemplary 3D printed miniaturized ultrasound transducer according to aspects of the present invention. Fig. 8D shows

an image of an exemplary 3D printed miniaturized ultrasound transducer with a focused micro-PZT element according to aspects of the present invention.

Fig. 9A through Fig. 9I show an exemplary miniaturized ultrasound transducer and test results. Fig. 9A shows a schematic of an experiment with a disclosed 3D printed transducer capturing the cavitation signal in a microbubble suspension with an enlarged view of microbubble fragmentation. Fig. 9B is a plot showing the captured signals (Input voltage: 15 Vpp, 40 Vpp, 90 Vpp and 180 Vpp) in time domain. Fig. 9C, Fig. 9D and Fig. 9E are plots showing frequency spectrums of the received signals driven by different input voltages. The sub-harmonic and broadband are identified as the generation of stable cavitation and inertial cavitation, respectively. Fig. 9F, Fig. 9G, Fig. 9H, and Fig. 9I are a series of images showing microbubble behavior during insonation, showing the processes of oscillation, growth, and collapse of a microbubble.

Fig. 10A through Fig. 10H show an exemplary miniaturized ultrasound transducer and induced localized cavitation in a blood vessel phantom. Fig. 10A depicts the transducer positioned at a target site or region of interest. Fig. 10B depicts injecting a microbubble suspension or solution into or near the target site or region of interest. Fig. 10C depicts Ultrasound-induced microbubble opening via the exemplary 3D printed miniaturized ultrasound transducer in the 3D printed blood vessel phantom. Fig. 10D is a plot showing microbubble opening vs. time, indicating that the opening rate is related to the input voltage. Fig. 10E depicts the transducer trajectory and microbubble on the inner wall of the phantom blood vessel. Fig. 10F depicts microbubble fragmentation as a result of the path of the transducer. Fig. 10G depicts microbubble fragmentation as a result of the path of the transducer. Fig. 10H depicts a localized drug delivery testing wherein the microbubbles can be controlled to open only at the focal area of the transducer.

Fig. 11A shows an exemplary two-step debonding process. Fig. 11B is a plot showing the debonding time-temperature curve of the process of Fig. 11A.

Fig. 12A is a plot showing peak sintering temperature optimized by $d_{33}$ constant. Fig. 12B is a plot showing breakdown electrical field of the exemplary samples. Fig. 12C is a plot showing an X-Ray diffraction analysis (XRD) of the sintered PZT sample.

Fig. 13A depicts an exemplary polarization setup or transducer design according to aspects of the present invention. Fig. 13B is a diagram depicting dipole alignment along the

applied electrical field. Fig. 13C is a plot showing polarization time and electrical field profile for the transducer design of Fig. 13A.

Fig. 14A depict exemplary transducer material samples prior to sintering. Fig. 14B depict exemplary transducer material samples after sintering, showing their dimension shrinkages were identical after the sintering process. Fig. 14C is a plot showing average linear shrinkage vs probability density (i.e., structural integrity measurement and results) of samples after sintering ($\mu$ is the mean value while $\sigma$ is the standard deviation). Fig. 14D depicts an exemplary curved transducer material sample with focusing feature prior to sintering. Fig. 14E depicts an exemplary curved transducer material sample with focusing feature after sintering, showing the curvature was well maintained during sintering. Fig. 14F is a plot showing probability distribution for curvature ($\mu$ is the mean value while $\sigma$ is the standard deviation) Fig. 14G depicts an exemplary 3D printed honeycomb lattice transducer (e.g., lattice sample). Fig. 14H is an XCT image of the unit cell of the lattice sample. Fig. 14I is a plot showing probability distribution for strut thickness ($\mu$ is the mean value while $\sigma$ is the standard deviation).

Fig. 15A is a diagram of an experimental set up for sound speed and acoustic attenuation measurement of ultrasound through a sample or material. Fig. 15B depicts an enlarged view of the material to be tested ($p$ : acoustic pressure) Fig. 15C are plots depicting the received signals with and without sample in between transducers.

Fig. 16A and Fig. 16B show Strain-Electric (S-E) field loop measurement of a commercial sample vs an exemplary 3D printed sample of the present invention. Fig 16A is a diagram showing the experimental the S-E loop testing system. Fig 16B is a plot showing the S-E curves of the commercial PZT sample and the exemplary 3D printed sample.

Fig. 17A through Fig. 17F depict various exemplary 3D printed transducers of different geometries and their related energy output capability. Fig. 17A depicts an exemplary transducer design and a plot showing the energy output. Fig. 17B is a diagram depicting a schematic of the acoustic pressure measurement setup. Fig. 17C is a plot of x-y coordinate vs intensity for the transducer of Fig. 17A. Fig. 17D depicts an exemplary transducer design and a plot showing the energy output. Fig. 17E depicts an exemplary transducer design and a plot showing the energy output. Fig. 17F depicts an exemplary transducer design and a plot showing the energy output.

Fig. 18A depicts exemplary transducer designs (one transducer comprising a disk element and an another comprising an element with concentric annular layers). Fig. 18B depicts the disk element transducer design. Fig. 18C depicts the transducer design comprising an element with concentric annular layers. Fig. 18D is a plot showing peak-to-peak acoustic pressure generated by the transducers. Fig. 18E and Fig. 18F show example finite element analysis (FEA) models to predict the acoustic pressure and the acoustic fields generated by the transducers.

Fig. 19 is a plot showing impedance curves of the fabricated PZT sample and standard PZT sample.

Fig. 20 is a plot showing pulse-echo signal and its frequency spectrum for a 3D printed miniatured ultrasound transducer.

Fig. 21 is a diagram with images depicting dye diffusion speed and uniformity calculation based on the pixel value of grayscale images of a disclosed transducer near or in a target site or region of interest.

Fig. 22A depicts a dye dispersion experiment set up in water. Fig. 22B depicts a 0.1 ml methylene blue drop is added to the media of the water experiment. Fig. 22C depicts where 9.75-MHz burst waves were input into the transducer, and the dye was stirred by the emitted acoustic wave in the water experiment. Fig. 22D depicts where after 15 seconds of ultrasound exposure, the dye partially dispersed in the water. Fig. 22E depicts a timeline across the experiments of Fig. 22A and Fig. 22F. Fig. 22F depicts a dye dispersion experiment set up in a microbubble suspension. Fig. 22G depicts a 0.1 ml methylene blue drop is added to the media of the microbubble experiment. Fig. 22H depicts where 9.75-MHz burst waves were input into the transducer, and the dye was stirred by the emitted acoustic wave in the microbubble experiment. Fig. 22I depicts where after 15 seconds of ultrasound exposure, the dye fully dispersed in the microbubble suspension.

Fig. 23 is a plot showing a digital image correlation curve of microbubble concentration in the blood vessel phantom vs. image mean pixel value.

Fig. 24A is a series of images depicting a progression of microbubble collapse and fragmentation. Fig. 24B is a series of images depicting a progression of microbubble collapse and fragmentation.

Fig. 25A is a series of images depicting a progression of dye dispersion from microbubble opening. Fig. 25B is a series of images depicting a progression of dye dispersion from microbubble opening. Fig. 25C is a series of images depicting a progression of dye dispersion from microbubble opening

Fig. 26A is a series of images depicting a progression of microbubble fragmentation. Fig. 26B is a series of images depicting a progression of microbubble fragmentation.

Fig. 27A is a series of images depicting a progression of microbubble fragmentation. Fig. 27B is a series of images depicting a progression of microbubble fragmentation.

## DETAILED DESCRIPTION

It is to be understood that the figures and descriptions of the present invention have been simplified to illustrate elements that are relevant for a clear understanding of the present invention, while eliminating, for the purpose of clarity many other elements found in related systems and methods. Those of ordinary skill in the art may recognize that other elements and/or steps are desirable and/or required in implementing the present invention. However, because such elements and steps are well known in the art, and because they do not facilitate a better understanding of the present invention, a discussion of such elements and steps is not provided herein. The disclosure herein is directed to all such variations and modifications to such elements and methods known to those skilled in the art.

### Definitions

Unless defined otherwise, all technical and scientific terms used herein have the same meaning as commonly understood by one of ordinary skill in the art to which the invention pertains. Although any methods and materials similar or equivalent to those described herein can be used in the practice for testing of the present invention, exemplary materials and methods are described herein. In describing and claiming the present invention, the following terminology will be used.

It is also to be understood that the terminology used herein is for the purpose of describing particular embodiments only, and is not intended to be limiting.

The articles "a" and "an" are used herein to refer to one or to more than one (i.e., to at least one) of the grammatical object of the article. By way of example, "an element" means one element or more than one element.

"About" as used herein when referring to a measurable value such as an amount, a temporal duration, and the like, is meant to encompass variations of ±20%, ±10%, ±5%, ±1%, or ±0.1% from the specified value, as such variations are appropriate.

The terms "patient," "subject," "individual," and the like are used interchangeably herein, and refer to any animal amenable to the systems, devices, and methods described herein. The patient, subject or individual may be a mammal, and in some instances, a human.

Ranges: throughout this disclosure, various aspects of the invention can be presented in a range format. It should be understood that the description in range format is merely for convenience and brevity and should not be construed as an inflexible limitation on the scope of the invention. Accordingly, the description of a range should be considered to have specifically disclosed all the possible subranges as well as individual numerical values within that range. For example, description of a range such as from 1 to 6 should be considered to have specifically disclosed subranges such as from 1 to 3, from 1 to 4, from 1 to 5, from 2 to 4, from 2 to 6, from 3 to 6 etc., as well as individual numbers within that range, for example, 1, 2, 2.7, 3, 4, 5, 5.3, and 6. This applies regardless of the breadth of the range.

Advanced Function Stent System

Aspects of the present invention relate to advanced function stent systems and methods thereof for producing or delivering one or more therapies to or near a target site on a subject (e.g., acoustic stimulation therapy, sonogenetic control of cells, acoustic modulation of cell function, targeted drug delivery, chronic on-demand drug delivery, etc). Referring now to Fig. 1A and Fig. 1B, shown is an exemplary stent system 100 according to aspects of the present invention. In some embodiments, stent system 100 comprises a support structure 101 (in some examples referred to as a stent scaffold or stent structure) having a first end 113 and second end 115 comprising one or more members 102 defining an interior or inner region 114 and an outer or peripheral region 116, a lattice 103 (in some examples referred to as a lattice structure) interfaced with support structure 101, at least one transducer 104 attached to lattice 103, one or more leads 105 electrically connected to the at least one transducer 104, and a power source (not

shown) connected to the one or more leads 105. It should be appreciated that stent system 100 may be positioned near, in, within, or in proximity to at least one target site or region of interest of a subject using any known method or device including but not limited to: catheters, cannulas, guide wires, push wires, pusher wires, or the like, or any combination thereof.

Aspects of the present invention relate to a support structure for stent system 100. Support structure 101 comprises one or more members 102 configured, patterned, and/or arranged to form a scaffold such that lattice 103 may interface with the members and form a stent. It should be appreciated that support structure 101 may comprise any number of members. For example, the one or more members 102 comprise 1, 2, 3, 4, 5, 6, 7, 8, 9, 10, 11, 12, 13, 14, 15, 16, 17, 18, 19 or 20 members. In some embodiments, the one or more members 102 and/or lattice 103 comprise one or more wires interfaced together to form a stent. In some embodiments, the one or more wires of support structure 101 and/or the one or more wires of lattice 103 are interfaced, latticed, braided, woven, meshed, laced, interwoven, intertwined, interlaced, reticulated, wired, crossed, crisscrossed, wound, or the like, or any combination thereof, in order to form the stent. Generally, the support structure 101 and/or lattice 103 comprise or are formed from rigid, flexible, compressible, or elastic materials. It should be appreciated that portions or all of support structure 101 and/or lattice 103 may have rigid, flexible, compressible and/or elastic portions, regions or areas. In some embodiments, lattice 103 partially encloses the members of support structure 101, or fully or partially encloses the members. Support Structure 101, lattice 103 and/or leads 105 may be fixedly and/or releasably attached with any known method including attachments, weldments, bondings, glues, brackets, windings, wire bonding, wire wrapping, wire twisting, thermosonic binding, solders, or the like, or combinations thereof. Further, portions or all of support structure 101 and/or lattice 103 may be formed as a single unit or component, or may be formed separately, or with one or more components or structures each.

Generally, support structure 101 and/or lattice 103 may be configured or formed to have at least an undeployed state and a deployed state for the delivery and deployment of the stent system. In one example, stent system 100 comprises a first state or configuration, and a second state or configuration, wherein the first state is a compressed delivery state against the spring bias of the support structure and/or lattice 103, and the second state is a relaxed, expanded delivery state or configuration. In some embodiments, support structure 101 and/or lattice 103

comprise a spring bias that allows them to return to their expanded, relaxed state. In some embodiments, support structure 101 and/or lattice 103 comprise one or more expanding sections, or the entirety of each expands, or portions of one or both expand. In some embodiments, portions or all of stent system 100 can be compressed into a delivery device, such as a catheter, and later expand upon deployment when implanted.

Although described herein as a support structure 101 having one or more members 102, it should be appreciated that the support structure may also comprise one or more scaffolds or lattice type structures in addition to the one or more members 102, or in replacement of the one or more members 102.

In some embodiments, the one or more members 102 of the support structure 101 are formed of one or more materials selected from the group consisting of: elastic material, superelastic material, sputtered superelastic material, resilient material, rigid materials, flexible materials, nonconductive metal or alloy, poorly conductive metal or alloy, platinum, magnesium, stainless steel, nickel-titanium alloy/nitinol, nitinol thin film (i.e., NiTi thin film), cobalt-nickel alloys, tantalum alloys, cobalt-chromium alloys, platinum-tungsten metal, cobalt alloy, platinum-iridium alloy, cobalt, chromium, conductive metal, gold, copper, silver, titanium, and titanium alloys. In some embodiments, portions or all of support structure 101 are any of braided, laser cut, and/or magnetron sputtered thin film.

In some embodiments, the support structure 101 has a length of 15 mm to 60 mm, and a width or diameter of 1.5 mm to 20 mm, or a length between 0.1 mm and 100 mm, and a diameter between 0.001 mm and 200 mm. In some embodiments, the one or more members 102 of the support structure have a width or diameter between 0.01 mm and 2 mm, or between 0.001 and 5 mm. In some embodiments, support structure 101 has a length of 1 mm to 35 mm and a diameter of 0.1 mm to 5 mm. In some embodiments, the lattice has repeating subunits or components with openings, wherein each subunit or component comprises one or more connected members, and each member has a diameter or width between 0.01 mm and 2 mm. In some embodiments, the openings of the lattice range between 0.1 mm and 5 mm.

In some embodiments, the lattice 103 is formed of one or more materials selected from the group consisting of: elastic material, superelastic material, sputtered superelastic material, resilient material, rigid materials, flexible materials, nonconductive metal or alloy, poorly conductive metal or alloy, platinum, magnesium, stainless steel, nickel-titanium

alloy/nitinol, nitinol thin film (i.e., NiTi thin film), cobalt-nickel alloys, tantalum alloys, cobalt-chromium alloys, platinum-tungsten metal, cobalt alloy, platinum-iridium alloy, cobalt, chromium, conductive metal, gold, copper, silver, titanium, and titanium alloys. In some embodiments, portions or all of lattice 103 are any of braided, laser cut, and/or magnetron sputtered thin film.

Aspects of the present invention relate to the configuration, positioning, arrangement or patterning of one or more transducers on stent system 100. It should be appreciated that the at least one transducer 104 may be configured on stent system 100 to direct, focus or beam energy over one or more focal areas or regions. In some embodiments, the at least one traducers 104 produces a focused beam, or a broad beam, or a hybrid beam. In some embodiments, the at least one transducer 104 is positioned at least partially in inner region 114. In some embodiments, the at least one transducer 104 is positioned at least partially in peripheral region 116. In some embodiments, the at least one transducer spans or is positioned across inner region 114 and peripheral region 116. In some embodiments, the at least one transducer 104 is arranged, configured, or positioned in one or more patterns or configurations selected from: radial, radially outward, radially inward, focused inward, focused outward, circumferential, peripheral, helical, double-helical, triplicate, staggered, eccentric, biased, symmetrical, asymmetrical, and grouped. In some embodiments, system 100 comprises a plurality of transducers (i.e., at least 2 transducer 104) arranged radially along peripheral region 116 of support structure 101. In some embodiments, the plurality of transducers are configured and/or attached eccentrically in a serial linear arrangement along the length of support structure 102. In some embodiments, the plurality of transducers are configured, arranged and/or attached rotationally along the length of support structure 101. In some embodiments, plurality of transducers are arranged and/or attached in a corkscrew arrangement along the length of support structure 101. Although example configurations are provided, it should be appreciated that the plurality of transducers may be arranged in any configuration along the length of support structure 101 in order to focus energy directed towards the inside of the stent or the outside of the stent. In some embodiments, the arrangement of the at least one transducer 104 confers tunable acoustic focusing properties for selective targeting of cells or tissue (e.g., neuronal populations) of interest. In some embodiments, stent system 100 and/or the at least one transducer 104 is configured to selectively target one or more areas or regions in our surrounding the system. For

example, but without limitation, stent system 100 may be configured or formed to selectively target within the inner region 114, or outwardly from the peripheral region 116, or both, either separately or simultaneously, or on a program or schedule.

It should be appreciated that stent system 100 may be positioned near, in, within, or in proximity to at least one target site or region of interest of a subject using any known method or device including but not limited to: catheters, cannula, guide wires, push wires, pusher wires, or the like, or any combination thereof. In some embodiments, the pusher wire fixedly attaches, releasably attaches, or connects to one end of support structure 102. In some embodiments, stent system 100 is moved along at least one trajectory to treat the at least one target site or region of interest. In some embodiments, a disclosed pusher wire length is 120 cm to 200 cm and a diameter of 0.035 mm to 0.80 mm.

Aspects of the present invention relate to one or more leads for stent system 100. It should be appreciated that the at least one transducer 104 is electrically connected to one or more leads 105 with any known method or material known by one of ordinary level of skill in the art. In some embodiments, the one or more leads 105 comprise one or more electrically conductive wires. It should be appreciated that the one or more lead wires may comprise positive and negative lead wires. In some embodiments, leads 105 further comprise one or more insulators. Further, transducers 104 may be electrically connected to the one or more lead wires in any configuration known by one of ordinary level of skill in the art (e.g., series connection, parallel connection). The one or more leads 105 may comprise any terminating connectors or plugs known in the art.

In some embodiments, the one or more leads 105 are interfaced with any of support structure 101, one or more members 102, and/or lattice 103. In some embodiments, the one or more leads 105, the one or more members 102, and/or lattice 103 are interfaced, latticed, braided, woven, meshed, laced, interwoven, intertwined, interlaced, reticulated, wired, crossed, crisscrossed, wound, or the like, or any combination thereof. In some embodiments, one or more leads 105 partially encloses the one or more members 102 of support structure 101, or the repeating components of lattice 103, or fully encloses the members and components. In some embodiments, the one or more leads 105 are formed of one or more materials selected from the group consisting of: conductive metal, conductive metal allow, gold, copper, aluminum, silver, insulating material, polymer, or plastics, or any combination thereof.

In some embodiments, at least one of the support structure 101, one or more members 102, lattice 103, and one or more leads 105 are at least partially coated with one or more coatings selected from the group consisting of: biocompatible coating, conductive coating, non-conductive coating, insulating coating, oxide-film, titanium-nitride-oxide, organic polymer, polyurethane, polyimide, bioactive/covalently bonded coating, covalently-linked heparin, polymerized allylamine, poly(dimethylsiloxane), phosphorylcholine, 2-methylacryloyloxyethyl phosphorylcholine, poly(2-methoxyethyl acrylate), enzyme-loaded inducible nitric acid oxide, synthase oxygenase on polyethylenimine, chromium, platinum, gold, silver, trimethylolpropane triacrylate (TMPTA), parylene, anti-moisture coating and/or any anti-corrosion coating.

Aspects of the present invention relate to novel transducer designs, configurations, shapes, and dimensions, and methods of using and fabricating thereof. Referring now to Fig. 2, shown is an exemplary transducer 104 according to aspects of the present invention. In some embodiments, stent system 100 and/or transducer 104 further comprises at least one piezoelectric device or stack. In some embodiments, transducer 104 comprises a housing 140, a backing layer 142, a matching layer 144, a PZT element 146 and at least one electrode 148. In some embodiments, transducer 104 comprises a bipolar ceramic stack, electrode(s), a back mass and a front mass. In some embodiments, the at least one transducer 104 is a piezoelectric device comprising a bipolar ceramic stack, at least one electrode, a back mass, a front mass, and at least one biocompatible coating covering at least a portion of the at least one transducer 104.

In some embodiments, the at least one transducer 104 is at least partially formed in one or more shapes selected from the group consisting of: non-planar, curved, cylindrical, concentrical circles, concentric circles with struts, hemispherical, annular, ring, half-ring, spherical, rectangular, prism, pyramidal, helical and polyhedral. In some embodiments, the at least one transducer 104 has length of 5 μm to 50 mm, or 15 μm to 25 mm a width or diameter of 5 μm to 50 mmm or 15 μm to 25 mm, and a height of 5 μm to 25 mm, or 15 μm to 25 mm. In some embodiments, the at least one transducer 104 has a curvature ranging from 0 degrees to 180 degrees, or 20 degrees to 160 degrees, or 40 degrees to 140 degrees, or 60 degrees to 120 degrees, or 80 degrees to 115 degrees, or 90 to 110 degrees, or 105 degrees to 115 degrees, or about 110 degrees, or an arc length ranging from 0.1 μm to 10 mm. It should be appreciated that the size of the transducer and the degree of curvature or arc length may create one or more focal

distance lengths for the transducer. In some embodiments, the at least one transducer 104 has one or more focal lengths, such as lengths of about 0.1 μm, 0.2 μm, 0.3 μm, 0.4 μm, 0.5 μm, 0.6 μm, 0.7 μm, 0.8 μm, 0.9 μm or between 0.1 μm and 200 μm, or between 0.1 μm and 2 mm, or about 0.1 mm, 0.2 mm, 0.3 mm, 0.4 mm, 0.5 mm, 0.6 mm, 0.7 mm, 0.8 mm, 0.9 mm, 1.0 mm, or between 0.1 mm and 5 mm, or about 1 mm, or about 1.5 mm, or between 1 mm and 100 mm, or between 1 mm and 50 mm, or between 1 mm and 10 mm. It should be appreciated that any known transducer material, geometry or size may be used or incorporated into the at least one transducer 104 in order to tune or configure the at least one transducer 104 for the applications discussed herein.

In some embodiments, the at least one transducer 104 is at least partially coated with one or more coatings selected from the group consisting of: biocompatible coating, conductive coating, non-conductive coating, insulating coating, oxide-film, titanium-nitride-oxide, organic polymer, polyurethane, polyimide, bioactive/covalently bonded coating, covalently-linked heparin, polymerized allylamine, poly(dimethylsiloxane), phosphorylcholine, 2-methylacryloyloxyethyl phosphorylcholine, poly(2-methoxyethyl acrylate), enzyme-loaded inducible nitric acid oxide, synthase oxygenase on polyethylenimine, chromium, platinum, gold, silver, trimethylolpropane triacrylate (TMPTA), parylene, anti-moisture coating and/or any anti-corrosion coating.

In some embodiments, transducer 104 comprises Lead Zirconate Titanate (PZT). In some embodiments, the transducer further comprises at least one biocompatible coating. In some embodiments, the biocompatible coating comprises trimethylolpropane triacrylate (TMPTA). In some embodiments, transducer 104 comprises a matching layer 144. In some embodiments, the matching layer 144 is a thin layer of material located between the transducer's piezoelectric crystal and the target to be treated. The matching layer 144 functions to improve acoustic energy transfer between the transducer and the target medium by reducing the impedance mismatch between these two materials. In some embodiments, the matching layer 144 comprises a mixture of carbon fiber (CF) and RIGID resin (Formlab, USA). RIGID resin is a mixture comprising urethane dimethacrylate and isobornyl methacrylate. In some embodiments, transducer 104 comprises a backing layer 142 and/or backing material. The backing layer 142 of an ultrasound transducer is a layer of material located behind the piezoelectric crystal. The function of the backing layer 142 is to absorb and dampen the sound waves generated by the

crystal, which helps to reduce the ringing or reverberation that can occur after each pulse of sound. In some embodiments, the backing layer 144 comprises an Fe magnetic particle-loaded FLEXIBLE resin (Formlab, USA). FLEXIBLE is a mixture comprising acrylated oligomers and acrylated monomers. In some embodiments, transducer 104 comprises a parylene coating. In some embodiments, transducer 104 comprises any FDA compliant coating, any anti-moisture coating and/or any anti-corrosion coating.

Aspects of the present invention relate to providing power at one or more voltages in one or more frequencies from the power source to the at least one transducer 104 for at least one duration. It should be appreciated that transducers, ultrasound transducers and pzeiolectric devices are disclosed herein that operate based on well-known parameters. This includes, but is not limited to, applying electrical power to the transducer in order to produce acoustic energy from the transducer. As discussed elsewhere herein, a controller 108 and/or computer 400 may comprise a power source capable of generating the electrical power, frequencies, signals and other parameters required to operate said transducers in order to perform targeted acoustic stimulation of one or more cells, one or more areas of interest, regions of interest, or target sites on a subject. Adjustable parameters for powering the disclosed transducers include, but are not limited to, voltage (e.g., Vpp), current, power, signal, frequency, duration, bursts, cycles, duty cycles, or the like, and any combination thereof. For example, in some embodiments, the one or voltages is between 0.1 V to 500 V, the one or more frequencies are between 0.1 Hz and 10000 MHz, the at least one duration is between 0.1 μs and 1 hour, and duty cycle between 0% and 100%. In another example, in some embodiments, the at least one transducer 104 is provided with 9.75-MHz burst waves with 50 cycles (20 ms burst period) with a 10% duty cycle. For localized cavitation experiments in blood vessel phantom, the 9.75-MHz burst waves were set up to have 10% duty cycle. In some embodiments, the arrangement and powering of the transducers confers tunable acoustic focusing properties for selective targeting of neuronal populations of interest, and thusly may be arranged or powered in any configuration known by one of ordinary level of skill in the art for achieving the selective targeting of the one or more cells. In some embodiments, the performance of transducer 104 may be enhanced by adjoining it with one or more application specific integrated circuits (ASICs).

Aspects of the present invention relate to microfluidic chambers for the disclosed stent systems. In some embodiments, system 100 comprises at least one microfluidic chamber.

Each microfluid chamber comprises one or more side walls having inside and outside surfaces and enclosing an interior region wherein a fluid or solution may be stored securely while the stent system 100 is positioned and/or configured. In some embodiments, system 100 further comprises a first microfluidic reservoir 130 external to the stent, connected to and in fluid communication with a first microfluidic chamber 110. In some embodiments, system 100 further comprises a second microfluidic reservoir 132 connected to and in fluid communication with second microfluidic chamber 112. In some embodiments, first microfluidic reservoir 130 and second microfluidic reservoir 132 are configured to receive drug, solutions, fluids, and/or microbubbles delivered percutaneously via needle and syringe or other methods as would be known by one of ordinary skill in the art.

In some embodiments, first microfluidic reservoir 130 comprises a first port 131 in fluid communication with first microfluidic chamber 110 and is configured to receive drug, fluid, solution, microbubbles, therapeutics etc delivered via needle and syringe. In some embodiments, second microfluidic reservoir 132 comprises a port 133 in fluid communication with second microfluidic chamber 112, and configured to receive fluid, solution, microbubbles, drug, therapeutics, etc via needle and syringe. Although exemplary configurations are provided, it should be appreciated that the each chamber may positioned at least partially within the stent of stent system 100 and is fluidly connected to a respective reservoir, wherein the chambers are connected in series, or connected individually to the respective reservoir. In one example, a single reservoir feeds all of the chambers connected in series, or parallel. Further, it should be appreciated that the size, location, shape etc of the at least microfluidic chamber may be impacted or controlled by the size, location and shape of the at least one transducer 104. For example, if the at least one transducer is directing energy towards inner region 114, then logically the at least one microfluidic chamber should be positioned in or near the focal area, focal region, or at or near the focal depth of the at least one transducer 104.

In some embodiments, the at least one microfluidic chamber is disposed or positioned within the inner region 114 of support structure 101. In some embodiments, the at least one microfluidic chamber spans at least a portion of inner region 114 and peripheral region 116. In some embodiments, the at least one microfluidic chamber is deformable. In some embodiments, the at least one microfluidic chamber is porous. In some embodiments, the at least one microfluidic chamber is configured to release drug and/or microbubbles. In some

embodiments, the at least one microfluidic chamber is configured to release drug and/or microbubbles when ultrasound is applied to the at least one microfluidic chamber.

Aspects of the present invention relate to one or more microfluidic reservoirs for stent system 100. In some embodiments, stent system 100 further comprises least one microfluidic reservoir positioned outside of the support structure 101 with at least one conduit 106 comprising at least one lumen fluidly connecting to the at least one microfluidic chamber.

Referring now to Fig 3, shown is an exemplary stent system 100 comprising at least one microfluid reservoir connected to at least one microfluidic reserervoir with at least one conduit. In some embodiments, stent system 100 comprises a support structure 101 having a first end 113, a second end 115, a length and diameter, and wherein at least one transducer 104 is connected or attached thereto. In some embodiments, support structure 101 interfaces with a cylindrical lattice 103 and forms an inner region 114, peripheral region 116. In some embodiment, support structure 101 and/or lattice 103 may form or be covered with an outer surface 118 and/or end caps, or end membranes.

In some embodiments, system 100 further comprises a power source (not shown) electrically connected to at least one transducer 104. In some embodiments, system 100 further comprises a controller 108 connected to the power source and/or the at least one transducer 104 or one or more leads 105 (not shown). In some embodiments, the at least one conduit 106 is a flexible hypotube with or more lumens connected to a position on support structure 101, and to a position on controller 108. In some embodiments, system 100 further comprises at least one microfluidic chamber disposed within support structure 101, and in fluid communication with one or more of the lumens of conduit 106. In some embodiments, the at least one microfluidic chamber comprises a first microfluidic chamber 110 and second microfluidic chamber 112, and the at least one microfluidic reservoir comprises a first microfluidic reservoir 130 and second microfluidic reservoir 132. In some embodiments, first microfluidic chamber 110 is a microbubble chamber, and the second microfluidic chamber 112 is a drug chamber.

In some embodiments, each microfluidic reservoir comprises at least one port configured to receive one or more fluids or solutions. In some embodiments, a first microfluidic reservoir 130 comprises a port 131 and second microfluidic reservoir 132 comprises a port 133. It should be appreciated the flow of fluid or solution may travel from the one or more microfluidic reservoir through the at least one conduit to the one or more microfluidic chambers

using any known method or device. In one example, that this may be achieved by modulating the flow or pressure of the one or more reservoir using any known method or device (e.g., a pump, a syringe fluidly connected to the port, a plunger, other mechanical means).

In some embodiments, system 100 further comprises an implantable housing 108 at least partially enclosing the power source (not shown), the first microfluidic reservoir 130, and the second microfluidic reservoir 132. In some embodiments, the at least one conduit 106 comprises a tubular conduit having at least one lumen extending from the housing 108 to a position on the first end 113 of the support structure 101. In some embodiments, the housing 108 is configured to be implanted subcutaneously in the thorax and support structure 101 and lattice 103 is configured to be placed intravascularly. Although example positions are provided, it should be appreciated that the housing may be at least partially transdermal, subdermal, or subcutaneous, and the stent may be positioned within any structure including vascular, organs and tissue. In some embodiments, the stent is implanted in a superior sagittal sinus of a subject, wherein a portion of the system 100 percutaneously exits to a connector block for power, programming and fluid introduction (e.g., housing 108).

The microfluidic chambers may be formed in one or more shapes, or at least partially in one or more shapes, and be positioned or configured to any portion or region of stent system 100, support structure 101 and/or lattice 103. In some embodiments, the at least one microfluidic chamber is at least partially formed in one or more shapes selected from: cylinder, disk, toroid, annulus, capsule, pill, cube, sphere, dome, arc, spiral, helix, double helix. For example, but without limitation, first microfluidic chamber 110 is formed as a capsule shape and positioned in inner region 114, and second microfluidic chamber 112 is formed as an annulus or ring configured or formed in or on peripheral region 116. Examples are provided with 1 or 2 microfluidic chambers, but there may be any number of microfluidic chambers, positioned in any configurations in or around the support structure 101 and/or lattice 103.

Aspects of the present invention relate to materials for the at least one microfluidic chamber and/or at least one microfluidic reservoir for system 100. In some embodiments, the at least one microfluid chamber comprises sidewalls formed of a permeable membrane, semi-permeable membrane, porous membrane, membrane, a hydrogel, a gel, a biomaterial, a biocompatible material, a bioresorbable material, a biodegradable material, a non-degradable material, a synthetic material, a polymer. It should be appreciated that the at least one

conduit is formed of a substantially non-porous material in order to direct fluid to the at least one microfluidic chamber, wherein the solution with drug may diffuse through the walls of the chamber. However, in another example, the at least microfluidic chamber is configured to lyse, burst, hemorrhage, bust, or pop the microfluidic chamber upon insonation and microbubble cavitation in order to disperse the contained fluid, and is formed of appropriate materials and thicknesses to achieve such.

In some embodiments, the at least one microfluidic chamber has a diameter ranging between about 0.100 mm to about 5 mm, or about 0.5 mm to 2 mm. For example, in some embodiments, the diameter range would be about 0.100 mm to about 0.35 mm. In some embodiments, the at least one microfluid chamber is formed at least partially in one or more shapes selected from cylinder, a toroid, a capsule, a pill, a cube, a sphere, a dome, an arc, a spiral, a double helix, irregular, non-planar, curved, banana.

In some embodiments, the at least one microfluid chamber has a volume ranging between 50 μl and 1000 μl, or 1 μl to 100 mL, or a diameter between 0.1 mm and 1 mm, the at least one microfluid reservoir has a volume ranging between 100 μl and 10 ml.

Aspects of the present invention relate to fluids, solutions, suspensions or the like that at least partially fluidly fill the disclosed microfluidic chambers and reservoirs. In some embodiments, the at least one microfluidic chamber and/or microfluidic reservoir are at least partially fluidly filled with one or more fluids, solutions, suspensions, drug suspensions, drug solutions, microbubble solutions, microbubble suspensions, drug-microbubble solutions, solution comprised drug-encapsulated microbubbles, or the like, or any combination thereof. In some embodiments, the first microfluidic chamber 110 and first microfluidic reservoir 130 are at least partially fluidly filled with a solution comprising microbubbles, and the second microfluidic chamber 112 and second microfluidic reservoir 132 are at least partially fluidly filled with a solution comprising at least one therapeutic.

Aspects of the present invention relate to delivering at least one therapeutic to a region of interest, an area of interest, or a target site on a subject. It should be appreciated that the at least one microfluidic chamber may be pre-filled with a solution prior to placement of the stent, or in another embodiment, the at least one microfluidic reservoir is filled, and the solution travels along one or more lumens of the at least one conduit to the at least one microfluidic chamber. In some embodiments, the at least one therapeutic is selected from the group

consisting of: gene therapy, Nusinersen, Levodopa, anti-seizure medication, DNA or RNA based biologic/viral-vector gene replacement therapies, CRISPR, Nusinersen for SMA, RGX-111, RGX-112, condensed tuberin, APOE2, hTERT, GBA, SOD-1, C9orf72, HTT, antibody-based biologic therapies, Lecanemab, small molecules and proteins.

Aspects of the present invention relate to an outer surface or layer and/or coating for a stent system 100. In some embodiments, outer surface 118 comprises any of a membrane, a porous membrane, a hydrogel, a gel, a biomaterial, a biocompatible material, a synthetic material, a polymer. In some embodiments, outer surface 118 comprises one or more coatings comprising at least one of oxide-film (e.g., titanium-nitride-oxide and the like), organic polymers (e.g., polyurethane, polyimide, and the like), or other bioactive/covalently bonded coatings (e.g., covalently-linked heparin, polymerized allylamine, poly(dimethylsiloxane), phosphorylcholine, 2-methylacryloyloxyethyl phosphorylcholine, poly(2-methoxyethyl acrylate), enzyme-loaded inducible nitric acid oxide synthase oxygenase on polyethylenimine, and the like), biocompatible coating, stealth coating, or any combination thereof.

Aspects of the present invention relate to the configuration of the components of stent system 100. In some embodiments, conduit 106 connects along the length of support structure 101. In some embodiments, conduit 106 connects to the first end 113, or the second end 115 of support structure 101. In some embodiments, conduit 106 connects to axially to first end 113 of support structure 101. In some embodiments, conduit 106 connects to second end 115 wherein conduit 106 is centered within the stent, or from the side of the stent. In another example, conduit 106 connects the first end 113 of support structure 101 eccentrically.

Aspects of the present invention relate to a controller for an advanced function stent system. In some embodiments, controller 108 is an electrical power source for providing power to the at least one transducer 104. In some embodiments, controller 108 comprises a housing and is configured to be implanted subcutaneously. In some embodiments, controller 108 is a programmable thorax implant. Again referring to Fig. 3, an exemplary system 100 with controller 108 is shown. In some embodiments, controller 108 comprises a console 126, a battery 128, a first microfluidic reservoir 130, a first port 131, a second microfluidic reservoir 132 and a second port 133. In some embodiments, controller 108 controls the release of fluid, solution or drug from the reservoirs. It should be appreciated that this may be achieved by modulating the flow or pressure of the at least one reservoir using any known method or device (e.g., a pump).

In some embodiments, controller 108 comprises a graphical user interface (GUI) that allows a user to control the release of fluid or drug from the at least one reservoir (e.g., from the first microfluidic reservoir 130). In some embodiments, controller 108 provides a schedule for the release of drug from the first microfluidic reservoir 130 and/or the acoustic stimulation from the at least one transducer 104. In some embodiments, system 100 and/or controller 108 comprise at least one sensor measuring at least one signal from the subject, wherein drug, fluid or solution from first microfluidic reservoir 130 is released when at least one threshold value is measured with the sensor (e.g., a temperature sensor, a pressure sensor). In some embodiments, system 100 is a closed-loop system wherein feedback from at least one sensor provides control over system 100. In some embodiments, system 100 is an open-loop system wherein control over the system is provided by at least one user or a health care professional.

In some embodiments, controller 108 comprises one or more computing devices (e.g., computing device 400 as elaborated upon herein). In some embodiments, controller 108 is a subcutaneous implant and is a programmable device that may be battery powered or wirelessly charged (near field radio frequency). In some embodiments, controller 108 encases reservoirs for the percutaneously injected bubbles and drugs. In some embodiments, controller 108 controls on/off functions and parameters for at least one transducer 102.

In some embodiments, system 100 further comprises a conduit 106 comprising a hyptotube. In some embodiments, conduit 106 comprises a first end 107, a second end 109, and a length therebetween. In some embodiments, conduit 106 comprises at least one lumen extending axially therethrough. In some embodiments, conduit 106 connects support structure 101 and controller 108. In some embodiments, the conduit 106 comprises at least one microfluidic tubular channel forming a lumen fluidly connected to the at least one microfluid chambers, and at least one channel forming a lumen for running a length of an electrical lead (e.g., one or more leads 105) or electrical wire connections for the at least one transducer 104. In some embodiments, at least one microfluidic tubular channel within conduit 106 fluidly connects microfluidic chamber 110 and first reservoir 130. In some embodiments, at least one microfluidic tubular channel fluidly connects second microfluidic chamber 112 and second microfluidic reservoir 132. In some embodiments, conduit 106 is configured to traverse through a blood vessel. In some embodiments, the conduit 106 comprises individual connections between the stent system 100 (e.g., microfluidic chambers, transducers , sensors, etc.) and traverses

through a vessel and out to a subcutaneous surgical implant on the body of the subject (e.g., the thorax).

Aspects of the present invention relates to at least one material for the at least one conduit 106 of stent system 100. In some embodiments, conduit 106 may be formed or comprise any suitable material, including but not limited to: flexible materials, synthetics, polymers, elastic materials, metal (e.g., stainless steel, nitinol, etc.), or an extruded polymer (e.g., PTFE, polydimethylsiloxane, silicone, etc.) or the like. Although example materials are provided, conduit 106 may comprise any material as would be known by one of ordinary level of skill in the art.

Aspects of the present invention relate to dimensions for the at least one conduit 106. In some embodiments, the at least one conduit 106 has a length ranging between 1 mm and 200 cm, and a diameter ranging between 0.01 mm and 3 mm. In some embodiments, conduit 106 has a length ranging between 1 mm and 1000 mm, and a width or diameter ranging between 0.01 mm and 2 mm. In some embodiments, conduit 106 comprises at least one lumen, wherein the lumen size ranges between about 0.01 mm and about 1 mm, or about 0.1 mm to about 0.35 mm.

Fabrication Method

Aspects of the present invention relate to a method of fabricating a stent system comprising fabricating a stent, fabricating at least one PZT transducer, fabricating at least one microfluidic chamber, fixing the at least one PZT transducer to the stent, disposing the at least one microfluidic chamber within the stent. In some embodiments, the step of fabricating the PZT transducer comprises 3D printing a PZT base layer on a polymer support layer, debonding the PZT base layer from the polymer support layer, sintering the PTZ base layer in a PTZ powder bed with heat to form a PTZ element, submerging the PTZ element into an isolation liquid, polarizing the dipoles within the sintered PTZ element, applying an electric field to the PTZ element and cooling the PTZ element.

Aspects of the present invention relate to exemplary fabrication methods for an advanced function stent system. In some embodiments, an exemplary method of fabricating a stent system comprises the steps of fabricating a stent, fabricating at least one PZT transducer, fabricating at least one microfluidic chamber, fixing the at least one PZT transducer to the stent, disposing the at least one microfluidic chamber within the stent. In some embodiments, the step

of fabricating the PTZ transducer comprises 3D printing a PZT base layer on a polymer support layer, debonding the PZT base layer from the polymer support layer, sintering the PTZ base layer in a PTZ powder bed with heat to form a PTZ element, submerging the PTZ element into an isolation liquid, polarizing the dipoles within the sintered PTZ element, applying an electric field to the PTZ element; and cooling the PTZ element.

Method of Use

Aspects of the present invention relate to spatiotemporal expression or control of genes (e.g., intrinsic or exogenous genes) with at least one therapy (e.g., targeted acoustic stimulation) of cells transfected with select Transient Receptor Potential channels using the disclosed stent system 100. In some embodiments, stent system 100 enhances precision treatment of neurologic diseases and disorders by activating, silencing, or modulating gene function by activating, silencing, or modulating gene function.

Aspects of the present invention relate to a method for spatiotemporal expression or control of intrinsic or exogenous genes comprising providing a stent system with transducers (e.g., system 100), implanting the stent system near or in a target site of a subject, providing power at one or more voltages in one or more frequencies from the power source to the at least one transducer for at least one duration. In some embodiments, the one or voltages is between 0.1 V to 500 V, the one or more frequencies are between 0.1 Hz and 10000 MHz, and the at least one duration is between 0.1 μs and 1 hour.

Aspects of the present invention relate to a drug delivery method comprising providing a stent system with at least one transducer and at least one microfluidic chamber (e.g, system 100), implanting the stent system in or near a target site of a subject, filling the at least one microfluidic chamber at least partially with a solution comprising at least one therapeutic and microbubbles, producing microbubble cavitation via the at least one transducer and delivering the at least one therapeutic to the target site.

Aspects of the present invention relate to methods of use for a smart stent system. In some embodiments, an exemplary method of use comprises a drug deliver method. In some embodiments, an exemplary drug delivery method comprises the steps of providing a system 100 of the present invention, supplying at least one therapeutic and microbubbles via at least one

microfluidic chamber, producing microbubble cavitation via the transducer and delivering the at least one therapeutic to a target site.

In some embodiments, a portion of system 100 is implanted in the superior sagittal sinus of a subject, and at least a portion of the system percutaneously exits the subject to a connector block or controller for power, programing and fluid introduction. In some embodiments, system 100 is an advanced function stent system that enables transient blood brain barrier disruption and direct drug delivery into the central nervous system.

Aspects of the present invention relates to an implantation method for an advanced stent system. In some embodiments, a 2.1 – 7 French catheter is used to implant at least a portion of system 100 at a target site. In some embodiments, a long sheath, a guide catheter, an intermediate catheter, a microcatheter, and/or a microguidewire is used to implant at least one of portion of system 100 at a target site. In some embodiments, the target site is reached via percutaneous access via the jugular, brachial, femoral, or subclavian veins or via the femoral, radial, carotid, or brachial arteries to the intracranial vessels (i.e., Superior sagittal sinus, straight sinus, great vein of galen, transverse sinus, sigmoid sinus, inferior petrosal sinus, internal cerebral vein, basal vein, vein of trolard, vein of Labbe, or the internal cerebral artery, middle cerebral artery, or anterior cerebral artery, respectively (or any of its branches with adequate diameters, generally > 1.5 mm) within the intracranial vault.

In some embodiments, a method of using system 100 comprises the steps of providing any system 100 of the present invention, implanting stent system 100 into a subject, supplying microbubble and at least one drug to system 100, and insonating the microbubbles.

In some embodiments, system 100 comprises a computing system (e.g., computer 400) communicatively connected to the transducers of system 100, comprising a processor and a non-transitory computer-readable medium with instructions stored thereon, which when executed by a processor, perform steps comprising applying an electrical current from the power source to the transducer for a predetermined period of time, or one or more durations.

In some embodiments, system 100 is used for on-demand transient blood brain barrier disruption, which may modulate cellular microenvironments. In some embodiments, system 100 is used adjunctively for enhanced drug delivery with or without microbubbles or some other carrier. In some embodiments, system 100 is used for sonogenetic control of cells. In some embodiments, system 100 is used for acoustic modulation of cell function. In some

embodiments, system 100 is used for sonogenetic control of cells transfected with TRP channels. In some embodiments, system 100 is used for acoustic wave mediated neuromodulation of brain circuits.

In some embodiments, at least a portion of system 100 is implanted to a target site, delivery site and/or delivery location. In some embodiments, the delivery location is the intracranial cerebral arteries such was the internal carotid artery, basilar artery, vertebral artery, middle cerebral artery, posterior cerebral artery, or anterior cerebral artery. Alternatively, in some embodiments, the venous structures may be the implantation site, such as the superior sagittal sinus, the straight sinus, the inferior sagittal sinus, transverse sinus, sigmoid sinus, or superior petrosal sinus, or inferior petrosal sinus.

Computing Device

In some aspects of the present invention, software executing the instructions provided herein may be stored on a non-transitory computer-readable medium, wherein the software performs some or all of the steps of the present invention when executed on a processor.

Aspects of the invention relate to algorithms executed in computer software. Though certain embodiments may be described as written in particular programming languages, or executed on particular operating systems or computing platforms, it is understood that the system and method of the present invention is not limited to any particular computing language, platform, or combination thereof. Software executing the algorithms described herein may be written in any programming language known in the art, compiled, or interpreted, including but not limited to C, C++, C#, Objective-C, Java, JavaScript, MATLAB, Python, PHP, Perl, Ruby, or Visual Basic. It is further understood that elements of the present invention may be executed on any acceptable computing platform, including but not limited to a server, a cloud instance, a workstation, a thin client, a mobile device, an embedded microcontroller, a television, or any other suitable computing device known in the art.

Parts of this invention are described as software running on a computing device. Though software described herein may be disclosed as operating on one particular computing device (e.g. a dedicated server or a workstation), it is understood in the art that software is intrinsically portable and that most software running on a dedicated server may also be run, for

the purposes of the present invention, on any of a wide range of devices including desktop or mobile devices, laptops, tablets, smartphones, watches, wearable electronics or other wireless digital/cellular phones, televisions, cloud instances, embedded microcontrollers, thin client devices, or any other suitable computing device known in the art.

Similarly, parts of this invention are described as communicating over a variety of wireless or wired computer networks. For the purposes of this invention, the words "network", "networked", and "networking" are understood to encompass wired Ethernet, fiber optic connections, wireless connections including any of the various 802.11 standards, cellular WAN infrastructures such as 3G, 4G/LTE, or 5G networks, Bluetooth®, Bluetooth® Low Energy (BLE) or Zigbee® communication links, or any other method by which one electronic device is capable of communicating with another. In some embodiments, elements of the networked portion of the invention may be implemented over a Virtual Private Network (VPN).

Fig. 4 and the following discussion are intended to provide a brief, general description of a suitable computing environment in which the invention may be implemented. While the invention is described above in the general context of program modules that execute in conjunction with an application program that runs on an operating system on a computer, those skilled in the art will recognize that the invention may also be implemented in combination with other program modules.

Generally, program modules include routines, programs, components, data structures, and other types of structures that perform particular tasks or implement particular abstract data types. Moreover, those skilled in the art will appreciate that the invention may be practiced with other computer system configurations, including hand-held devices, multiprocessor systems, microprocessor-based or programmable consumer electronics, minicomputers, mainframe computers, and the like. The invention may also be practiced in distributed computing environments where tasks are performed by remote processing devices that are linked through a communications network. In a distributed computing environment, program modules may be located in both local and remote memory storage devices.

Fig. 4 depicts an illustrative computer architecture for a computer 400 for practicing the various embodiments of the invention. The computer architecture shown in Fig. 4 illustrates a conventional personal computer, including a central processing unit 450 ("CPU"), a system memory 405, including a random access memory 410 ("RAM") and a read-only memory

("ROM") 415, and a system bus 435 that couples the system memory 405 to the CPU 450. A basic input/output system containing the basic routines that help to transfer information between elements within the computer, such as during startup, is stored in the ROM 415. The computer 400 further includes a storage device 420 for storing an operating system 425, application/program 430, and data.

The storage device 420 is connected to the CPU 450 through a storage controller (not shown) connected to the bus 435. The storage device 420 and its associated computer-readable media provide non-volatile storage for the computer 400. Although the description of computer-readable media contained herein refers to a storage device, such as a hard disk or CD-ROM drive, it should be appreciated by those skilled in the art that computer-readable media can be any available media that can be accessed by the computer 400.

By way of example, and not to be limiting, computer-readable media may comprise computer storage media. Computer storage media includes volatile and non-volatile, removable and non-removable media implemented in any method or technology for storage of information such as computer-readable instructions, data structures, program modules or other data. Computer storage media includes, but is not limited to, RAM, ROM, EPROM, EEPROM, flash memory or other solid state memory technology, CD-ROM, DVD, or other optical storage, magnetic cassettes, magnetic tape, magnetic disk storage or other magnetic storage devices, or any other medium which can be used to store the desired information and which can be accessed by the computer.

According to various embodiments of the invention, the computer 400 may operate in a networked environment using logical connections to remote computers through a network 440, such as TCP/IP network such as the Internet or an intranet. The computer 400 may connect to the network 440 through a network interface unit 445 connected to the bus 435. It should be appreciated that the network interface unit 445 may also be utilized to connect to other types of networks and remote computer systems.

The computer 400 may also include an input/output controller 455 for receiving and processing input from a number of input/output devices 460, including a keyboard, a mouse, a touchscreen, a camera, a microphone, a controller, a joystick, or other type of input device. Similarly, the input/output controller 455 may provide output to a display screen, a printer, a speaker, or other type of output device. The computer 400 can connect to the input/output device

460 via a wired connection including, but not limited to, fiber optic, Ethernet, or copper wire or wireless means including, but not limited to, Wi-Fi, Bluetooth, Near-Field Communication (NFC), infrared, or other suitable wired or wireless connections.

As mentioned briefly above, a number of program modules and data files may be stored in the storage device 420 and/or RAM 410 of the computer 400, including an operating system 425 suitable for controlling the operation of a networked computer. The storage device 420 and RAM 410 may also store one or more applications/programs 430. In particular, the storage device 420 and RAM 410 may store an application/program 430 for providing a variety of functionalities to a user. For instance, the application/program 430 may comprise many types of programs such as a word processing application, a spreadsheet application, a desktop publishing application, a database application, a gaming application, internet browsing application, electronic mail application, messaging application, and the like. According to an embodiment of the present invention, the application/program 430 comprises a multiple functionality software application for providing word processing functionality, slide presentation functionality, spreadsheet functionality, database functionality and the like.

The computer 400 in some embodiments can include a variety of sensors 465 for monitoring the environment surrounding and the environment internal to the computer 400. These sensors 465 can include a Global Positioning System (GPS) sensor, a photosensitive sensor, a gyroscope, a magnetometer, thermometer, a proximity sensor, an accelerometer, a microphone, biometric sensor, barometer, humidity sensor, radiation sensor, or any other suitable sensor.

## EXPERIMENTAL EXAMPLES

The invention is further described in detail by reference to the following experimental examples. These examples are provided for purposes of illustration only, and are not intended to be limiting unless otherwise specified. Thus, the invention should in no way be construed as being limited to the following examples, but rather, should be construed to encompass any and all variations which become evident as a result of the teaching provided herein.

Without further description, it is believed that one of ordinary skill in the art can, using the preceding description and the following illustrative examples, make and utilize the

present invention and practice the claimed methods. The following working examples therefore are not to be construed as limiting in any way the remainder of the disclosure.

The blood brain barrier is a major impediment to drug therapy into the central nervous system. Pulsed Ultrasound in conjunction with intravenous ultrasound transiently disrupts the blood brain barrier. The skull remains a significant barrier to effective ultrasound energy delivery. To overcome this known impediment, a device referred to as the SonoCloud has been developed for neuro-oncologic clinical indications and is currently undergoing clinical trials, but it requires drilling a hole into the skull. The invasiveness of the device limits its generalizability for the treatment of a variety of other neurological disorders. The use of sputtered Niti Thin film as a scaffold for sophisticated microelectronic mechanical systems has been demonstrated to be a versatile method of maintaining the structural integrity of MEMS components embedded on a stent structure. The development of smart stent systems is only in its infancy, and the prime example of one such device is the Stentrode, which utilizes a laser cut stent embedded with electrodes to transduce brain signals for computer interfacing in patients with motor disability, which is also undergoing clinical trials now with promising preliminary results.

Printing and Processing of 3D Transducers with Near-pristine Piezoelectric Ceramics for Localized Cavitations and Drug Delivery: Additive manufacturing has seen tremendous growth in the past decade, which provides the ability to create free-form objects with tailorable properties. The potential of printing functional devices from active materials is still elusive, as most printed products have mainly focused on single structural materials such as polymers, metals, and ceramics. Printing functional devices is compelling, as a 3D assembly of electronic, dielectric and functional materials could open up unprecedented design space and capabilities not offered by current fabrication approaches.

Fig. 5A, Fig. 5B, and Fig. 5C show an exemplary design and additive manufacturing of fully packaged freeform ultrasonic transducers capable of traveling inside millimeter-sized channels and the delivery of ultrasound energy to precise locations within sub-$mm^2$ and achieve cavitation-enabled drug delivery. This is achieved through a novel integrated printing and sintering technique that achieves dense 3D printable piezoceramic elements with properties matching pristine ceramics. To demonstrate the applications of the approach, an intravascular ultrasound (IVUS) transducer with microscale focusing features was 3D printed,

which is capable of generating high and localized acoustic pressure in blood vessels with diameters as low as 2 mm, allowing localized cavitation triggering and intravenous drug delivery.

Several fundamental scientific breakthroughs stand out from this transformative approach. First, 3D printing functional materials requires the introduction of active material inclusions and binders, such as UV sensitive monomers or inks as the matrix material where functional feedstock is embedded in. This results in a significant trade-off between processability and functionality. The disclosed 3D printing and liquid phase sintering method results in properties matching that of the fully dense pristine ceramics, making 3D printing a viable path for high-performance functional materials. Second, a design and printing library that enables the selection and 3D assembly of active, backing and matching layers into focusing ultrasonic transducer architectures for a myriad of medium for maximum acoustic energy output. Third, the novel 3D printable transducer technology enables localized energy delivery in the sub-mm domain. The energy density is capable of reaching the threshold of triggering cavitations via bursting microbubbles, paving the way for precision drug delivery, therapeutics and diagnostics.

3D Printing and Processing of Intravascular Ultrasound Transducers with Near-pristine Piezoelectric Ceramics for Localized Cavitation: Owing to the capability of piezoelectric materials to convert mechanical to electrical energy and vice versa, they are widely used in sensing [1], actuation [2], energy harvesting [3; 4], cleaning [5], and ultrasound imaging [6; 7]. Recently, the emergence of new structural designs and computations has led to the prediction that incorporating 3D microfeatures into piezoelectric materials could provide unprecedented properties or functionalities, including designed anisotropy [8] and the ability to emit tailored and localized ultrasound fields [9], as well as sensors and actuators for miniaturized robots and transducers. The manufacturing of these architectures is either dependent on conventional machining methods, including etching, dicing and hot pressing [10], or limited to 3D printed composite materials containing piezoelectric nanoparticles and polymer matrices [15]. The mechanical stress caused by the machining processes results in grain pullout, reduced strength and depolarization, leading to significant degradation of the piezoelectricity of the manufactured elements [12]. As a result, the piezoelectric materials with these architectures exhibit piezoelectric coefficients much lower than those of their pristine ceramic counterparts and weak emission pressures when used as ultrasonic transducers. Printing piezoceramic

transducer elements with precise microscale features, free form factors and high piezoelectric responses capable of acoustic focusing, impedance matching and serving as a backing layer is highly desirable in applications that require small sizes, high emission pressures and localized energy outputs that could open a myriad of new applications, including intravascular thrombolysis [20], deep-brain stimulation [22; 23], and in vivo drug delivery via cavitation [24].

An avenue addressing the challenge relies on precision additive manufacturing (AM) processes such as light-based stereolithography (SLA) approaches [25] or two-photon lithography [26] and post-processing (sintering) of the printed part [27]. During the SLA process, piezoelectric nanoparticles are mixed with photosensitive monomers to form composite colloids, which are used for UV curing to construct 3D composite elements in a layer-by-layer manner. The viscosity of the highly particle-loaded composite colloids makes printing a uniform layer difficult, and the light scattering effect [28] of the particles induces broadening of the printed features, making printing precise features challenging. To generate dense piezoceramics, the as-fabricated composites ("green parts") are sintered at high temperature to burn off the polymer matrices and regrow the ceramic grains. While piezoceramics, including sodium potassium niobate (KNN) [29] and barium titanate (BTO) [30], are most commonly used for 3D printing, the printing of lead-based piezoceramics, featuring a high piezoelectric constant and affordability, remains elusive because of the lead evaporation that occurs during the high-temperature sintering process [31], which suppresses the functional performance of the sintered elements. Moreover, the conventional sintering process induces deformation, cracks, and high porosity in the 3D printed elements, resulting in degraded mechanical and piezoelectric properties.

Disclosed herein is an SLA-based AM method with an optimized post-sintering process for printing dense lead zirconate titanate (PZT) elements and packaged transducers with microscale features and a high piezoelectric response. The process starts with high-resolution projection micro-stereolithography (PμSL) combined with a tape-casting recoating process to ensure accurate control of the features of the green parts. A liquid phase sintering method compatible with 3D printed parts was developed and a liquid sealing method to suppress lead evaporation at high temperature, which reduces the porosity and lead loss of 3D printed piezoceramics. The as-fabricated PZT elements reached a piezoelectric strain constant and an

electromechanical coupling factor of up to 583 pC/N, corresponding to 92.5% of that of the pristine material, outperforming currently printable piezoelectric materials.

In addition to active materials, printable packaging material pallets were developed that include a backing layer, an impedance matching layer and physical housing with a large range of tailorable impedances and attenuation coefficients to ensure optimal target performance for targeted applications. To demonstrate the applications of the approach, an intravascular ultrasound (IVUS) transducer was printed with microscale focusing features, which is capable of generating high and localized acoustic pressure in blood vessels with diameters as low as 2 mm, allowing localized cavitation triggering and intravenous drug delivery. The 3D printable microscale features together with the high piezoelectric properties of the printed piezoceramic materials will make a great leap forward toward new applications of 3D transducers.

3D Printing and Processing of Miniaturized Transducers with Near-pristine Piezoelectric Ceramics for Localized Cavitation: The performance of ultrasonic transducers is largely determined by the piezoelectric properties and machining methods, including etching, dicing and hot pressing [10] due to the brittle nature of piezoelectric ceramic [11–14], or limited to 3D printed composite materials containing piezoelectric nanoparticles and polymer matrices [15]. The mechanical stress caused by the machining processes results in grain pullout, reduced strength and depolarization, leading to significant degradation of the piezoelectricity of the manufactured elements [12]. As a result, the piezoelectric materials with these architectures exhibit piezoelectric coefficients much lower than those of their pristine ceramic counterparts and weak emission pressures when used as ultrasonic transducers. Printing piezoceramic transducer elements with precise microscale features, free form factors and high piezoelectric responses capable of acoustic focusing, impedance matching and serving as a backing layer is highly desirable in applications that require small sizes, high emission pressures and localized energy outputs that could open a myriad of new applications, including in situ imaging [16], sonogenetic cellular modulation [17–19], intravascular thrombolysis [20], blood brain barrier disruption [21], neuromodulation [22,23], and enhanced drug delivery via cavitation [24].

An avenue addressing the challenge relies on precision additive manufacturing (AM) processes such as light-based stereolithography (SLA) approaches [25] or two-photon lithography [26] and post-processing (sintering) of the printed part [27]. During the SLA process,

piezoelectric nanoparticles are mixed with photosensitive monomers to form composite colloids, which are used for UV curing to construct 3D composite elements in a layer-by-layer manner. The viscosity of the highly particle-loaded composite colloids makes printing a uniform layer difficult, and the light scattering effect [28] of the particles induces broadening of the printed features, making printing precise features challenging. To generate dense piezoceramics, the as-fabricated composites ("green parts") are sintered at high temperature to burn off the polymer matrices and regrow the ceramic grains. While piezoceramics, including sodium potassium niobate (KNN) [29] and barium titanate (BTO) [30], are most commonly used for 3D printing, the printing of lead-based piezoceramics, featuring a high piezoelectric constant and affordability, remains elusive because of the lead evaporation that occurs during the high-temperature sintering process [31], which suppresses the functional performance of the sintered elements. Moreover, the conventional sintering process induces deformation, cracks, and high porosity in the 3D printed elements, resulting in degraded mechanical and piezoelectric properties.

Disclosed herein is an SLA-based AM approach with an optimized post-sintering process for printing dense lead zirconate titanate (PZT) elements and packaged transducers with microscale features and a high piezoelectric response. The process starts with high-resolution projection micro-stereolithography (PμSL) combined with a tape-casting recoating process to ensure accurate control of the features of the green parts. Inspired by the liquid phase sintering (LPS) [5], which implements liquid phase of sintering additives during sintering to promote grain growth and improve the sintering behavior of ceramics, a liquid phase sintering method was incorporated compatible with SLA-based 3D printed PZT samples. Further, a liquid sealing method [32] was developed to suppress lead evaporation at high temperature, which reduces the porosity and lead loss of sintered elements. The as-fabricated PZT elements reached a piezoelectric charge constant and an electromechanical coupling factor of up to 583 pC/N, corresponding to 92.5% of that of the pristine material, outperforming currently printable piezoelectric materials.

In addition to active materials, printable packaging material pallets were developed that include a backing layer, an impedance matching layer and physical housing with a large range of tailorable impedances and attenuation coefficients to ensure optimal target performance for targeted applications. To demonstrate the applications of the approach, a

miniaturized ultrasound transducer was printed with microscale focusing features, which is capable of generating high and localized acoustic pressure in blood vessels with diameters as low as 2 mm, allowing localized cavitation triggering, enhanced drug delivery, and ultrasonic modulation of cellular activity. The 3D printable microscale features together with the high piezoelectric properties of the printed piezoceramic materials will make a great leap forward toward new applications of 3D printed transducers.

3D printing of a highly loaded PZT composite and liquid phase sintering: The free-form fabrication achievable with 3D printing technology allows one to exploit acoustic pressure and focusing capabilities with ranges and resolutions that are not feasible with conventional piezoelectric transducers comprising flat piezoelectric elements. The miniatured ultrasound transducer is widely used for blood vessel disease diagnosis and treatment. However, currently existing miniatured ultrasound transducers have limited focusing or acoustic energy emitting capability [33–36] due to the inability to fabricate high-resolution focusing features. Herein, the generated acoustic beam of the ultrasound transducers was manipulated by tuning the PZT element curvature. This curved shape leverages the ability to focus emitted acoustic energy along one line to improve the element sensitivity and acoustic beam resolution, as shown in Fig. 6A.

The disclosed fabrication method starts with UV-sensitive piezoelectric preparation. In one example, the highly particle-loaded slurry comprises 15~45 vol% PZT nanoparticles (APC 855), 5~15 vol% liquid phase sintering (LPS) agent, lead nitrate (PbNO3) and a UV-sensitive resin made from a mixture of monomers (polyethylene glycol diacrylate, PEGDA) and a photoinitiator, as shown in Fig. 6B. Compared to other PZT nanoparticles, APC 855 features a high piezoelectric charge constant (630 pC/N), which ensures the high performance of the printed part. LPS has been widely used in piezo ceramic fabrication [37,38] and has been implemented in powder-based 3D printing techniques of piezoelectric materials [39]. However, incorporating LPS for light-based additive manufacturing is challenging as most sintering additives (lead oxide [38] and CdBiB [40]) introduce additional light absorbance and increases viscosity, thus decrease the slurry printability. In this study, lead nitrate was used as the LPS agent due to its low UV light absorption, ensuring the high printability of the slurry. High PZT loading in the slurry could improve the piezoelectric properties but limited the printability.

Here, the combination of 35 vol% PZT and 5 vol% lead nitrates was chosen, which was experimentally optimized to guarantee the printability and piezoelectrical properties.

As illustrated in Fig. 5B and Fig. 5C, the slurry was fed to the resin tray of a custom-made PμSL system for 3D printing. A printing window (2 mm) made of polydimethylsiloxane (PDMS) was utilized during the process of separating the printed part and the printing window, which prevents small features from being damaged. The oxygen permeability of the PDMS window leads to an oxygen inhibition layer between the printing window and resin that increases the distance between the printed part and printing window and reduces the suction force [41]. In addition, compared to other printing windows, including fluorinated ethylene propylene (FEP) film [42], acrylic board [43] and glass window [44], the high compliance of the PDMS window results in a slower separation process and protects the high precision features of the printed parts.

The as-printed piezocomposites were then sintered to grow the PZT grain size and form the dense PZT ceramic with designed geometries. First, the printed sample was debonded using a two-step debonding process (Fig. 11) to remove the supportive polymer, as shown in Fig. 6D. The two-step debonding process reduced the deformation of the printed elements compared to the currently existing direct debonding process, allowing fabrication of small-scale features. During the debonding process, lead nitrate within the elements decomposes into lead oxide at around 470 °C. After debonding, extra PZT powders were placed on the bottom of an alumina crucible, and the printed element was placed on top of the powder bed. A smaller crucible was used to cover the element and pushed down into the powder bed. The temperature was then increased to 1100 °C in 1.5 hours and held for 3 hours to grow the PZT grains and form a dense ceramic (see Fig. 12A and Fig. 12B). LPS started at an elevated temperature. Lead oxide melted at 888 °C and contracted the PZT particles via surface tension, densifying the PZT architecture, as shown in Fig. 6E. The lead oxide inside the element also serves as a lead source during sintering to prevent lead loss [45]. The liquid sealing method was implemented by placing lead oxide along the edge of the small crucible (see Fig. 6F) to further reduce the lead loss at high temperatures. During the sintering process, lead oxide melted, sealed the crucible, and created a lead-rich environment to avoid lead loss during the high-temperature sintering. Then, the samples were cooled down to room temperature at a rate of 10 °C/min. The sintered PZT material kept perovskite structure after high-temperature heat-treatment (see Fig. 12C).

The sintering was followed by a polarization process to align the dipoles within the sintered PZT element and activate the piezoelectric effect (see Fig. 13A and Fig. 13B). The polarization was conducted in an isolation liquid (silicone oil) to prevent the breakdown in air with a polarization electric field higher than 3 V/μm. Based on the Curie temperature and breakdown electric field (6.5 V/μm) of the sintered PZT elements, the temperature and electric field profile of the polarization process was optimized (see Fig. 13C). After reaching the peak value, the electric field was maintained during the cooling process of the isolation liquid to prevent depolarization of the printed element.

The optimized sintering procedure ensured the formation of a dense ceramic with low porosity and well-maintained lead content, leading to high piezoelectric charge constant and coupling factor. The acoustic pressure generated by the fabricated 9.75-MHz transducer can be effectively increased by using the curvature design of the elements (Fig. 6G). Notably, the acoustic pressure is tunable according to the change in the element curvature degree and can exceed some medical thresholds [46–50] at 9.75 MHz, enlarging the range of applications of the fabricated device.

Piezoelectric performance of the as-fabricated piezoelectric elements: The technique allows the fabrication of high-performance piezoelectric transducers with complex 3D geometries that are not achievable by any conventional fabrication methods for piezoceramics, including hot-pressing, molding, sanding, and dicing. These complex shapes allow for potential custom transducer applications. Fig. 7A shows curved elements with designed curvatures for potential miniatured transducer applications. Other examples include hemisphere elements (see Fig. 7B) for medical imaging and nondestructive testing, cylindrical transducer elements with multiple concentric annular layers filled with a polymer (see Fig. 7C) for reducing the traverse vibration and enhancing the thickness vibration, helical elements (see Fig. 7D) for generating acoustic beams with vortex motion for ultrasound manipulation [9], and architected piezo sensors (see Fig. 7E, Fig. 7F) for underwater sensing.

To quantify the deformation induced during the sintering process, the linear shrinkage and curvature change of the element after sintering was measured. The results showed an average linear shrinkage as high as 27.73 % and a curvature change within 0.5 % (see Fig. 14A through Fig. 14I). Fig. 7G shows the SEM image comparison of an element between the conventional sintering method and the optimized sintering method, confirming the low porosity

of the as-fabricated elements. The density of the sintered elements was measured on a set of PZT disks (diameter 5 mm, thickness 390 μm, n = 5). The density of the sintered elements reached 7.2g/cm$^3$, which is 94.7% of the pristine material (APC 855). The porosity of the elements, 5.3%, is calculated from the density of the printed samples. The sound speed within both the 3D printed element and its pristine material counterpart were measured within multiple PZT plates with the same cross section area (5 x 5 mm) and different thicknesses to verify the low porosity of samples with different volumes. The sound traveling time in each element was captured to calculate the sound speed (Fig. 15). As shown in Fig. 7H, the sound speed in the 3D printed samples reaches approximately 93.2% of the speed in the pristine material, which is consistent with the density measurements.

The piezoelectric properties (hysteresis loops, piezoelectric charge constant, $k_t$) of the as-fabricated PZT elements were measured to compare with the pristine materials. Fig. 7H plots the hysteresis of the polarization of the PZT element measured by precision multiferroic analyzer (Radiant Technology. Inc, USA), showing a remnant polarization ($P_r$) as high as 32.4μC/cm$^2$. The strain-electric field loops of the 3D printed and the pristine elements were captured (see Fig. 16A and Fig. 16B), showing that the 3D printed sample can generate near-pristine strain under the same electric field. The piezoelectric charge constant, $d_{33}$, was measured using a $d_{33}$ meter (YE2730A, APC Piezo, USA) and reached 583 pC/N, 92.5% of the value of the pristine material. The electromechanical coupling factor in the thickness direction, $k_t$, was measured as 0.57 (see Fig. 19). Fig. 7J compares the $d_{33}$ and $k_t$ of the 3D printed PZT with those of the state-of-the-art 3D printed piezoceramics [11, 51–55].

Packaging: The acoustic signal resolution and energy output of ultrasonic transducers highly depend on the packaging due to the mismatch of acoustic properties of the ceramic transducer element and transmission medium. To achieve optimal resolution and acoustic energy output, the acoustic properties of the matching layer and backing layer of the transducer package need to be optimized for target applications. In addition, the microscale features and complex shapes of a 3D printed transducer require conformal packaging to ensure tight contact with and encapsulation with the transducer element. Herein, 3D printable composite material pallets were developed with acoustic impedance ranging from 3 Mrayl to 6.7 Mrayl and attenuation coefficient ranging from -4.3 dB/mm to -10 dB/mm, as shown in Fig. 8A. The acoustic properties of the materials can be tuned by changing the ratio of the resin composites.

The matching layer composite, featuring low attenuation coefficient and a large range of acoustic impedances, was used as the matching layer, while a backing layer composite, featuring a large range of attenuation coefficients, was used as the backing layer. The large tunable range of impedances and attenuation coefficients allows us to fabricate transducers with optimal performances for targeted applications. To maximize the acoustic wave transmissivity and output pressure, the acoustic impedance ($Z_m$) of a single matching layer should follow the rule [56]:

$$Z_m = (ZZ_1^2)^{1/3}$$

**Equation 1**

Where Z and $Z_1$ are the piezo element acoustic impedance and medium acoustic impedance, respectively. Fig. 8A demonstrates the optimal matching layer composition when the transducer is used in different tissues, including blood, muscle, fat, and bone. The selection of the backing layer depends on the applications. For acoustic imaging, as an example, the backing layer requires high attenuation to prevent the ringing effect [57]. For high acoustic pressure output, a large impedance mismatch between the backing layer and the transducer is required to maximize the bounce-back pressure [6]. Moreover, during in vivo operation, the encapsulation material of the transducer is directly in contact with the tissue and requires biocompatibility. A biocompatible material was used, trimethylolpropane triacrylate (TMPTA), as the encapsulation material to minimize the damage to the tissues. The energy output performance variation of the representative packaged transducers along with their geometries are discussed herein and in Fig. 18A through Fig. 18D.

3D printed focused ultrasonic transducers: The effect of transducer shape factors was then explored, including curvature and arc length, and the driving voltage on the acoustic pressure of the transducer. As shown in Fig. 8B, piezo element curvatures ranging from 0 deg to 180 deg and arc lengths ranging from 1 mm to 6 mm, which fit a typical portal vein inner diameter (6 – 12 mm) [58], were simulated in COMSOL Multiphysics for different voltage inputs. The width of the simulated elements was 2.5 mm to ensure steerability of the transducer inside a blood vessel. The bold curves with a curvature equal to zero denote the flat piezoelectric transducers with limited acoustic pressure outputs, while the surface plots denote the output pressure range enabled by the 3D printed curved elements. The focusing feature enabled the transducer to minimize its focal zone by 78.6 %, as shown in the subfigure in Fig. 8B. The

results show that the miniaturized ultrasound transducer with 3D printed focusing features reaches higher pressure and lateral resolution than the reported ultrasound transducers (see Fig. 17A through Fig. 17F). Remarkably, the 3D printed focusing elements reach the FDA defined pressure limit [50] and many other medical threshold [46–49] at 9.75 MHz. The highly localized acoustic pressure may open the door for applications for targeted ultrasonic therapy, such as non-contact cellular modulation, localized drug delivery, and transient blood brain barrier opening in small areas with length scales under 2 mm.

The acoustic pressures were then experimentally verified with an element with a curvature of 120 deg and an arch length of 2.3 mm. The schematic (Fig. 8C) of the miniaturized ultrasound transducer shows the package component assembly used for experimental verification. To maximize the pressure output in blood, using the chart in Fig. 8A, the optimal matching layer (CF (28wt%) – matching layer composite) and backing layer (Fe (3wt%) – backing layer composite) were chosen. Fig. 8D shows an optical image of the 3D printed miniaturized ultrasound transducer. Two copper cables (300 mm length, 0.5 mm diameter) were used to connect the device electrodes with the power supply and allow the transducer to be placed in veins. The as-fabricated piezo element was designed with a resonant frequency of 9.75 MHz, which is ideally suited for high resolution focusing and high output pressure in the usual range of the medical ultrasound for procedure guidance [59, 60]. 9.75-MHz burst waves were used to drive the miniaturized ultrasound transducer. The output pressures of the transducer with different voltage inputs were captured by a commercial hydrophone (HGL-0400, OND) in DI water and are plotted in Fig. 8B (with "X" shaped dots), which well match the simulated results.

Underwater cavitation generated by the as-fabricated transducer: The highly localized acoustic output of the 3D printed transducer allows us to exploit its applications for localized cavitation. Cavitation refers to the process in which vapor- or gas-filled cavities formation and undergo oscillation or growth and implosion in liquids upon exposure to acoustic radiation [61]. It can generally be classified into two types: stable cavitation and inertial cavitation. Stable cavitation [62] is identified by sustained small amplitude oscillations of the cavities at about their equilibrium, which induces microstreaming in the liquid. Inertial cavitation is characterized by the process of cavities growth and collapse, which induces microjets, causing pitting on solid surface [61]. In biomedical applications, inertial cavitation disrupts the structure of the carrier vesicle and triggers the release of drugs; the induced microstreaming and microjet

also makes cell membranes and capillaries more permeable for drug transportation from the blood, making the cavitation a powerful tool for localized endogenous drug delivery. However, triggering cavitation usually requires high acoustic pressure. The cavitation and the triggering ultrasound can cause collateral damage, including tissue burning, hemolysis and blood temperature increase [61–64]. Additionally, the treatment of diseases such as cancer, degenerative and inflammatory diseases, or thromboembolic diseases requires a high concentration of certain drugs to be delivered that have toxic side effects on other tissues [24]. Precise control and localize cavitation at target tissue sites is desired to minimize those side effects. Using microbubble as the cavities can effectively induce the cavitation, making it more controllable [20]. But the localized cavitation induced by the microbubble oscillation or fragmentation requires precise delivery of acoustic pressure in a controlled manner within a confined volume as small as hundreds of microns, which cannot be achieved by conventional miniatured ultrasonic elements without focusing features.

Inspired by this challenge, it was demonstrated that the 3D printed high-pressure miniaturized ultrasound transducer with focusing features to precisely burst microbubbles and generate cavitation. The piezo element has a curvature of 120 deg and an arch length of 2.3 mm, yielding a focal depth of 0.9 mm. The center frequency of the fabricated transducer is 9.75 MHz, as shown in the pulse-echo signal frequency spectrum (see Fig. 20).

To verify the cavitation generated by the 3D printed transducer, 25 mg microbubbles (Lumason, BRACCO, USA) were diluted in a 5 ml 0.9% sodium chloride injection and burst by the 3D printed transducer driving by 9.75-MHz burst waves with 50 cycles. The input voltage of the transducer was adjusted from 15 $V_{pp}$ to 180 $V_{pp}$ and captured the ultrasound signal with a cavitation detector (Sonic Concepts Inc., Bothell, WA, USA) in a large water tank (free field), as shown in Fig. 9A and Fig. 9B. The captured signals were transformed (Fast Fourier Transform) into frequency spectrums to verify cavitation (Fig. 9C, Fig. 9D, and Fig. 9E). As shown in Fig. 9C, with a 40 $V_{pp}$ excitation, the spectrum clearly shows the sub-harmonic of the fundamental frequency (9.75 MHz), which is an indication of the stable cavitation generation [65]. As the input voltage increases, both broadband noise and sub-harmonic were captured (see Fig. 9D), indicating that stable cavitation and inertial cavitation [66] were activated by the transducer simultaneously. With a higher voltage, the sub-harmonic disappeared while and the

broadband noise increased by 40 dB (see Fig. 9E) compared to that of 15 $V_{pp}$ excitation, showing the microbubbles were undergoing stronger inertial cavitation [67].

The process of microbubble fragmentation was captured by an inverted microscope (IX71, Olympus America Inc., Center Valley, PA, USA). As shown in Fig. 9F, Fig. 24A and Fig. 24B, the microbubbles fragmented and collapsed in the focal area when the transducer was excited by 9.75 MHz 180 $V_{pp}$ pulses. The microbubble behavior during insonation was captured when transducer was driving by 50 $V_{pp}$ pulses with 50 cycles (Fig. 9G through Fig. 9J, Fig. 24A and Fig. 24B). The microbubbles experienced oscillation, growth, and collapse, indicating both stable cavitation and inertial cavitation can be generated by the 3D printed transducer [62]. The microbubble-induced cavitation shows the capability of the miniatured transducer to assist the drug delivery and diffusion (Cavitation-assisted dye diffusion is shown in Fig. 21, Fig. 22, Fig. 25A, Fig. 25B, and Fig. 25C).

Localized cavitation: To demonstrate the potential of the transducer for precision transvascular drug delivery via low sound pressure cavitation, a 3D printed transparent blood vessel phantom was prepared with multiple internal channels to mimic the in vivo physical environment and inject the transducer and microbubbles inside it. As shown in Fig. 10A, the transducer was focused on the marked "lesion" location. During this time the microbubble suspension (5 mg/ml) was injected into the blood vessel phantom (see Fig. 10B). Next, pulses were applied to the transducer to generate acoustic pressure. A transparent region appearing in the focal area (see Fig. 10B, Fig. 26A and Fig. 26B) was caused by microbubble fragmentation and acoustic radiation force. Fig. 10D plots the bubble content as a function of time captured by digital image correlation (see Fig. 23), showing that the bubbles were fragmented within 0.15 s and 0.08 s for 50 $V_{pp}$ and 90 $V_{pp}$ driving voltages. With a driving voltage lower than the cavitation threshold, no microbubble fragmentation was observed. To demonstrate the high precision focusing, bubbles were deposited on the internal wall of the vessel phantom (Fig. 10E) and used the transducer to fragment the bubbles. As shown in Fig. 10E through Fig. 10H, Fig. 27A, and Fig. 27B, as the transducer moved, only the bubbles within the focal area (0.2 $mm^2$) were fragmented, showing high-precision cavitation.

In summary, via a combination of high-resolution piezoceramic matrix printing and a liquid agent-assisted sintering approach, a 3D printed micro-structured transducer was demonstrated with near-pristine piezoelectricity, which enabled the delivery of ultrasound to

focal areas confined within areas on the order of sub-$mm^2$ and achieved target cavitation and cavitation-enabled drug delivery. Liquid phase sintering and sealing reduced the PZT lead loss, sample porosity, and the deformation. The piezoelectric properties of the materials such as the $d_{33}$ and $k_t$ outperformed those of existing 3D printed piezoceramics. The effect of micro-structures and curvatures enabled by the printing approach was studied on the focusing resolution and power output and optimized the spatial resolution and acoustic pressure of the output acoustic beam. Additionally, the 3D printed packaging components with tunable acoustic properties adapt the PZT elements to different transmission media and applications, diversifying the versatility of the fabricated ultrasound transducers in medical treatments.

The reported processing approach achieves the high energy output application of an ultrasound transducer driven by a 3D printed piezo element. Optimization of the microstructural effect, along with tunable matching and backing layer properties, enables high acoustic pressure confined within sub-$mm^2$. Beyond the drug delivery, the localized acoustic energy output could enable future applications including intravascular thrombolysis, in situ imaging, neuromodulation, sonogentic control, and oncology applications.

Fabrication of the 3D piezoelectric nanocomposites: The fabrication process started with the preparation of the UV sensitive piezocomposite colloid comprising PZT 855 (APC Piezo, USA) particles, lead nitrate (MilliporeSigma, USA) and the UV sensitive resin. The UV sensitive resin was comprised of 1 wt% to 3 wt% photoinitiator Irg819 (MilliporeSigma, USA) and PEGDA (MilliporeSigma, USA). 15 vol% to 45 vol% of PZT, 5 vol% to 15 vol% lead nitrate was ball milled together with the UV sensitive resin to form the colloid. These materials were subsequently used for printing on a high-resolution projection micro-stereolithography system integrated with the tape casting method [8]. The designed 3D structure was created in Autodesk Inventor (Autodesk, inc. USA), and then sliced into 2D images with Netfabb (Autodesk, inc. USA) for the printing process. During the printing, the colloid was coated on the printing window with one layer thickness by controlling the height of the casting blade [8]. One slice of the printing model was projected by the UV projector (light power intensity: 14.8 $mW/cm^2$) onto the printing window and used to solidify one layer of the colloid. The solidified layer was attached to the building platform, or the previous layer and the printing stage was lifted from the printing window, preparing for the coating and curing process of the next layer. The piezoelectric composite with designed 3D geometry was fabricated by repetition of the coating

and UV curing processes. The printing resolutions in x-y plane and along z-axis were 20 μm and 15 μm, respectively.

Debonding and sintering: The two-step debonding process is shown in Fig. 11A. The debonding temperature profile is shown in Fig. 11B. Firstly, the printed sample was heated under an argon environment. The temperature was increased from 0 °C to 600 °C at a rate of 1 °C/min in 10 hours, and held at 600 °C for three hours, during which the supportive polymer (PEGDA) was carbonized and utilized to maintain the shape of the PZT composite structure. Then, the carbonized polymer was burnt out in the air at 600 °C for 3 hours. The two-step debonding process reduced the deformation of the printed elements compared to the direct debonding process [54], allowing the fabrication of small-scale features.

After debonding, the temperature increased to 1100 °C for grain growth and dense ceramic formation. The peak sintering temperature was optimized according to the $d_{33}$ testing results and sample breakdown electric field. With a peak sintering temperature higher than 1100 °C, the $d_{33}$ dropped due to lead loss caused by high temperature (see Fig. 12A). When the peak sintering temperature was lower than 1100 °C, the sample would have a low density, resulting in a low breakdown electric field (see Fig. 12A).

Polarization: The polarization process was conducted in silicone oil to avoid electric breakdown when the polarization field is over 3 V/μm, which is the breakdown field of the air. Both surfaces of the sample were covered by silver electrode plates wired to the high voltage supply, as shown in Fig. 11A. The piezoelectric sample was polarized under 6.5 V/μm electric field, resulting in dipole alignment in the direction of the applied field (see Fig. 13B). A combination of an electric field profile and a temperature profile was used to polarize the as-fabricated piezoelectric nanocomposite, as shown in Fig. 13C.

Hysteresis loops measurement: The P-E loop was measured by Precision Multiferroic Analyzer from Radiant technology. Oil drops were applied to the sample to prevent electric breakdown. The S-E loop measurement was performed by Thin Film Piezoelectric Test Bundles (Radiant technologies, Inc, USA). The testing bundle comprises a precision materials analyzer (Precision Multiferroic II, Radiation technologies, Inc) and a laser vibrometer (VibroOne, Polytec, Inc. USA) (Fig. 16). The tested samples had the same dimensions (2.5 x 2 x 0.25 mm). In S-E loop testing, the samples were polarized under 6.5 V/μm electric fields using the same poling method described in the manuscript.

Electromechanical coupling factor: The electromechanical coupling factor $k_t$ was calculated using resonance frequency $f_r$ and anti-resonance frequency $f_a$ [68] via:

$$k_t = \sqrt{\frac{\pi f_r}{2f_a} \times cot\frac{\pi f_r}{2f_a}}$$

**Equation 2**

$f_r$ and $f_a$ were extracted from the impedance curve measured using an E4991B impedance analyzer (Keysight Technology, USA). The spectrum of impedance of the as-fabricated elements (2.1×1.9×0.15 mm) is shown in Fig. 19. The resonant frequency and anti-resonant frequency were 8.27 MHz and 9.77 MHz, respectively, leading to an electromechanical coupling factor of 57.2%.

Equivalent medical threshold calculation: The equivalent thresholds at the working frequency of the transducer in this study was calculated using M.I. value [50] via:

$$M.I. = \frac{p_{negative}}{\sqrt{f}}$$

**Equation 3**

where $p_{negative}$ is the peak negative pressure and $f$ is the ultrasound wave frequency.

Ultrasound setup: A function generator (*SDG1025, SIGLENT, China*) was connected to a radio frequency power amplifier (100A250A, Amplifier Research, USA) to drive the transducer. 9.75-MHz burst waves with 50 cycles (20 ms burst period) were input into the transducer. For localized cavitation experiments in blood vessel phantom, the 9.75-MHz burst waves were set up to have 10% duty cycle.

Miniaturized ultrasound transducer pulse-echo signal: The pulse-echo profile of the as-fabricated transducer with optimized packaging is shown in the Fig. 20. JSR pulser receiver (DPR300, JSR Ultrasonics, USA) was used to drive the transducer and receive the echo signal. The frequency spectrum indicates that the transducer has the largest output at frequency is 9.75 MHz. The -6 dB bandwidth of the signal is 57%, which is also suitable for imaging application [69].

3D printable packaging material: The 3D printable composite material pallets contain two resin composite systems for matching and backing layer of a transducer. The loaded

fiber/particle were sonicated and uniformly mixed with the UV curable resin using ball mill. The acoustic properties (acoustic impedance, attenuation coefficient) of the cured composite can be tuned by adjusting the loading of fibers in the composites. The 3D printable composite materials were printed using the same custom PμSL fabrication system as the PZT fabrication.

Acoustic Simulation: The acoustic simulations were conducted using COMSOL Multiphysics 6.0. The transmission medium was set to water. The boundaries of simulation models were set to perfect matching layer to avoid reflection. The materials' properties (piezoelectric properties, acoustic impedance and sound speed) in the model were using the tested properties of the samples.

Dye diffusion coefficient and microbubble concentration: The dye diffusion coefficient and concentration of microbubble in the container were calculated by a self-developed digital image correlation method based on the transparency of the solution. The screenshots of the target location were converted into gray scale image using MATLAB (MathWorks, USA). The mean pixel values of images were used for computing the dye diffusion speed and microbubble concentration change (see Fig. 21, Fig. 22 and Fig. 23).

Fabrication resolution of the 3D piezoelectric nanocomposites: During the curing process, the resolution of the custom PμSL fabrication system in x-y plane (20x20 μm) is determined by the pixel size of the projector. The resolution along z-axis is determined by the curing depth of colloid. The curing depth of the solid layer is given as [70]:

$$Z_{ct} = \frac{1}{\alpha}\ln(\frac{E}{E_c})$$

**Equation 4**

where, $\alpha$ is the resin absorption coefficient, $E$ and $E_c$ are the actual and critical exposure, respectively. In the disclosed fabrication process, the layer thickness was set as 15 μm, which is smaller than half of the cure depth to ensure tight bonding between two consecutive layer [71]. This optimized cure depth for each layer was modulated by tuning the exposure time [72]. A reductive lens was utilized to increase the fabrication resolution of the printed structure [72]. The range of achievable 3-3 vibration mode frequency of a 3D printed thin-film sample is determined by the range of thickness that can be achieved, which is around 10.8 μm. This corresponds to the highest achievable frequency on the order of 171 MHz. Higher frequency can

be potentially achieved by reducing the minimal layer thickness of the printing apparatus (employing Z-stage with higher resolution).

Element shrinkage during sintering and its effects on the structural integrity: To evaluate the effects of shrinkage on structural integrity, three types of geometrical parameters were measured before and after sintering, including length change (characterized on flat samples), curvature deviation (measured on concave samples) and strut thickness deviations. Here, 20 rectangular samples (3 x 2.6 x 0.2 mm) were fabricated and the dimension change before and after sintering was measured, as shown in Fig. 14A through Fig. 14B. Fig. 14C shows the deviation distribution of the average linear shrinkage ratio with an average value of 27.73 % and a standard variation of 1.9 %, [50] indicating a uniform shrinkage ratio among samples. Fig. 14D and Fig. 14E show the representative sample before and after sintering. The average curvature change is within 0.5° (0.51 % of the original curvature) with a standard deviation of 2.2° (see Fig. 14E and Fig. 14F). The resultant acoustic pressure change is within 0.04 Mpa based on Fig. 8D, which was negligible in the experiments. Furthermore, the strut thickness uniformity in 3D architectures was evaluated. X-ray computed tomography was used (CT, Bruker microCT, Model Skyscan 1174) to capture the morphology of a sintered lattice sample containing 84 struts. Fig. 14I shows the deviation distribution of the strut thicknesses. The thickness of the sintered struts is less than 1.58% thicker than the as-designed value (300 μm) with a standard deviation of 6.6 μm, indicating that the structural integrity was well kept after sintering.

Acoustic properties of as-fabricated material: Measurement of acoustic impedance: The schematic of the setup that was used to measure sound speeds is shown in Fig. 15A. The sound speed in the material $Vmaterial$ is calculated using the phase change $\Delta\phi$ of the received signal after inserting the material in between the two standard transducers (see Fig. 15C) via:

$$V_{material} = \frac{tV_{water}}{t - \Delta\phi V_{water}}$$

**Equation 5**

where, t indicates the thickness of the material to be tested, $V_{water}$ is the sound speed in water. The acoustic impedance is calculated by [73]:

$$Z = \rho V_{material}$$

**Equation 6**

where, $\rho$ is the density of the material.

Measurement of attenuation coefficients: The transmission ratio, $t_p$, between the transmitted wave acoustic pressure and the incident wave acoustic pressure on the interface [74] can be represented by:

$$t_p = \frac{2Z_2}{Z_1 + Z_2}$$

**Equation 7**

where the $Z_1$ and $Z_2$ indicates the acoustic impedance of the two materials. Thus, the acoustic pressure $p$ in the material near the interface I and interface II (see Fig. 15B) are represented using the transmission ratio $t_{p12}$ at interface I and $t_{p34}$ at interface II via:

$$p_2 = t_{p12} p_1$$

**Equation 8**

$$p_2 = t_{p34} p_4$$

**Equation 9**

Since the acoustic pressure $p$ has a linear relationship with the voltage $V$ generated by the transducer for measuring, the acoustic pressure ratio between top and bottom side within material can be represented using the voltage amplitude V by:

$$\frac{p_3}{p_2} = \frac{(z_1 + z_2)^2 V_4}{4 Z_1 Z_2 V_1}$$

**Equation 10**

where, $Z_1$and $Z_2$ are the acoustic impedance of the medium (water) and the material to be tested. $V_1$ and $V_4$ are the measured voltage generated by ultrasound transducer placed at the top and bottom side of the material. For a given frequency, converting the unit of Equation 10 into (dB/mm) can yield the attenuation coefficient of the material via:

$$\alpha = \frac{\frac{20}{d}\log(z_1 + z_2)^2 V_4}{4Z_1 Z_2 V_1}$$

**Equation 11**

where, d is the thickness of the material.

Strain – electric field curves of the as-fabricated material: For the S-E loop, the strain in the thickness direction was measured (3-3 mode) of the 3D printed material and a standard commercial material against the applied electric fields (S-E curves) using Thin Film Piezoelectric Test Bundles (Radiant technologies, Inc, USA) at room temperature (21.3 °C), as shown in Fig. 16A. The system comprises a precision materials analyzer (Precision Multiferroic II, Radiation Technologies, Inc) and a laser vibrometer (VibroOne, Polytec, Inc. USA). The precision materials analyzer applied voltage long the polarization direction (thickness direction) of the sample and the displacements of the samples were collected by the laser vibrometer and sent back to material analyzer for processing. The tested samples had the same dimensions (2.5 x 2 x 0.25 mm). The S-E loops of the 3D printed sample and commercial sample are plotted and compared in Fig. 16B, showing that the 3D printed sample can generate near-pristine strain under the same electric field.

3D printable packaging material: The matching material was formed by mixing carbon fiber (CF) with RIGID resin (Formlab, USA). RIGID resin is the mixture of urethane dimethacrylate and isobornyl Methacrylate. The acoustic impedance of the matching material reached the values from 3 Mrayl to 6.7 Mrayl by tuning the matching layer's CF loading from 25 wt% to 45 wt%. The CF could increase the composite density and sound speed with a little increment of attenuation coefficient [75]. The thickness of the fabricated matching layer was designed as the one-quarter of the wavelengths of the transmitted ultrasound to reduce the acoustic loss [76].

The backing material is the Fe magnetic particle-loaded Flexible resin (Formlab, USA). Flexible is the mixture of acrylated oligomers and acrylated monomers. By tuning the Fe magnetic particle loading in the backing layer from 3 wt% to 20 wt%, the attenuation coefficient of the backing materials can range from -4.3 dB/mm to -10 dB/mm for 10-MHz sound waves damping. The Fe magnetic particle loading can increase sound dissipation by increase the thermal loss caused by the friction of particles [77]. The acoustic impedance of the backing

material ranged from 2.6 Mrayl to 8 Mrayl, making it suitable for many transducer applications mentioned in the main text.

The design, material selection, and assembly of the matching layers depend on the intended applications and the function of the transducers. Using the transducers with 3-3 working modes as an example, which is also a commonly used ultrasonic transducer type for imaging and nondestructive testing, the matching layer is designed based on the shape of the aperture of the transducer. The material selection is determined by the sound propagation medium, as discussed in this disclosure. The thickness of matching layer was controlled to be less than one-fourth of the ultrasound wavelength to minimize the acoustic attenuation [78]. For the focused miniatured transducer, the matching layer was 3D printed to fit the size of the sintered piezo element and glue the matching layer with the piezo part using the same photocurable material used for the matching layer. For the transducer with microarchitectures, such as the lattice transducers, the matching layer was designed as flat membranes and glue it onto the surface that receives sound wave.

Benchmark the energy output capability and sound beam lateral resolution of the disclosed 3D-printed transducer with the state-of-the-art: The 3D-printed transducer was benchmarked with reported micro transducers in Table 1. Normalized $prms$ is defined as the negative acoustic pressure generated by the element per unit voltage input per surface area and used to describe the energy output capability. For the studies that use acoustic intensity to characterize the performance of the transducers, the spatial-peak-pulse-average intensity $I_{sppa}$ was converted into the root-mean-square acoustic pressure $prms$ via [79]:

$$p_{rms} = \sqrt{I_{sppa}\rho_0 c}$$

**Equation 12**

where $\rho_0$ is the density of sound propagation medium and $c$ is the sound velocity in the medium. As shown in the table below, our transducer has the highest values (3.48 Mpa ($p_{rms}$ = 2.46 Mpa) at 150 $V_{pp}$) for the normalized $p_{rms}$ compared with other miniatured transducers.

**Table 1:** Transducer energy output capability comparison

| Element geometry | Input signal | Working frequency (MHz) | Surface area ($mm^2$) | Normalized $p_{rms}$ (kPa/V x $mm^2$) |
|---|---|---|---|---|
| Stacked plates [80] | Sin wave, 10% duty cycle | 0.62 | 1.5 x 1.5 | 3.11 |
| Plate [81] | Sin wave, 4% duty cycle | 8.5 | 2 x 1.5 | 0.73 |
| Stacked plates [82] | Sin wave, 10% duty cycle | 1.92 | 2 x 2 | 2.83 |
| Disk [83] | Sin wave, 10% duty cycle | 5.3 | 16 x π | 0.28 |
| Curved plate [84] | Sine wave, 2% duty cycle | 11 | 2.5 x 7.5 | 0.18 |
| Curved plate (This work) | Sin wave, 10% duty cycle | 9.75 | 2.5 x 2 | 3.28 |

The lateral resolution of ultrasonic transducers is determined by the geometries and driving frequencies of piezo elements [85]. The acoustic intensity field of the transducer was simulated with COMSOL by inputting transducer aperture geometry and working frequency (see Fig. 17A) and verified the result with experiments (see Fig. 17C). The hydrophone (HGL-0200, ONDA, USA) was controlled by motors to capture the sound signal of the transducer, as shown in Fig. 17B. The resolution is defined by the -6 dB threshold of the acoustic intensity field. The simulated and measured resolutions of our transducer are 0.08 mm and 0.18 mm, respectively. Compared with the simulated results of the reported transducers (Fig. 17D, Fig. 17E and Fig. 17F), our transducer has the highest lateral resolution owing to its focusing feature and high working frequency.

Energy output performance variations of the ultrasound transducers along with the shapes: To demonstrate the performance of the elements with complex geometries, disk elements (Fig. 18B) and elements with concentric annular layers (Fig. 18C) were fabricated and packaged them with the same procedure and material as the curved elements (matching layer (CF (28wt%) – matching layer composite) and backing layer (Fe (3wt%) – backing layer composite). The element with concentric annular layers was filled with epoxy, which can suppress the transverse vibration of the elements [86]. The acoustic pressure was measured using standard hydrophone

(HGL-0400, ONDA, USA) by placing it at the focal area [87] of the transducers, as shown in Fig. 18A. The negative acoustic pressure of the as-fabricated transducers is plotted in Fig. 18D. The disk element can generate the negative acoustic pressure of 0.86 MPa under the voltage of 150 $V_{pp}$, while the negative acoustic pressure produced by element with concentric layers can be up to 0.99 Mpa. Finite element analysis (COMSOL, USA) was used to show the generated acoustic field of the transducers (Fig. 18E and Fig. 18F).

Dye diffusion coefficient and microbubble concentration: The transducer achieves cavitation assisted diffusion of molecules. Here, the efficiency was tested in the diffusion of methylene blue, a salt used as a dye and as a medication in aqueous solutions. The experiment was prepared by gently dropping methylene blue into aqueous solution and measuring its diffusion coefficient [19] with and without the assistance of microbubble cavitation at 90 $V_{pp}$ (Fig. 25A, Fig. 25B, and Fig. 25C). The container was divided into six sections. The change of their pixel value standard deviation was used to evaluate the diffusion uniformity (Fig. 21). The ultrasound radiation force-assisted diffusion and cavitation-assisted diffusion can be calculated based on the methylene blue diffusion coefficient in the water [88].

The methylene blue in both the water and microbubble suspensions started to disperse, as shown in Fig. 22 and Fig. 25A through Fig. 25C. The dispersion in the microbubble suspension rapidly began when the cavitation threshold was reached, and the corresponding standard deviations decreased faster than that in the tap water group. At the $15^{th}$ second of the ultrasound exposure, methylene blue in the microbubble suspension was fully dissolved in the solution, and the standard deviation was decreased by 97 % compared to its original value, while the methylene blue in tap water was mainly dispersed in the bottom part with a 21 % drop in the standard deviation. With the assistance of cavitation, the diffusion coefficient reached 36.2 x $10^{-5}$ $cm^2/s$, which is 6.4 times of the value calculated for the tap water group. Without cavitation, both the diffusion coefficient and pixel standard deviation change in the microbubble suspension remained the same as those in the tap water group, showing that the microbubble suspension alone has no effect on the dye dispersion.

In localized cavitation experiment, microbubble solution with different concentrations was injected into the transparent blood vessel phantom. The pixel value – microbubble concentration digital imaging correlation (DIC) curve was plotted in Fig. 23. The

microbubble fragmentation speeds were achieved by correlating frames of experiment videos at different times and the DIC curve.

The following publications are each hereby included by reference in their entirety:

1. Huang, C.-T., Shen, C.-L., Tang, C.-F. & Chang, S.-H. A wearable yarn-based piezo-resistive sensor. Sensors and Actuators A: Physical 141, 396–403 (2008).

2. Karpelson, M., Wei, G.-Y. & Wood, R. J. Driving high voltage piezoelectric actuators in microrobotic applications. Sensors and Actuators A: Physical 176, 78–89 (2012).

3. Harb, A. Energy harvesting: State-of-the-art. Renewable Energy 36, 2641–2654 (2011).

4. Jiang, L. et al. Flexible piezoelectric ultrasonic energy harvester array for bio-implantable wireless generator. Nano Energy 56, 216–224 (2019).

5. Fuchs, F. Ultrasonic Cleaning Fundamental Theory and Application. 14.

6. Shung, K. K. & Zippuro, M. Ultrasonic transducers and arrays. IEEE Engineering in Medicine and Biology Magazine 15, 20–30 (1996).

7. Jiang, L. et al. Fabrication of a (K,Na)NbO3-based lead-free 1-3 piezocomposite for high-sensitivity ultrasonic transducers application. Journal of Applied Physics 125, 214501 (2019).

8. Cui, H. et al. Three-dimensional printing of piezoelectric materials with designed anisotropy and directional response. Nature Mater 18, 234–241 (2019).

9. Chen, X. et al. Helical-Like 3D Ultrathin Piezoelectric Element for Complicated Ultrasonic Field. Advanced Functional Materials 29, 1902912 (2019).

10. Zhou, Q., Lau, S., Wu, D. & Kirk Shung, K. Piezoelectric films for high frequency ultrasonic transducers in biomedical applications. Progress in Materials Science 56, 139–174 (2011).

11. Chen, Z. et al. 3D printing of piezoelectric element for energy focusing and ultrasonic sensing. Nano Energy 27, 78–86 (2016).

12. Goat, C. A. & Whatmore, R. W. The Effect of Grinding Conditions on Lead Zirconate Titanate Machinability. Journal of the European Ceramic Society 19, 1311–1313 (1999).

13. Smay, J. E., Cesarano III, J., Tuttle, B. A. & Lewis, J. A. Directed Colloidal Assembly of Linear and Annular Lead Zirconate Titanate Arrays. Journal of the American Ceramic Society 87, 293–295 (2004).

14. Sun, J., Ngernchuklin, P., Vittadello, M., Akdoğan, E. K. & Safari, A. Development of 2-2 piezoelectric ceramic/polymer composites by direct-write technique. J Electroceram 24, 219–225 (2010).

15. Yao, D. et al. Achieving the Upper Bound of Piezoelectric Response in Tunable, Wearable 3D Printed Nanocomposites. Advanced Functional Materials 29, 1903866 (2019).

16. Rabut, C. et al. Ultrasound Technologies for Imaging and Modulating Neural Activity. Neuron 108, 93–110 (2020).

17. Azadeh, S. S., Lordifard, P., Soheilifar, M. H., Esmaeeli Djavid, G. & Keshmiri Neghab, H. Ultrasound and Sonogenetics: A New Perspective for Controlling Cells with Sound. Iran J Pharm Res 20, 151–160 (2021).

18. Huang, Y.-S. et al. Sonogenetic Modulation of Cellular Activities Using an Engineered Auditory-Sensing Protein. Nano Lett 20, 1089–1100 (2020).

19. Tzanakis, I., Lebon, G. S. B., Eskin, D. G. & Pericleous, K. A. Characterizing the cavitation development and acoustic spectrum in various liquids. Ultrasonics Sonochemistry 34, 651–662 (2017).

20. Suo, D., Jin, Z., Jiang, X., Dayton, P. & Jing, Y. Microbubble mediated dual-frequency high intensity focused ultrasound thrombolysis: An In vitro study. Applied Physics Letters 110, (2016).

21. Epelbaum, S. et al. Pilot study of repeated blood-brain barrier disruption in patients with mild Alzheimer's disease with an implantable ultrasound device. Alzheimer's Research & Therapy 14, 40 (2022).

22. Zhou, H. et al. Noninvasive Ultrasound Deep Brain Stimulation for the Treatment of Parkinson's Disease Model Mouse. Research 2019, 1–13 (2019).

23. Lu, G. et al. Transcranial Focused Ultrasound for Noninvasive Neuromodulation of the Visual Cortex. IEEE Transactions on Ultrasonics, Ferroelectrics, and Frequency Control 68, 21–28 (2021).

24. Ultrasound Cavitation/Microbubble Detection and Medical Applications | SpringerLink. 10.1007/s40846-018-0391-0.

25. Xu, Z. et al. Vat photopolymerization of fly-like, complex micro-architectures with dissolvable supports. Additive Manufacturing 47, 102321 (2021).

26. Marino, A. et al. Two-Photon Lithography of 3D Nanocomposite Piezoelectric Scaffolds for Cell Stimulation. ACS Appl. Mater. Interfaces 7, 25574–25579 (2015).

27. Sikder, P., Koju, N., Lin, B. & Bhaduri, S. B. Conventionally Sintered Hydroxyapatite–Barium Titanate Piezo-Biocomposites. Trans Indian Inst Met 72, 2011–2018 (2019).

28. Sinclair, David. & La Mer, V. K. Light Scattering as a Measure of Particle Size in Aerosols. The Production of Monodisperse Aerosols. Chem. Rev. 44, 245–267 (1949).

29. Chen, W., Wang, F., Yan, K., Zhang, Y. & Wu, D. Micro-stereolithography of KNN-based lead-free piezoceramics. Ceramics International 45, 4880–4885 (2019).

30. Cheng, J., Chen, Y., Wu, J.-W., Ji, X.-R. & Wu, S.-H. 3D Printing of BaTiO3 Piezoelectric Ceramics for a Focused Ultrasonic Array. Sensors 19, 4078 (2019).

31. Ananta, S. & Thomas, N. W. Relationships between Sintering Conditions, Microstructure and Dielectric Properties of Lead Iron Niobate. Journal of the European Ceramic Society 19, 1873–1881 (1999).

32. Safar, M., Button, T. W. & Zabcik, M. Control of PbO loss during sintering of PZT: Laboratory vs industry. In 2017 Joint IEEE International Symposium on the Applications of Ferroelectric (ISAF)/International Workshop on Acoustic Transduction Materials and Devices (IWATMD)/Piezoresponse Force Microscopy (PFM) 83–88 (2017). Doi:10.1109/ISAF.2017.8000218.

33. Khan, K., Yamamura, D., Vargas, C., Alexander, T. & Surani, S. The Role of EkoSonic Endovascular System or EKOS® in Pulmonary Embolism. Cureus 11, e6380.

34. Peng, C., Wu, H., Kim, S., Dai, X. & Jiang, X. Recent Advances in Transducers for Intravascular Ultrasound (IVUS) Imaging. Sensors (Basel) 21, 3540 (2021).

35. Frijlink, M. E., Goertz, D. E., Van Damme, L. C. a., Krams, R. & W. Van Der Steen, A. F. Intravascular ultrasound tissue harmonic imaging in vivo. IEEE Transactions on Ultrasonics, Ferroelectrics, and Frequency Control 53, 1844–1852 (2006).

36. Combined chirp coded tissue harmonic and fundamental ultrasound imaging for intravascular ultrasound: 20-60MHz phantom and ex vivo results | Elsevier Enhanced Reader. doi:10.1016/j.ultras.2012.07.003.

37. Corker, D. L., Whatmore, R. W., Ringgaard, E. & Wolny, W. W. Liquid-phase sintering of PZT ceramics. Journal of the European Ceramic Society 20, 2039–2045 (2000).

38. Wang, D., Guo, H., Morandi, C. S., Randall, C. A. & Trolier-McKinstry, S. Cold sintering and electrical characterization of lead zirconate titanate piezoelectric ceramics. APL Materials 6, 016101 (2018).

39. Deckers, J. P. et al. Shaping ceramics through indirect selective laser sintering. Rapid Prototyping Journal 22, 544–558 (2016).

40. Yi, J., Shen, M., Liu, S. & Jiang, S. Effects of PbO-B2O3 Glass Doping on the Sintering Temperature and Piezoelectric Properties of 0.35Pb (Ni1/3Nb2/3)O3-0.65Pb(Zr0.41Ti0.59)O3 Ceramics. Journal of Electronic Materials 44, (2015).

41. Tumbleston, J. R. et al. Continuous liquid interface production of 3D objects. Science 347, 1349–1352 (2015).

42. LCD-SLA 3D printing of BaTiO3 piezoelectric ceramics | Elsevier Enhanced Reader. doi:10.1016/j.ceramint.2021.07.216.

43. Bagheri, A. & Jin, J. Photopolymerization in 3D Printing. ACS Appl. Polym. Mater. 1, 593–611 (2019).

44. Beer, M. P. de et al. Rapid, continuous additive manufacturing by volumetric polymerization inhibition patterning. Science Advances (2019) doi:10.1126/sciadv.aau8723.

45. Hammer, M. & Hoffmann, M. J. Sintering Model for Mixed-Oxide-Derived Lead Zirconate Titanate Ceramics. Journal of the American Ceramic Society 81, 3277–3284 (1998).

46. Kubanek, J. et al. Ultrasound modulates ion channel currents. Sci Rep 6, 24170 (2016).

47. Choi, T., Bae, S., Suh, M. & Park, J. A Soft Housing Needle Ultrasonic Transducer for Focal Stimulation to Small Animal Brain. Ann Biomed Eng 48, 1157–1168 (2020).

48. Kubanek, J., Shukla, P., Das, A., Baccus, S. A. & Goodman, M. B. Ultrasound elicits behavioral responses through mechanical effects on neurons and ion channels in a simple nervous system. J. Neurosci. (2018) doi:10.1523/JNEUROSCI.1458-17.2018.

49. Mannaris, C. & Averkiou, M. A. Investigation of microbubble response to long ultrasonic pulses used in therapeutic applications. The Journal of the Acoustical Society of America 129, 2512–2512 (2011).

50. Şen, T., Tüfekçioğlu, O. & Koza, Y. Mechanical index. Anatol J Cardiol 15, 334–336 (2015).

51. Zeng, Y. et al. 3D-Printing Piezoelectric Composite with Honeycomb Structure for Ultrasonic Devices. Micromachines 11, 713 (2020).

52. Song, X. et al. Piezoelectric component fabrication using projection-based stereolithography of barium titanate ceramic suspensions. Rapid Prototyping Journal 23, 44–53 (2017).

53. Chen, Z. et al. Three-Dimensional Printed Piezoelectric Array for Improving Acoustic Field and Spatial Resolution in Medical Ultrasonic Imaging. Micromachines 10, 170 (2019).

54. Chen, Y. et al. PZT ceramics fabricated based on stereolithography for an ultrasound transducer array application. Ceramics International 44, 22725–22730 (2018).

55. Chabok, H. et al. Ultrasound Transducer Array Fabrication Based on Additive Manufacturing of Piezocomposites. In 433–444 (American Society of Mechanical Engineers Digital Collection, 2013). Doi:10.1115/ISFA2012-7119.

56. Desilets, C. S., Fraser, J. D. & Kino, G. S. The design of efficient broad-band piezoelectric transducers. IEEE Transactions on Sonics and Ultrasonics 25, 115–125 (1978).

57. Brown, L. F. Design considerations for piezoelectric polymer ultrasound transducers. IEEE Transactions on Ultrasonics, Ferroelectrics, and Frequency Control 47, 1377–1396 (2000).

58. Wanless, I. R. & Huang, W.-Y. 12 – Vascular disorders. In MacSween's Pathology of the Liver (Sixth Edition) (eds. Burt, A. D., Portmann, B. C. & Ferrell, L. D.) 601–643 (Churchill Livingstone, 2012). Doi:10.1016/B978-0-7020-3398-8.00012-X.

59. Jiang, L. et al. Multichannel Piezo-Ultrasound Implant with Hybrid Waterborne Acoustic Metastructure for Selective Wireless Energy Transfer at Megahertz Frequencies. Advanced Materials n/a, 2104251.

60. Bhatia, A. & Peng, P. Chapter 79 – Ultrasound-Guided Procedures for Pain Management: Spine Injections and Relevant Peripheral Nerve Blocks. In Essentials of Pain Medicine (Fourth Edition) (eds. Benzon, H. T., Raja, S. N., Liu, S. S., Fishman, S. M. & Cohen, S. P.) 725-736.e1 (Elsevier, 2018). Doi:10.1016/B978-0-323-40196-8.00079-6.

61. Brennen, C. E. Cavitation in medicine. Interface Focus 5, 20150022 (2015).

62. Chowdhury, S. M., Abou-Elkacem, L., Lee, T., Dahl, J. & Lutz, A. M. Ultrasound and microbubble mediated therapeutic delivery: Underlying mechanisms and future outlook. Journal of Controlled Release 326, 75–90 (2020).

63. Wischhusen, J. & Padilla, F. Ultrasound-Targeted Microbubble Destruction (UTMD) for Localized Drug Delivery into Tumor Tissue. IRBM 40, 10–15 (2019).

64. Qin, P., Xu, L., Zhong, W. & Yu, A. C. H. Ultrasound-Microbubble Mediated Cavitation of Plant Cells: Effects on Morphology and Viability. Ultrasound in Medicine & Biology 38, 1085–1096 (2012).

65. Bader, K. B. & Holland, C. K. Gauging the likelihood of stable cavitation from ultrasound contrast agents. Phys. Med. Biol. 58, 127–144 (2012).

66. Datta, S. et al. CORRELATION OF CAVITATION WITH ULTRASOUND ENHANCEMENT OF THROMBOLYSIS. Ultrasound Med Biol 32, 1257–1267 (2006).

67. Rayes, A. et al. Estimating Thrombus Elasticity by Shear Wave Elastography to Evaluate Ultrasound Thrombolysis for Thrombus with Different Stiffness. IEEE Transactions on Biomedical Engineering 1–9 (2022) doi:10.1109/TBME.2022.3186586.

68. IEEE Standard on Piezoelectricity. ANSI/IEEE Std 176-1987 0_1- (1988) doi:10.1109/IEEESTD.1988.79638.

69. Lee, W., Idriss, S. F., Wolf, P. D. & Smith, S. W. A miniaturized catheter 2-D array for real-time, 3-D intracardiac echocardiography. IEEE Transactions on Ultrasonics, Ferroelectrics, and Frequency Control 51, 1334–1346 (2004).

70. Walker, D. A., Hedrick, J. L. & Mirkin, C. A. Rapid, large-volume, thermally controlled 3D printing using a mobile liquid interface. Science 366, 360–364 (2019).

71. Cui, H. et al. Three-dimensional printing of piezoelectric materials with designed anisotropy and directional response. Nature Mater 18, 234–241 (2019).

72. Yao, D. et al. Achieving the Upper Bound of Piezoelectric Response in Tunable, Wearable 3Dprinted Nanocomposites. Advanced Functional Materials 29, 1903866 (2019).

73. Dukhin, A. S. & Goetz, P. J. Chapter 7 – Acoustic and Electroacoustic Measurement Techniques.in Studies in Interface Science (eds. Dukhin, A. S. & Goetz, P. J.) vol. 24 261–301 (Elsevier, 2010).

74. Dukhin, A. S. & Goetz, P. J. Chapter 3 – Fundamentals of Acoustics in Homogeneous Liquids:Longitudinal Rheology. In Studies in Interface Science (eds. Dukhin, A. S. & Goetz, P. J.) vol. 24 91–125 (Elsevier, 2010).

75. Yan, Z., Pu, Z., Haijun, F. & Yi, Z. Experiment Study on Sound Properties of Carbon Fiber Composite Material. IOP Conference Series: Materials Science and Engineering 542, 012001 (2019).

76. Shung, K. K. & Zippuro, M. Ultrasonic transducers and arrays. IEEE Engineering in Medicine and Biology Magazine 15, 20–30 (1996).

77. Cao, L., Fu, Q., Si, Y., Ding, B. & Yu, J. Porous materials for sound absorption. Composites Communications 10, 25–35 (2018).

78. Zhou, Q., Lam, K. H., Zheng, H., Qiu, W. & Shung, K. K. Piezoelectric single crystals for ultrasonic transducers in biomedical applications. Prog Mater Sci 66, 87–111 (2014).

79. Mickiewicz, W., Raczyński, M. & Parus, A. Performance Analysis of Cost-Effective Miniature Microphone Sound Intensity 2D Probe. Sensors (Basel, Switzerland) 20, (2020).

80. Kim, J. et al. Intravascular forward-looking ultrasound transducers for microbubble-mediated sonothrombolysis. Sci Rep 7, 3454 (2017).

81. Shih, C.-C. et al. Development of an intravascular ultrasound elastography based on a dual-element transducer. R. Soc. Open sci. 5, 180138 (2018).

82. Kim, H., Wu, H., Goel, L. & Jiang, X. Miniaturized Ultrasound Transducer Composed of a Composite of Multiple Piezoelectric Stacks. In (American Society of Mechanical Engineers Digital Collection, 2020). Doi:10.1115/IMECE2019-12208.

83. Lim, H. G. et al. Thermal Ablation and High-Resolution Imaging Using a Back-to-Back(BTB) Dual-Mode Ultrasonic Transducer: In Vivo Results. Sensors 21, 1580 (2021).

84. Bouchoux, G. et al. Dual-Mode Ultrasound Transducer for Image-Guided Interstitial Thermal Therapy. Ultrasound in Medicine & Biology 34, 607–616 (2008).

85. Basak, A. & Bhunia, S. Chapter 13 – Implantable imaging system for automated monitoring of internal organs. In Implantable Biomedical Microsystems (eds. Bhunia, S., Majerus, S. J. A. & Sawan, M.) 281–312 (William Andrew Publishing, 2015). Doi:10.1016/B978-0-323-26208-8.00013-3.

86. Hu, H. et al. Stretchable ultrasonic transducer arrays for three-dimensional imaging on complex surfaces. Science Advances 4, eaar3979 (2018).

87. Sadeghi Gougheri, H., Dangi, A., Kothapalli, S.-R. & Kiani, M. A Comprehensive Study of Ultrasound Transducer Characteristics in Microscopic Ultrasound Neuromodulation. IEEE Trans Biomed Circuits Syst 13, 835–847 (2019).

88. Selifonov, A. A., Shapoval, O. G., Mikerov, A. N. & Tuchin, V. V. Determination of the Diffusion Coefficient of Methylene Blue Solutions in Dentin of a Human Tooth using Reflectance Spectroscopy and Their Antibacterial Activity during Laser Exposure. Optics and Spectroscopy 126, 758–768 (2019).

89. Chaussy, C., Tilki, D. & Thüroff, S. Transrectal High-Intensity Focused Ultrasound for the Treatment of Localized Prostate Cancer: Current Role. 2013, (2013).

90. Lee, Jungpyo, et al. "A MEMS ultrasound stimulation system for modulation of neural circuits with high spatial resolution in vitro." Microsystems & Nanoengineering 5.1 (2019): 28.

91. Wu, Sheng-Kai, et al. "Characterization of different microbubbles in assisting focused ultrasound-induced blood-brain barrier opening." Scientific reports 7.1 (2017): 46689.

92. Arvanitis, Costas D., et al. "Controlled ultrasound-induced blood-brain barrier disruption using passive acoustic emissions monitoring." (2012): e45783.

93. Mulgaonkar, Amit P., et al. "Design of a minimally invasive low-frequency microtransducer for ultrasonic neuromodulation." 2014 IEEE International Ultrasonics Symposium. IEEE, 2014.

94. Manbachi, Amir, and Richard SC Cobbold. "Development and application of piezoelectric materials for ultrasound generation and detection." Ultrasound 19.4 (2011): 187-196.

95. Dixon, Adam J., et al. "Efficacy of sonothrombolysis using microbubbles produced by a catheter-based microfluidic device in a rat model of ischemic stroke." Annals of biomedical engineering 47 (2019): 1012-1022.

96. Neudorfer, Clemens, et al. "Endovascular deep brain stimulation: investigating the relationship between vascular structures and deep brain stimulation targets." Brain Stimulation 13.6 (2020): 1668-1677.

97. Chen, Ko-Ting, Kuo-Chen Wei, and Hao-Li Liu. "Focused ultrasound combined with microbubbles in central nervous system applications." Pharmaceutics 13.7 (2021): 1084.

98. Idbaih, Ahmed, et al. "Safety and Feasibility of Repeated and Transient Blood–Brain Barrier Disruption by Pulsed Ultrasound in Patients with Recurrent GlioblastomaBlood–Brain Barrier Disruption by Ultrasound in GBM." Clinical Cancer Research 25.13 (2019): 3793-3801.

99. Fan, Ching-Hsiang, et al. "Sonogenetic-based neuromodulation for the amelioration of Parkinson's disease." Nano letters 21.14 (2021): 5967-5976.

100. Azadeh, Seyedeh Sara, et al. "Ultrasound and sonogenetics: A new perspective for controlling cells with sound." Iranian Journal of Pharmaceutical Research: IJPR 20.3 (2021): 151.

101. Vasan, Aditya, et al. "Ultrasound mediated cellular deflection results in cellular depolarization." Advanced Science 9.2 (2022): 2101950.

102. Ferrara, Katherine, Rachel Pollard, and Mark Borden. "Ultrasound microbubble contrast agents: fundamentals and application to gene and drug delivery." Annu. Rev. Biomed. Eng. 9 (2007): 415-447.

103. Aryal, Muna, et al. "Ultrasound-mediated blood–brain barrier disruption for targeted drug delivery in the central nervous system." Advanced drug delivery reviews 72 (2014): 94-109.

104. Rabut, Claire, et al. "Ultrasound technologies for imaging and modulating neural activity." Neuron 108.1 (2020): 93-110.

105. Cadoni, S., et al. "Sonogenetic stimulation of the brain at a spatiotemporal resolution suitable for vision restoration." BioRxiv (2021): 2021-11.

Lu, H., Cui, H., Lu, G. et al. 3D Printing and processing of miniaturized transducers with near-pristine piezoelectric ceramics for localized cavitation. Nat Commun 14, 2418 (2023).

U.S. Patent Publication No. US 10,512,555 B2

U.S. Patent Publication No. US 9,526,922 B2

U.S. Patent Publication No. US 2019/0175372 A1

The disclosures of each and every patent, patent application, and publication cited herein are hereby each incorporated herein by reference in their entirety. While this invention has been disclosed with reference to specific embodiments, it is apparent that other embodiments and variations of this invention may be devised by others skilled in the art without departing from the true spirit and scope of the invention. The appended claims are intended to be construed to include all such embodiments and equivalent variations.

## CLAIMS

What is claimed is:

1. A stent system comprising:

a support structure having first and second ends, comprising one or more members defining interior and peripheral regions for the structure;

a lattice interfaced with the support structure;

at least one transducer attached to the lattice;

one or more leads electrically connected to the at least one transducer; and

a power source connected to the one or more lead wires.

2. The system of claim 1, wherein the at least one transducer is at least partially formed in one or more shapes selected from the group consisting of: non-planar, curved, cylindrical, concentrical circles, concentric circles with struts, hemispherical, annular, ring, half-ring, spherical, rectangular, prism, pyramidal, helical and polyhedral.

3. The system of claim 2, wherein the at least one transducer is arranged in one or more patterns or configurations selected from: radial, radially outward, radially inward, focused inward, focused outward, circumferential, peripheral, helical, double-helical, triplicate, staggered, eccentric, biased, symmetrical, asymmetrical, or grouped.

4. The system of claim 3, wherein the at least one transducer has length of 5 μm to 50 mm, a width or diameter of 5 μm to 50 mm, and a height of 5 μm to 50 mm.

5. The system of claim 4, wherein the at least one transducer has a curvature ranging from 0 degrees to 180 degrees, a focal depth ranging between 0.1 mm and 25 mm, or an arc length ranging from 0.1 μm to 10 mm.

6. The system of claim 5, wherein the support structure has a length of 10 mm to 60 mm, and a width or diameter of 0.5 mm to 20 mm.

7. The system of claim 6, wherein the one or more members of the support structure have a width or diameter between 0.01 mm and 2 mm.

8. The system of claim 7, wherein the openings of the lattice range between 0.1 mm and 5 mm.

9. The system of claim 8, wherein the one or more members of the support structure are formed of one or more materials selected from the group consisting of: elastic material, superelastic material, sputtered superelastic material, resilient material, nonconductive metal or alloy, poorly conductive metal or alloy, platinum, magnesium, stainless steel, nickel-titanium alloy/nitinol, nitinol thin film (i.e., NiTi thin film), cobalt-nickel alloys, tantalum alloys, cobalt-chromium alloys, platinum-tungsten metal, cobalt alloy, platinum-iridium alloy, cobalt, chromium, conductive metal, gold, copper, silver, titanium, and titanium alloys.

10. The system of claim 9, wherein the lattice is formed of one or more materials selected from the group consisting of: elastic material, superelastic material, sputtered superelastic material, resilient material, nonconductive metal or alloy, poorly conductive metal or alloy, platinum, magnesium, stainless steel, nickel-titanium alloy/nitinol, nitinol thin film (i.e., NiTi thin film), cobalt-nickel alloys, tantalum alloys, cobalt-chromium alloys, platinum-tungsten metal, cobalt alloy, platinum-iridium alloy, cobalt, chromium, conductive metal, gold, copper, silver, titanium, and titanium alloys.

11. The system of claim 10, wherein the lead wires are formed of one or more materials selected from the group consisting of: conductive metal, conductive metal allow, gold, copper, aluminum, silver, insulating material, biocompatible material, polymer material, synthetic material, or plastic.

12. The system of claim 11, wherein at least one of the support structure, lattice, at least one transducer and one or more lead wires are at least partially coated with one or more coatings selected from the group consisting of: biocompatible coating, conductive coating, non-conductive coating, insulating coating, oxide-film, titanium-nitride-oxide, organic polymer, polyurethane, polyimide, bioactive/covalently bonded coating, covalently-linked heparin,

polymerized allylamine, poly(dimethylsiloxane), phosphorylcholine, 2-methylacryloyloxyethyl phosphorylcholine, poly(2-methoxyethyl acrylate), enzyme-loaded inducible nitric acid oxide, synthase oxygenase on polyethylenimine, chromium, platinum, gold, silver, stealth coating and trimethylolpropane triacrylate (TMPTA).

13. The system of claim 12, wherein the at least one transducer is a piezoelectric device comprising a bipolar ceramic stack, at least one electrode, a back mass, a front mass, and at least one biocompatible coating covering at least a portion of the at least one transducer, wherein the transducer is coated in trimethylolpropane triacrylate (TMPTA).

14. The system of claim 1, further comprising:

a computing system communicatively connected to the power source, comprising a processor and a non-transitory computer-readable medium with instructions stored thereon, which when executed by a processor, perform steps comprising:

providing power at one or more voltages in one or more frequencies from the power source to the at least one transducer for at least one duration.

15. The system of claim 12, wherein the one or voltages is between 0.1 V to 500 V, the one or more frequencies are between 0.1 Hz and 10000 MHz, and the at least one duration is between 0.1 μs and 1 hour.

16. The system of claim 1 or claim 15, further comprising at least one microfluidic chamber positioned in the interior region of the support structure fluidly connected to at least one microfluidic reservoir positioned outside of the support structure with at least one conduit comprising at least one lumen.

17. The system of claim 16, wherein the at least one microfluid chamber is at least partially formed in one or more shapes selected from: cylinder, disk, toroid, annulus, capsule, pill, cube, sphere, dome, arc, spiral, helix, double helix.

18. The system of claim 17, wherein the at least one microfluid chamber has a volume ranging between 1 μl and 1000 μl or a diameter between 0.1 mm and 1 mm, the at least one microfluid reservoir has a volume ranging between 100 μl and 2 ml.

19. The system of claim 18, wherein the at least one conduit has a length ranging between 1 mm and 200 cm.

20. The system of claim 19, wherein the at least one microfluidic chamber comprises first and second microfluidic chambers, and the at least one microfluidic chamber comprises first and second microfluidic chambers.

21. The system of claim 20, wherein the first microfluidic chamber and first microfluidic reservoir are at least partially fluidly filled with a solution comprising microbubbles, and the second microfluid chamber and second microfluidic reservoir are at least partially fluidly filled with a solution comprising at least one therapeutic.

22. The system of claim 21, wherein the at least one therapeutic is selected from the group consisting of: gene therapy, Nusinersen, Levodopa, anti-seizure medication, DNA or RNA based biologic/viral-vector gene replacement therapies, CRISPR, Nusinersen for SMA, RGX-111, RGX-112, condensed tuberin, APOE2, hTERT, GBA, SOD-1, C9orf72, HTT, antibody-based biologic therapies, Lecanemab, small molecules and proteins.

23. The system of claim 22, further comprising at least one port in each microfluidic reservoir configured to receive one or more fluids or solutions.

24. The system of claim 23, further comprising an implantable housing at least partially enclosing the power source, the first microfluidic reservoir, and the second microfluidic reservoir.

25. The system of claim 24, further comprising at least one tubular conduit having at least one lumen extending from the housing to a position on the first end of the support structure.

26. A method for spatiotemporal control of intrinsic or exogenous genes, comprising:

providing the system of claim 1;

implanting the stent system near or in a target site of a subject;

providing power at one or more voltages in one or more frequencies from the power source to the at least one transducer for at least one duration.

27. The method of claim 23, wherein the one or voltages is between 0.1 V to 500 V, the one or more frequencies are between 0.1 Hz and 10000 MHz, and the at least one duration is between 0.1 μs and 1 hour.

28. A drug delivery method, comprising:

providing the system of claim 16;

implanting the stent system in or near a target site of a subject;

filling the at least one microfluidic chamber at least partially with a solution comprising at least one therapeutic and microbubbles;

producing microbubble cavitation via the at least one transducer; and

delivering the at least one therapeutic to the target site.

29. A method of fabricating a stent system comprising:

fabricating a stent;

fabricating at least one PZT transducer;

fabricating at least one microfluidic chamber;

fixing the at least one PZT transducer to the stent;

disposing the at least one microfluidic chamber within the stent.

30. The method of claim 29, wherein the step of fabricating the PZT transducer comprises:

3D printing a PZT base layer on a polymer support layer;

debonding the PZT base layer from the polymer support layer;

sintering the PTZ base layer in a PTZ powder bed with heat to form a PTZ element;

submerging the PTZ element into an isolation liquid;

polarizing the dipoles within the sintered PTZ element;

applying an electric field to the PTZ element; and

cooling the PTZ element.

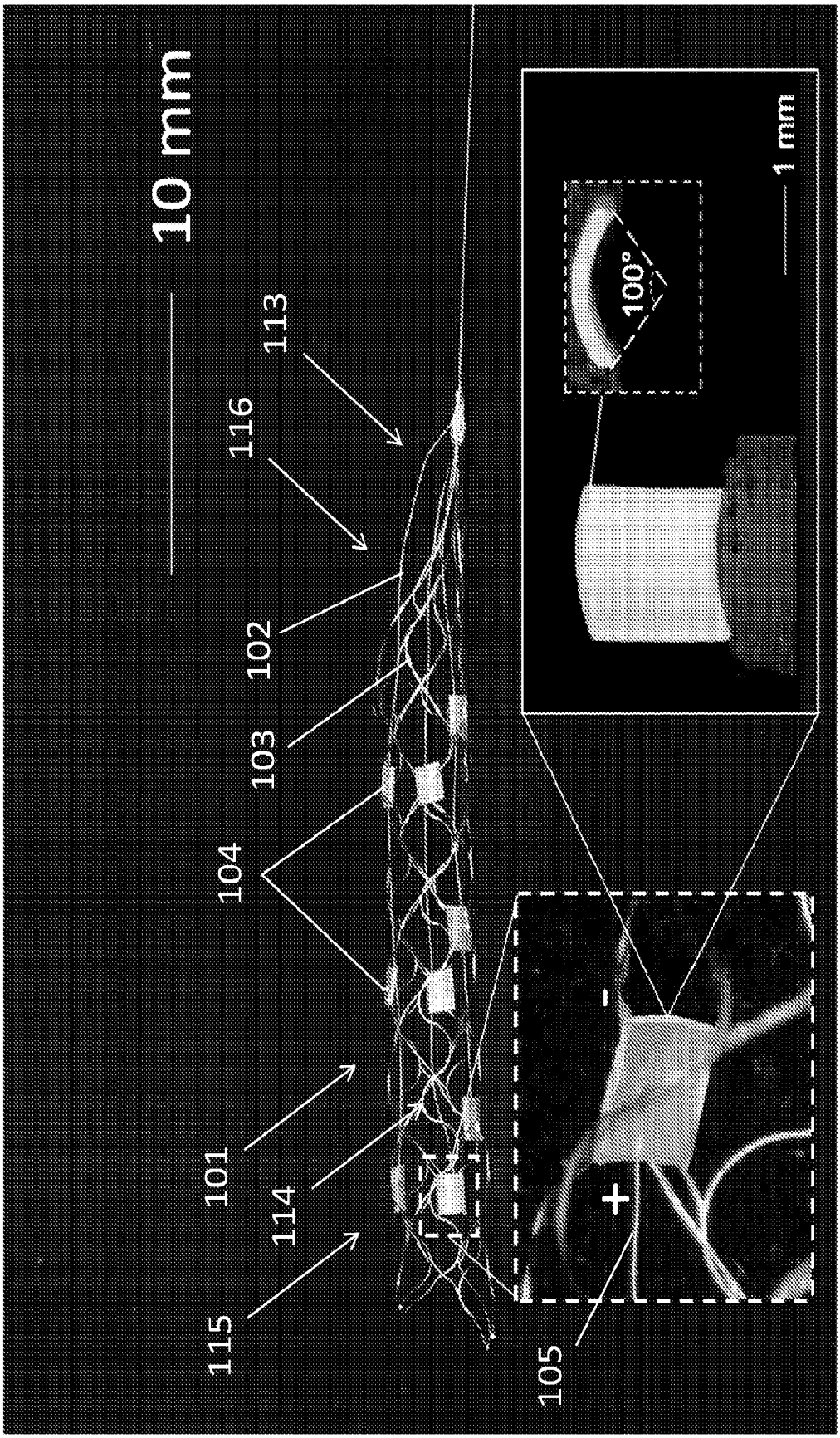


Fig. 1A

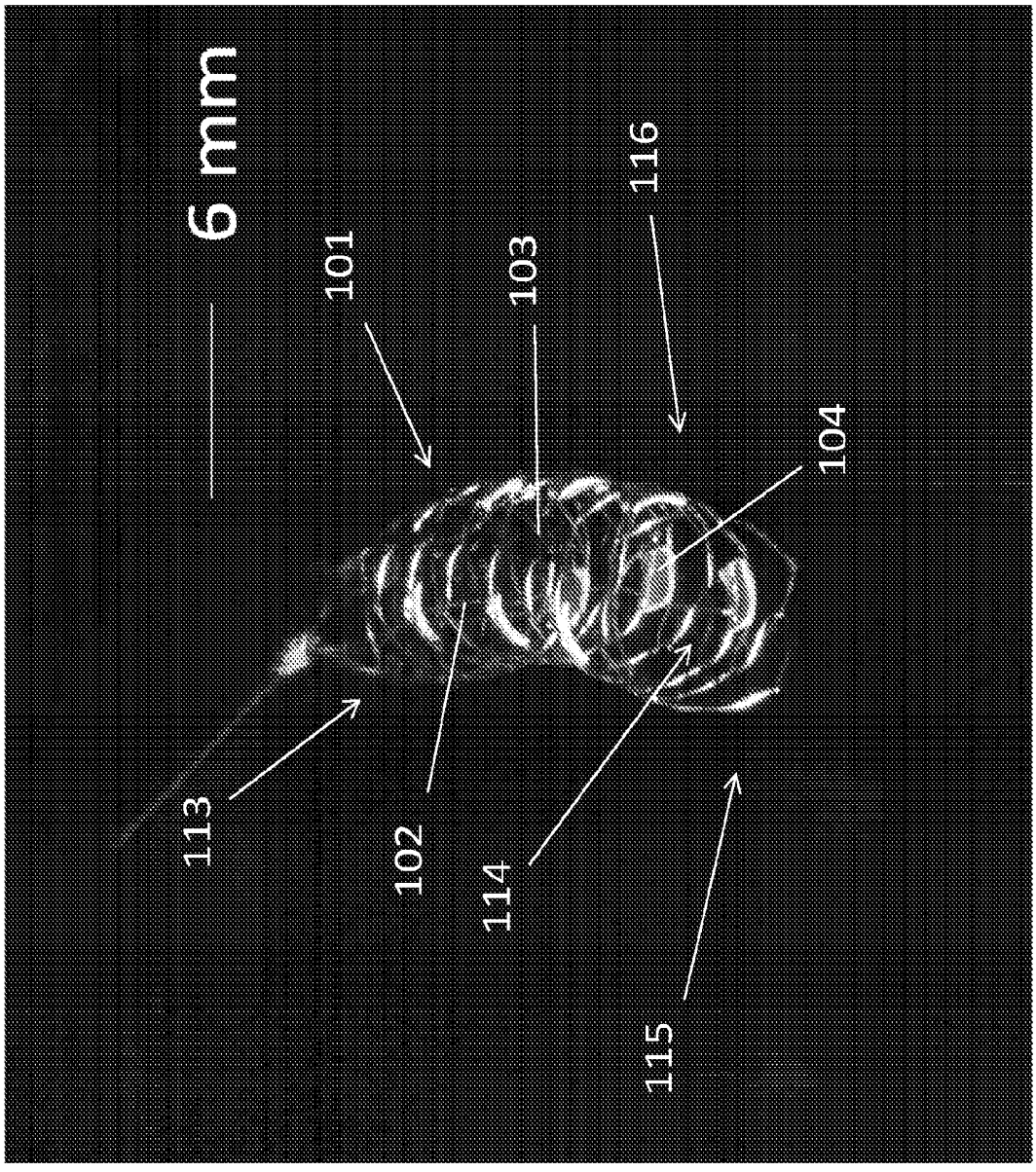


Fig. 1B

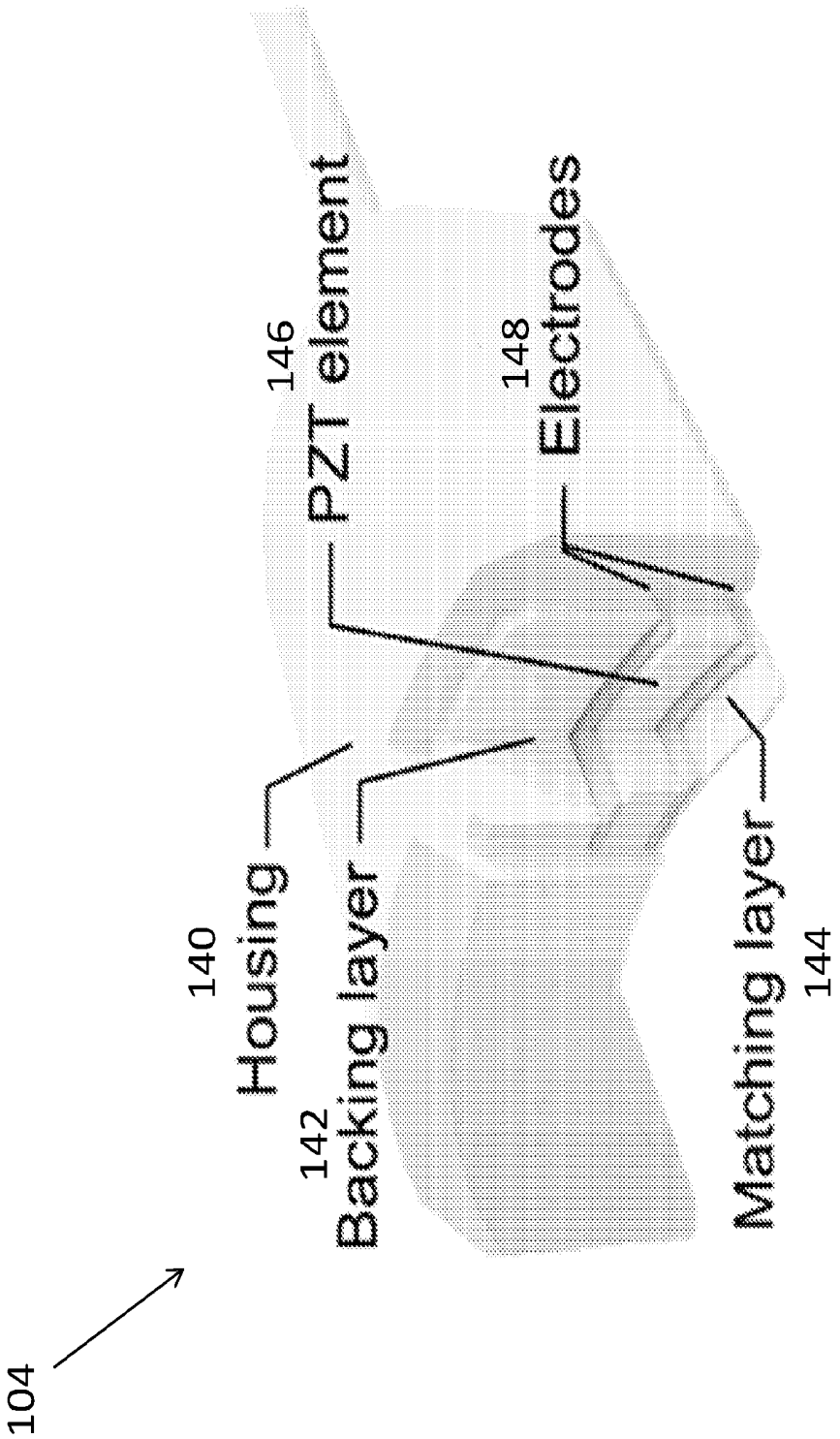
104
140
Housing
142
Backing layer
146
PZT element
148
Electrodes
144
Matching layer

Fig. 2

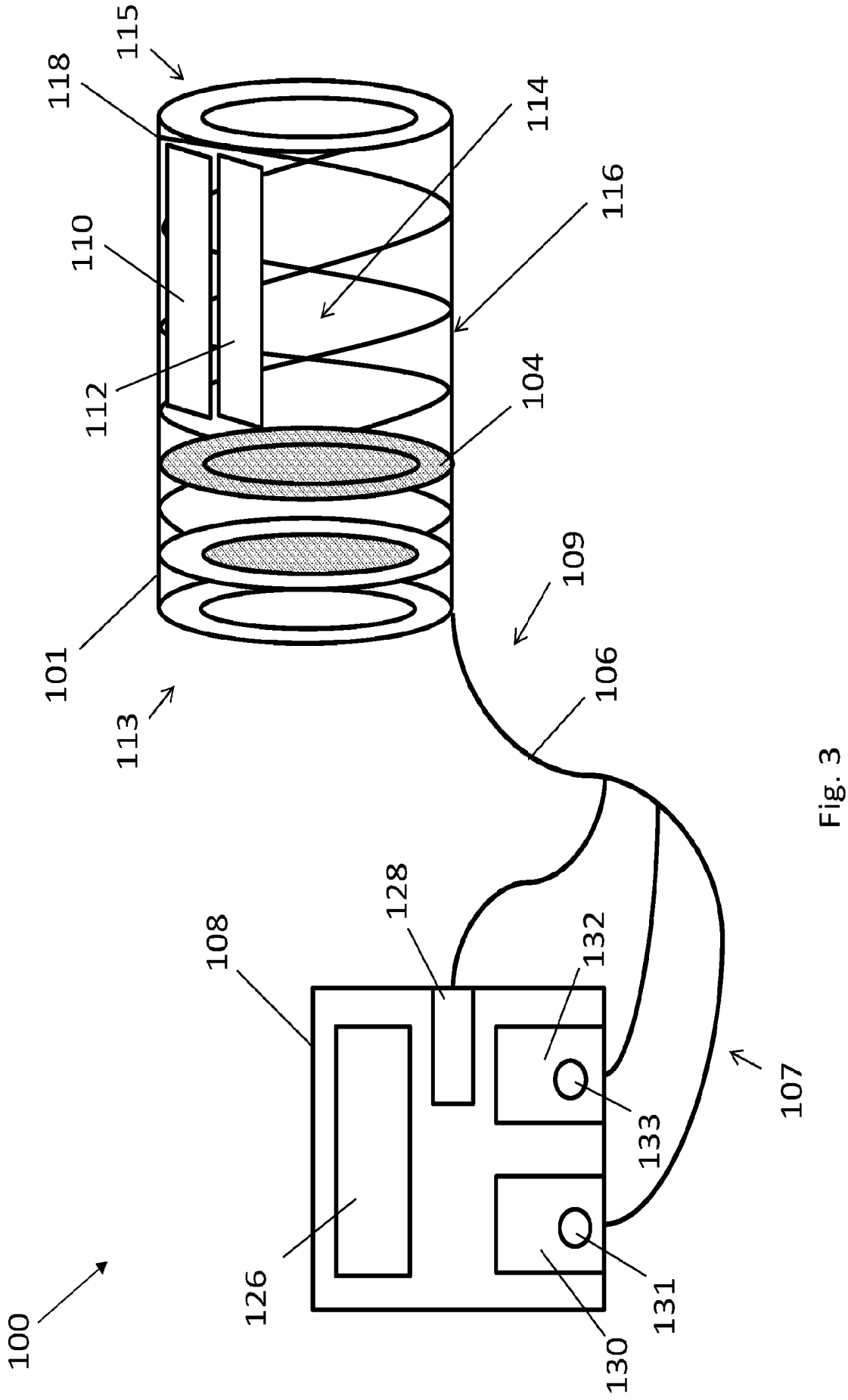
115
118
114
116
110
112
104
109
101
106
113
128
108
132
133
107
126
131
130
100

Fig. 3

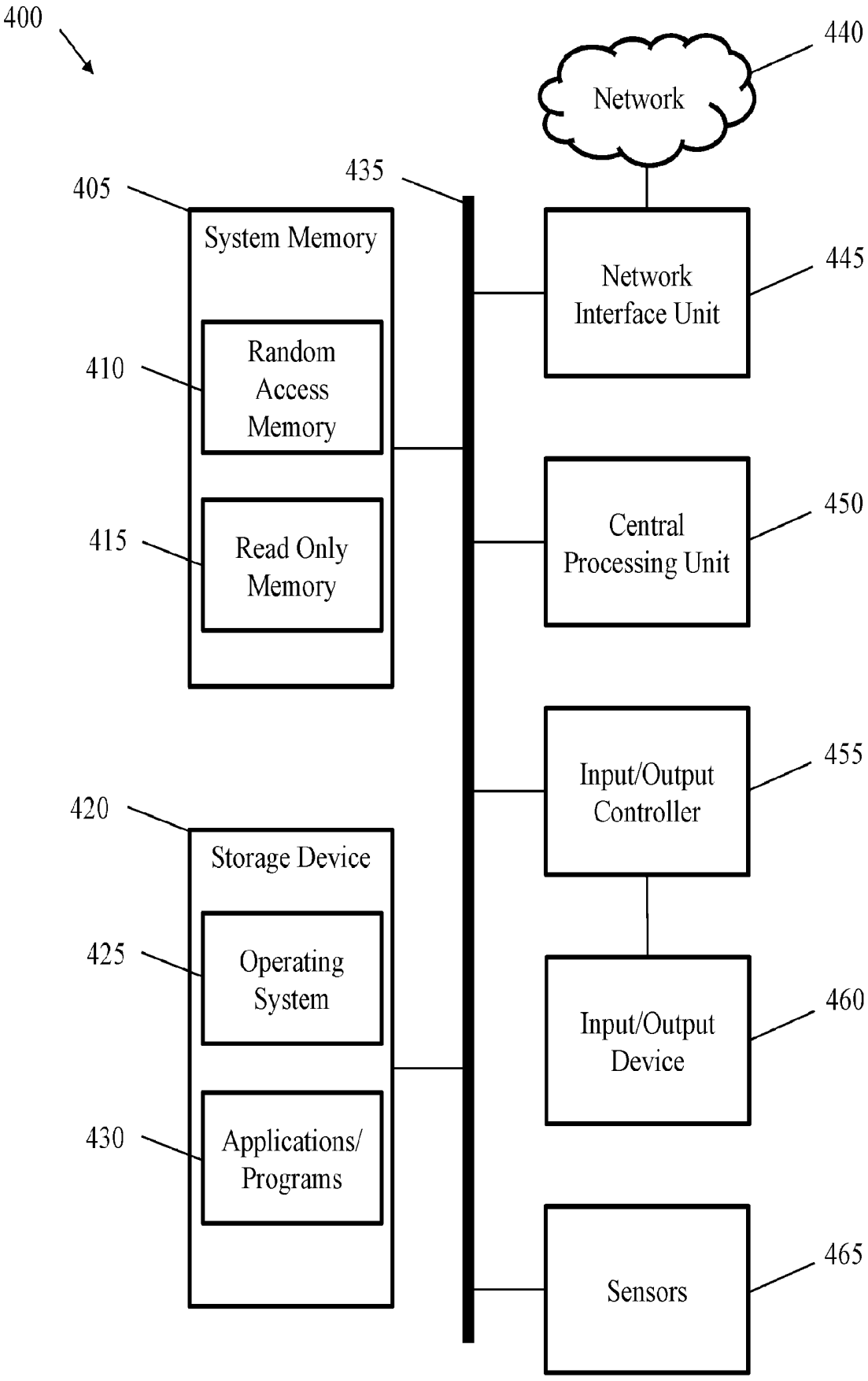
400
440
Network
435
405
System Memory
445
Network Interface Unit
410
Random Access Memory
415
Read Only Memory
450
Central Processing Unit
455
Input/Output Controller
420
Storage Device
425
Operating System
460
Input/Output Device
430
Applications/ Programs
465
Sensors

Fig. 4

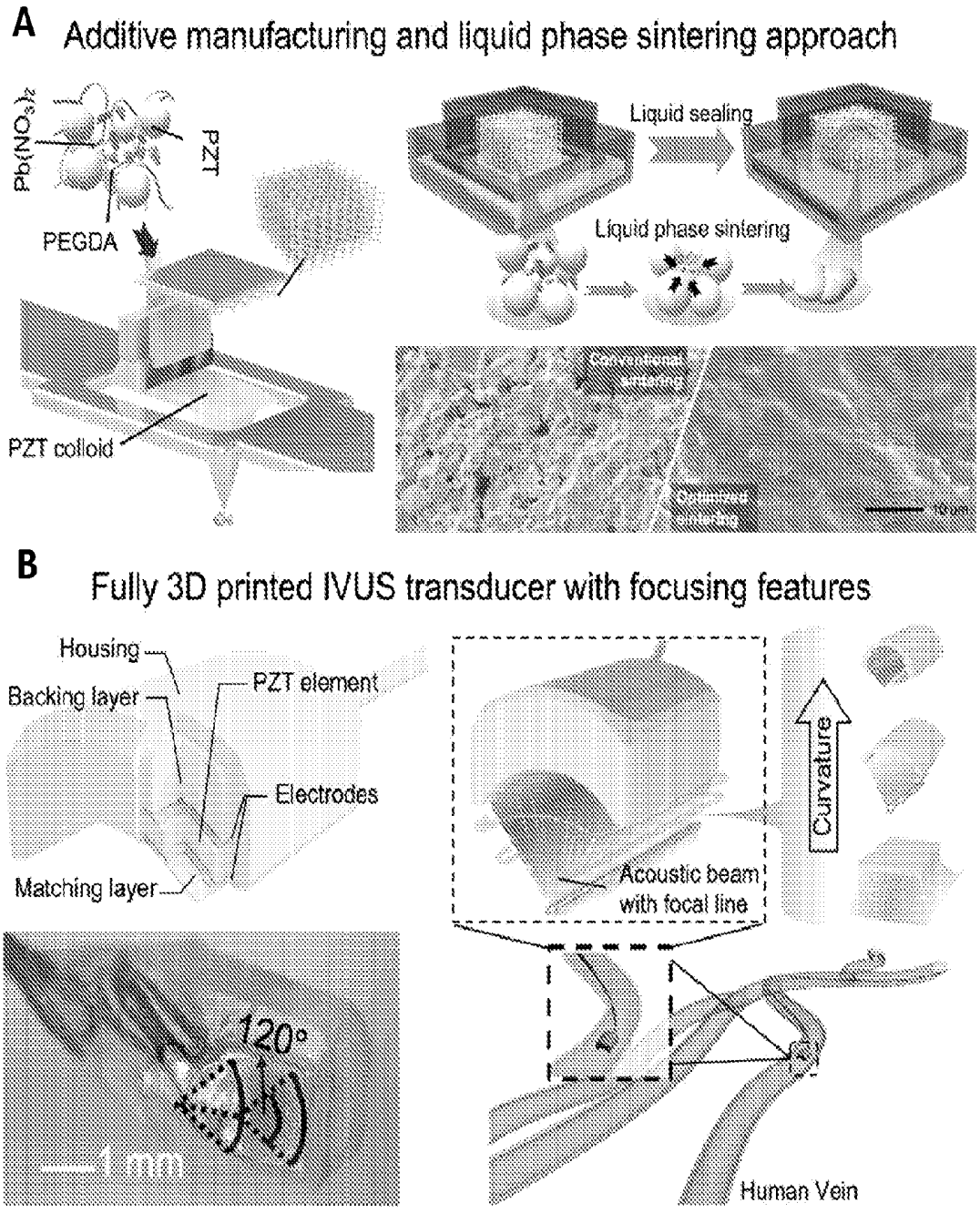
A
Additive manufacturing and liquid phase sintering approach
$Pb(NO_3)_2$
PZT
PEGDA
PZT colloid
Liquid sealing
Liquid phase sintering
B
Fully 3D printed IVUS transducer with focusing features
Housing
Backing layer
PZT element
Electrodes
Matching layer
120°
1 mm
Curvature
Acoustic beam with focal line
Human Vein
C
Ultrasound-enabled localized cavitation in blood vessel phantom
Blood vessel phantom
Target location
4.5 mm
Microbubble opening

Fig. 5

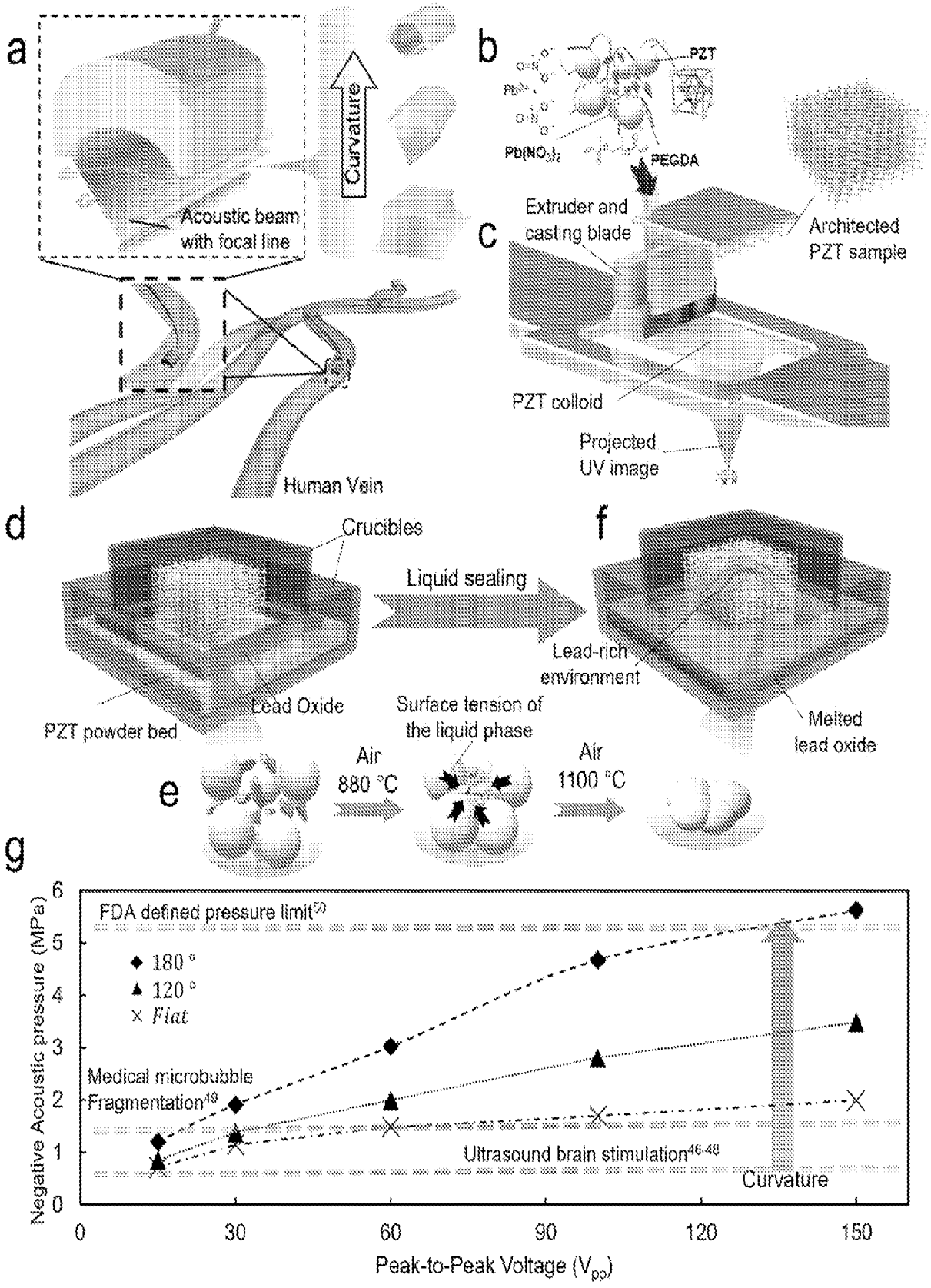
a
Curvature
Acoustic beam with focal line
Human Vein
b
PZT
$Pb(NO_3)_2$
PEGDA
c
Extruder and casting blade
Architected PZT sample
PZT colloid
Projected UV image
d
Crucibles
Liquid sealing
PZT powder bed
Lead Oxide
Surface tension of the liquid phase
f
Lead-rich environment
Melted lead oxide
e
Air
880 °C
Air
1100 °C
g
FDA defined pressure limit[50]
180 °
120 °
Flat
Medical microbubble Fragmentation[49]
Ultrasound brain stimulation[46-48]
Curvature
Negative Acoustic pressure (MPa)
Peak-to-Peak Voltage ($V_{pp}$)
0
1
2
3
4
5
6
0
30
60
90
120
150

Fig. 6

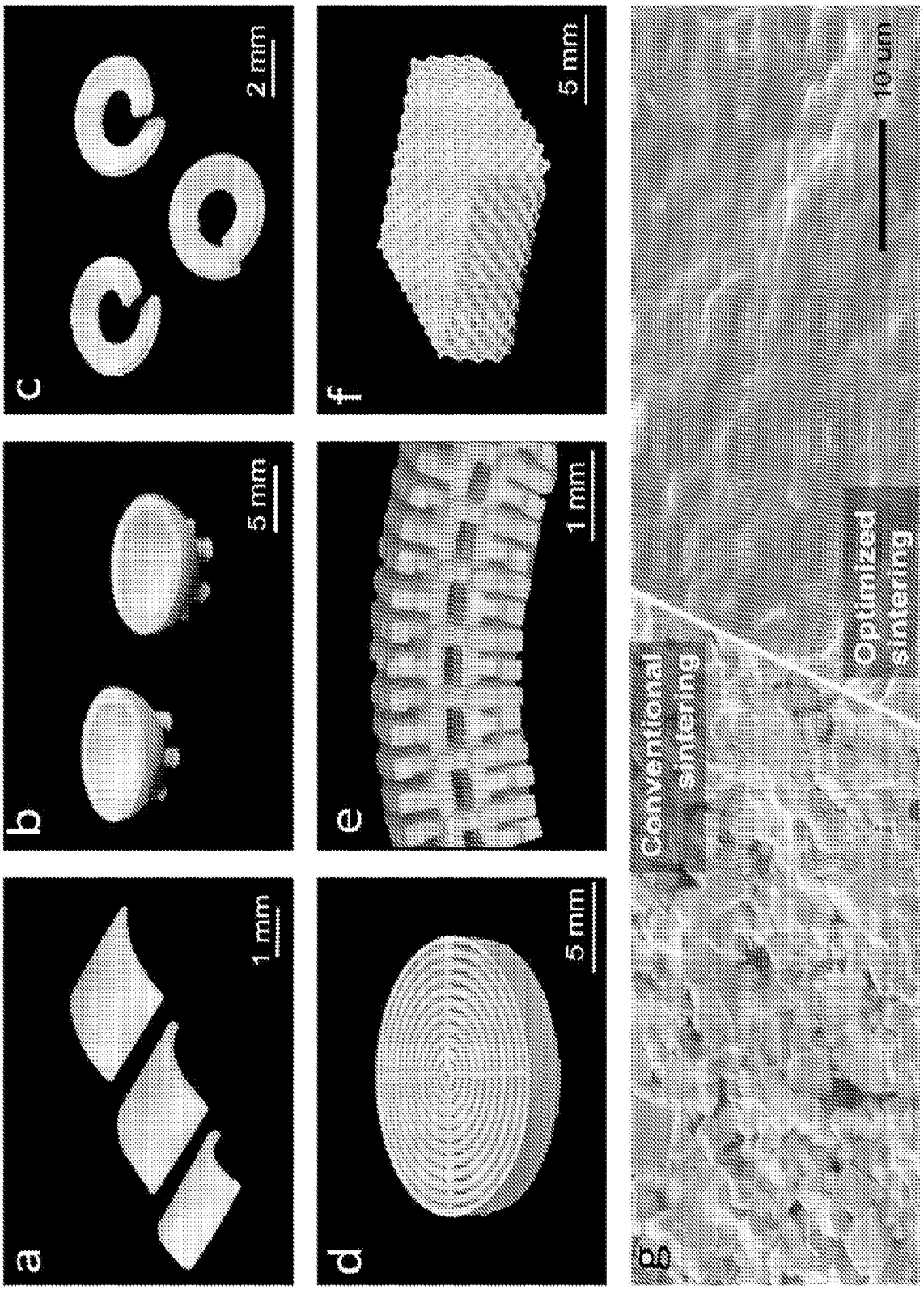
a
1 mm
b
5 mm
c
2 mm
d
5 mm
e
1 mm
f
5 mm
g
Conventional sintering
Optimized sintering
10 um

Fig. 7

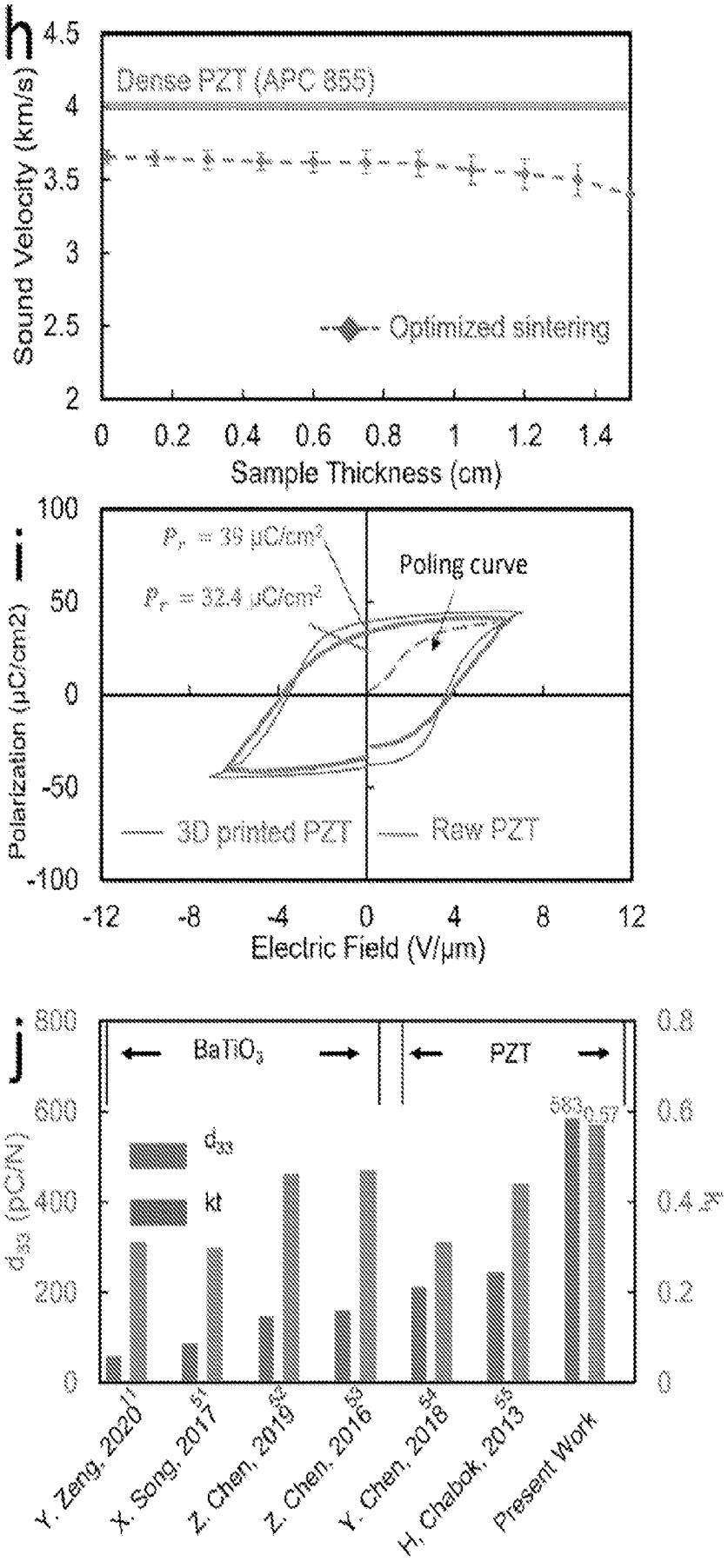
h
Sound Velocity (km/s)
Dense PZT (APC 855)
Optimized sintering
Sample Thickness (cm)
i
Polarization (μC/cm2)
$P_r$ = 39 μC/cm²
$P_r$ = 32.4 μC/cm²
Poling curve
3D printed PZT
Raw PZT
Electric Field (V/μm)
j
$d_{33}$ (pC/N)
BaTiO3
PZT
$d_{33}$
kt
583
0.57
Y. Zeng, 2020 [11]
X. Song, 2017 [51]
Z. Chen, 2019 [52]
Z. Chen, 2016 [53]
Y. Chen, 2018 [54]
H. Chabok, 2013 [55]
Present Work

Fig. 7 (cont.)

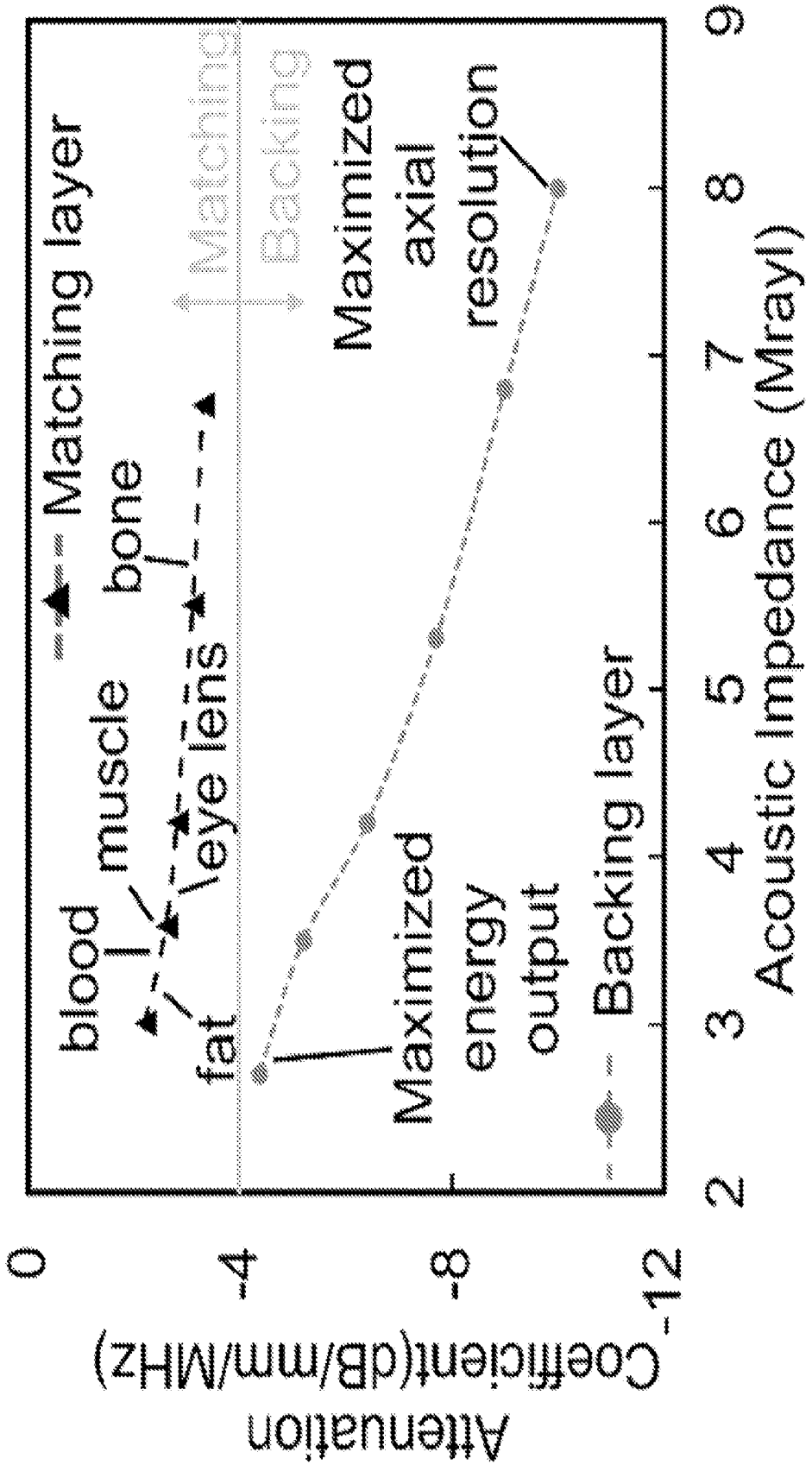
Attenuation Coefficient(dB/mm/MHz)
0
-4
-8
-12
2
3
4
5
6
7
8
9
Acoustic Impedance (Mrayl)
Matching layer
blood
muscle
bone
fat
eye lens
Backing layer
Maximized energy output
Maximized axial resolution
Matching
Backing

Fig. 8A

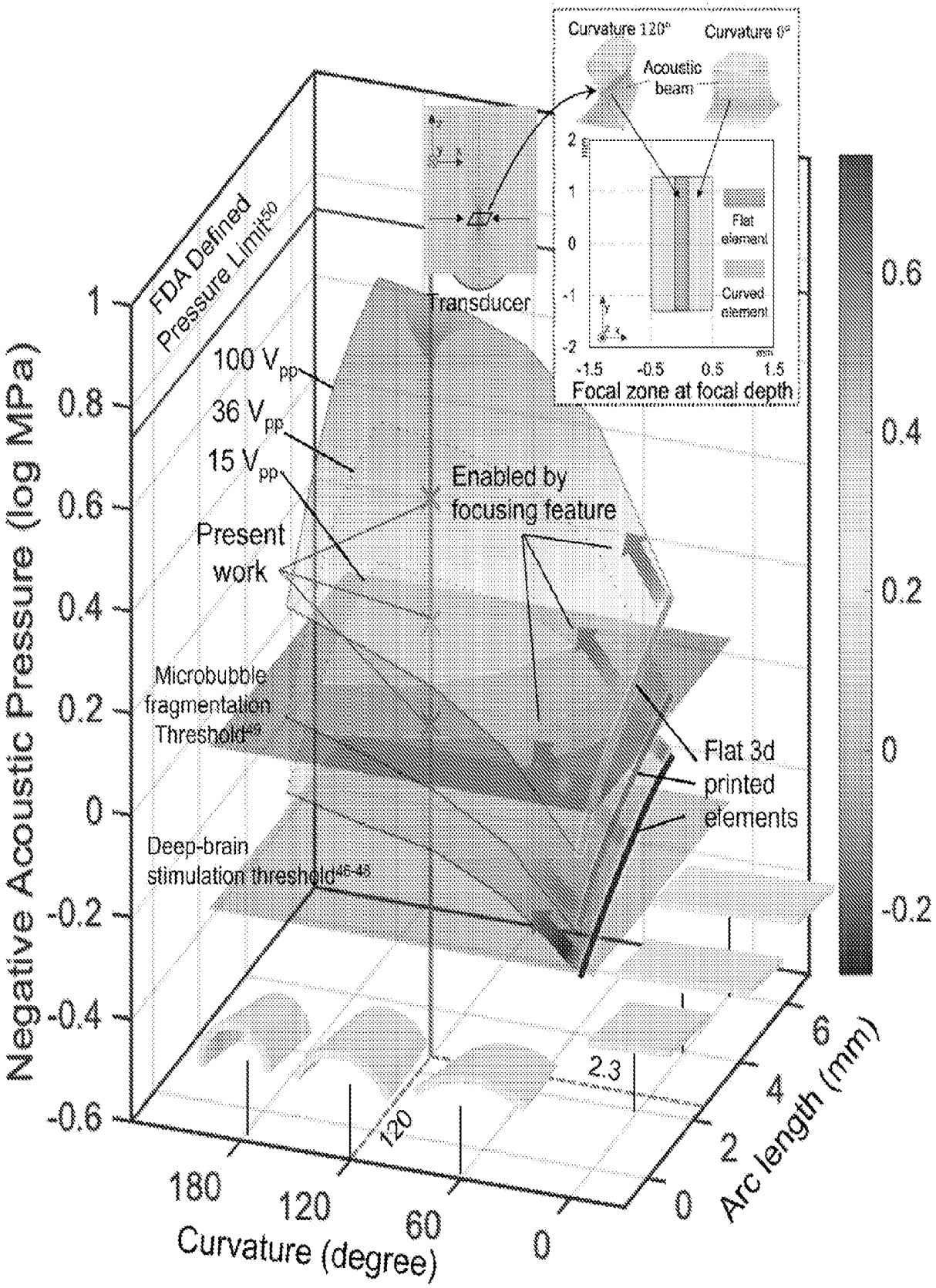
Curvature 120°
Curvature 6°
Acoustic beam
Flat element
Curved element
Focal zone at focal depth
Transducer
FDA Defined Pressure Limit[50]
100 Vpp
36 Vpp
15 Vpp
Present work
Enabled by focusing feature
Microbubble fragmentation Threshold[48]
Deep-brain stimulation threshold[46-48]
Flat 3d printed elements
Negative Acoustic Pressure (log MPa)
Curvature (degree)
Arc length (mm)

Fig. 8B

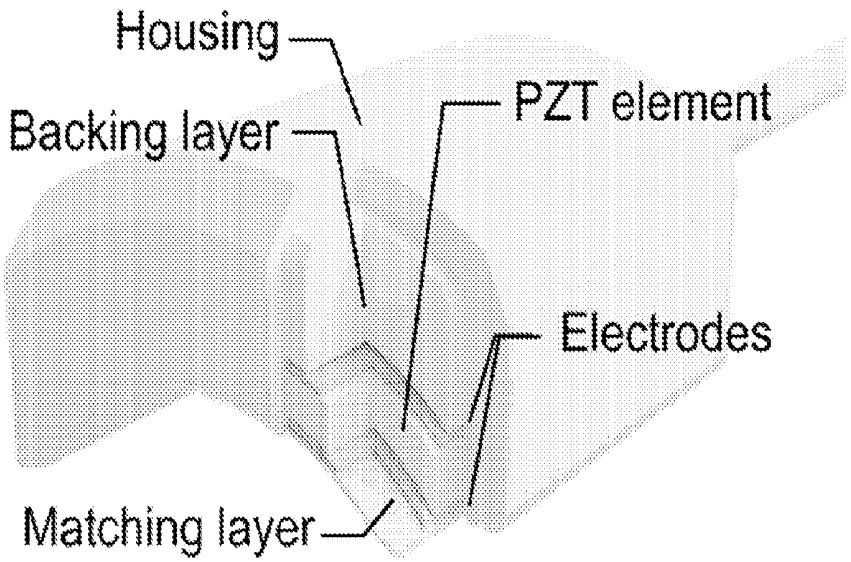
Housing
Backing layer
PZT element
Electrodes
Matching layer

Fig. 8C

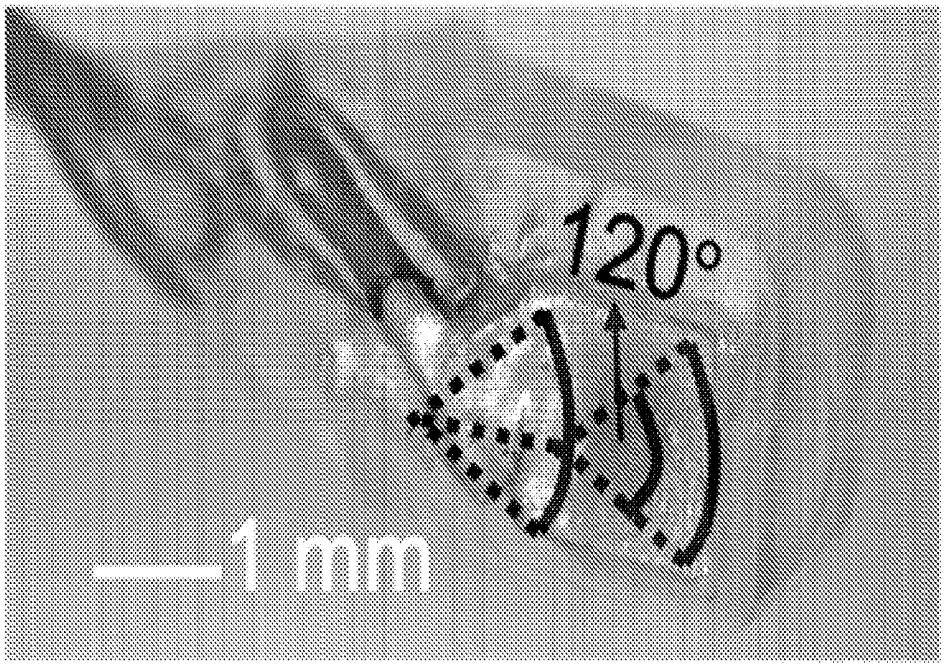
120°
1 mm

Fig. 8D

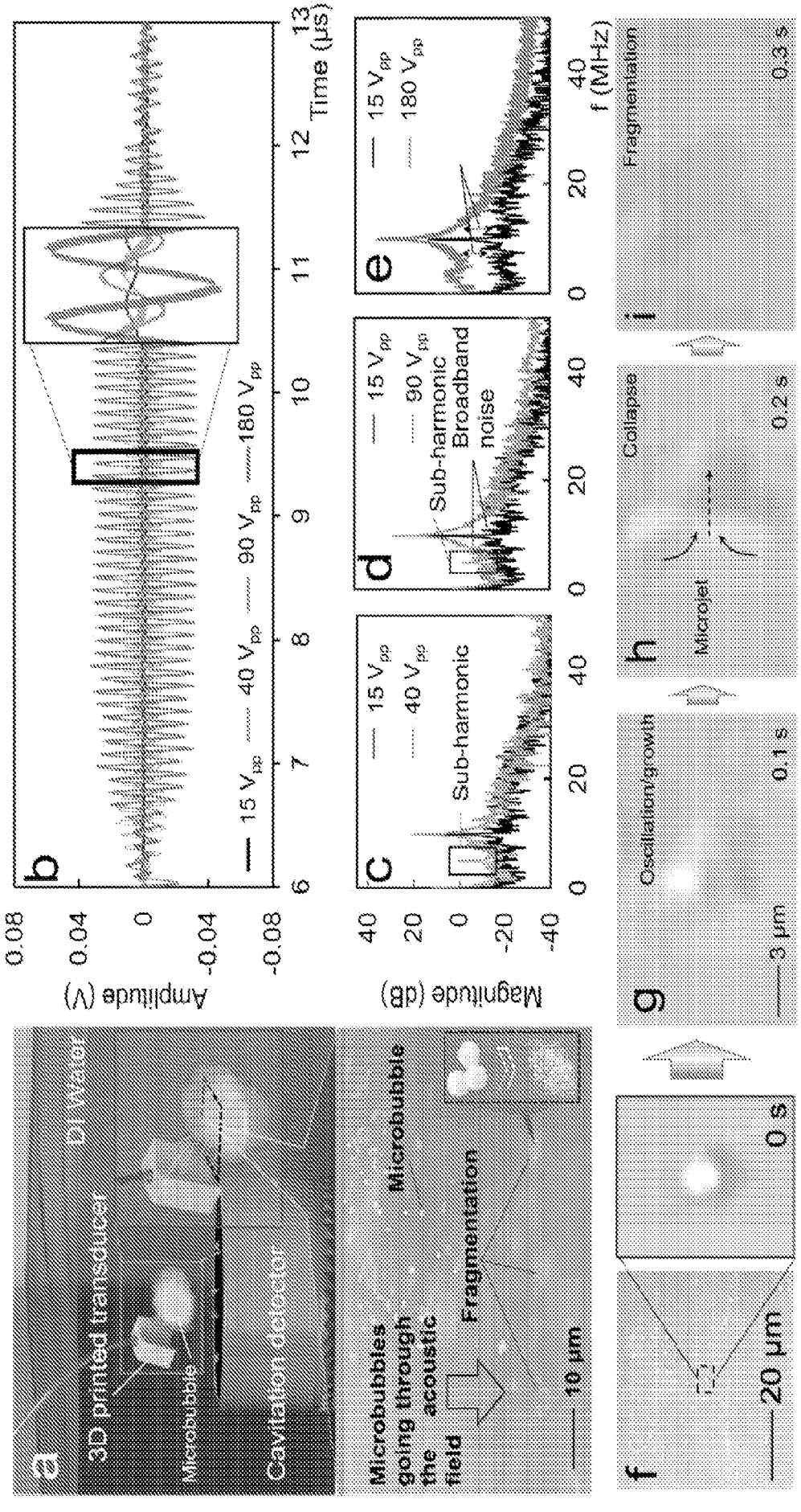
a
3D printed transducer
DI Water
Microbubbles
Cavitation activity
Microbubbles going through the acoustic field
Fragmentation
10 µm
b
Amplitude (V)
Time (µs)
15 Vpp
40 Vpp
90 Vpp
180 Vpp
c
Sub-harmonic
d
Sub-harmonic
Broadband noise
e
f (MHz)
f
20 µm
0 s
g
Oscillation/growth
3 µm
0.1 s
h
Collapse
Microjet
0.2 s
i
Fragmentation
0.3 s

Fig. 9

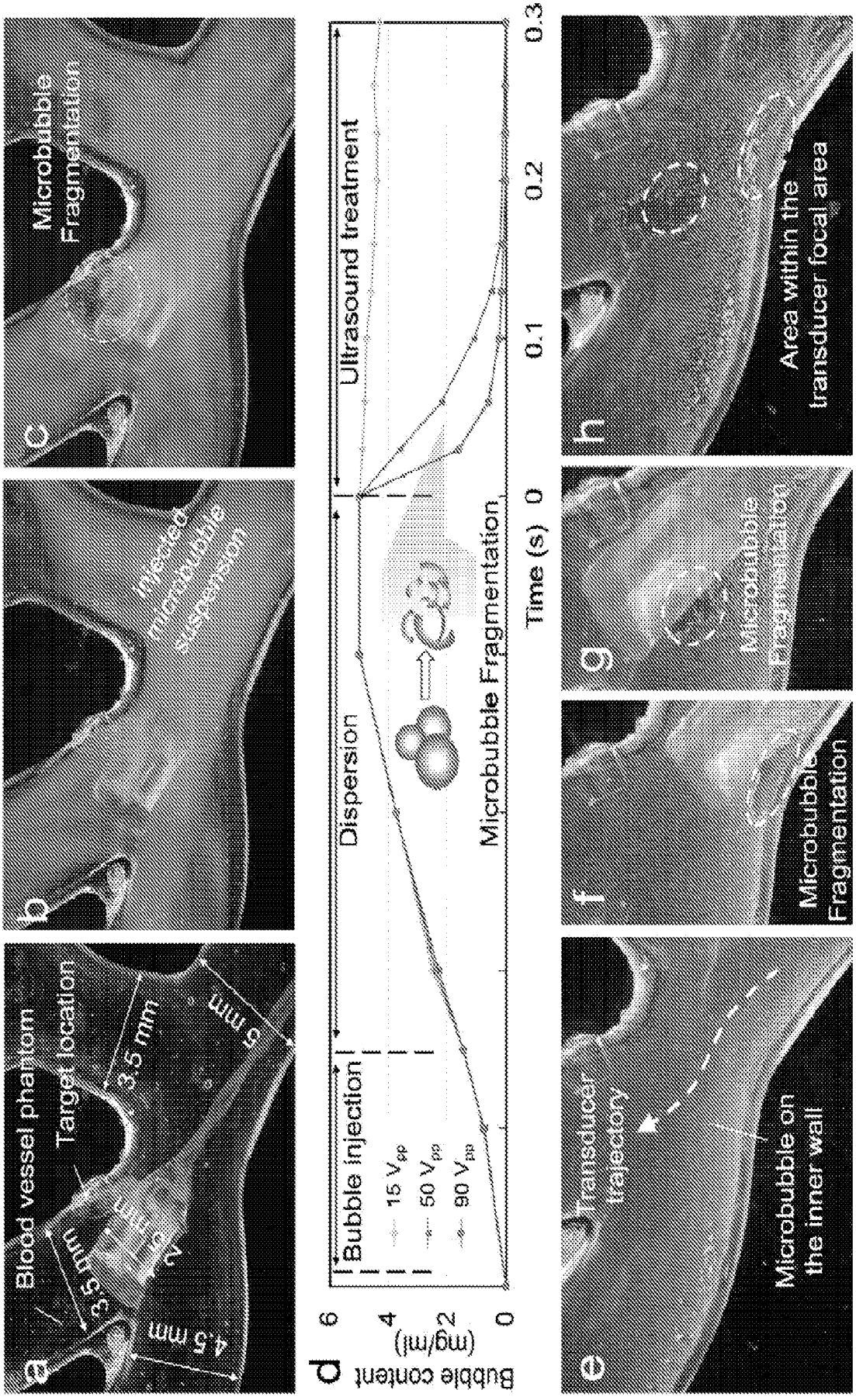
a
Blood vessel phantom
Target location
3.5 mm
5 mm
4.5 mm
b
Injected microbubble suspension
c
Microbubble Fragmentation
d
Bubble content (mg/ml)
Bubble injection
Dispersion
Ultrasound treatment
15 Vpp
50 Vpp
90 Vpp
Microbubble Fragmentation
Time (s)
e
Transducer trajectory
Microbubble on the inner wall
f
Microbubble Fragmentation
g
Microbubble Fragmentation
h
Area within the transducer focal area

Fig. 10

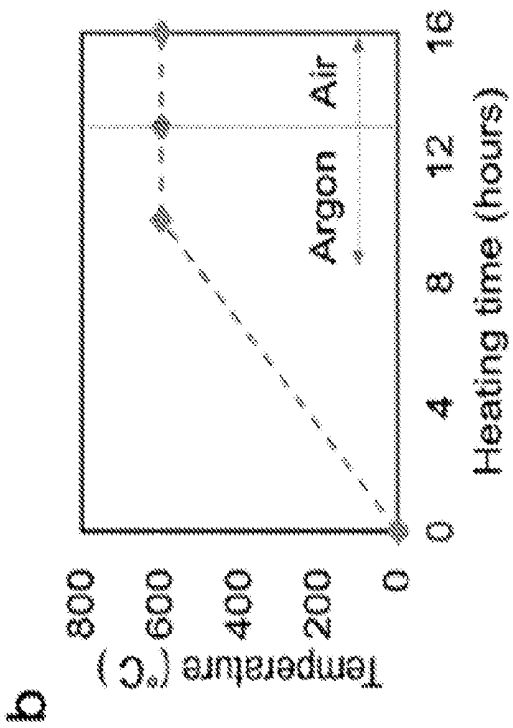
b
Temperature (°C)
800
600
400
200
0
0
4
8
12
16
Heating time (hours)
Argon
Air

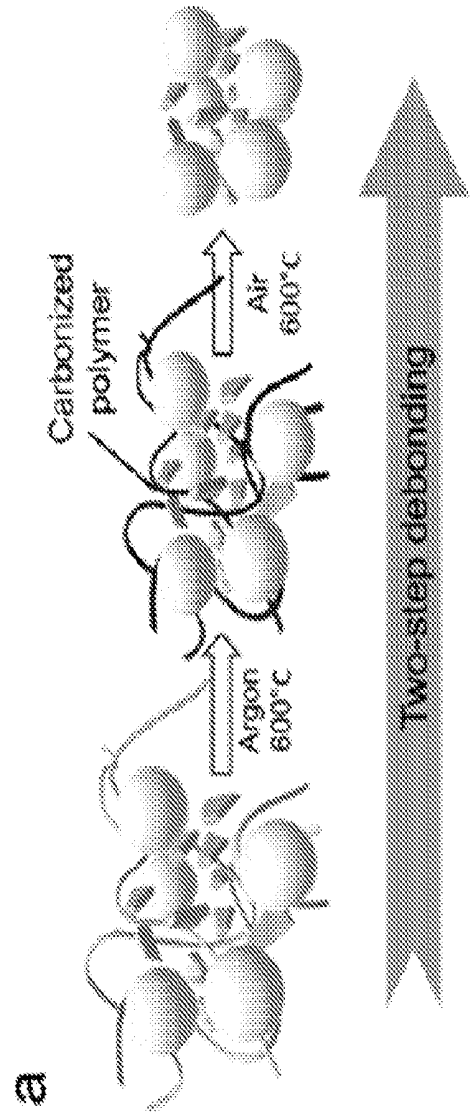
a
Argon
600°C
Carbonized
polymer
Air
600°C
Two-step debonding

Fig. 11

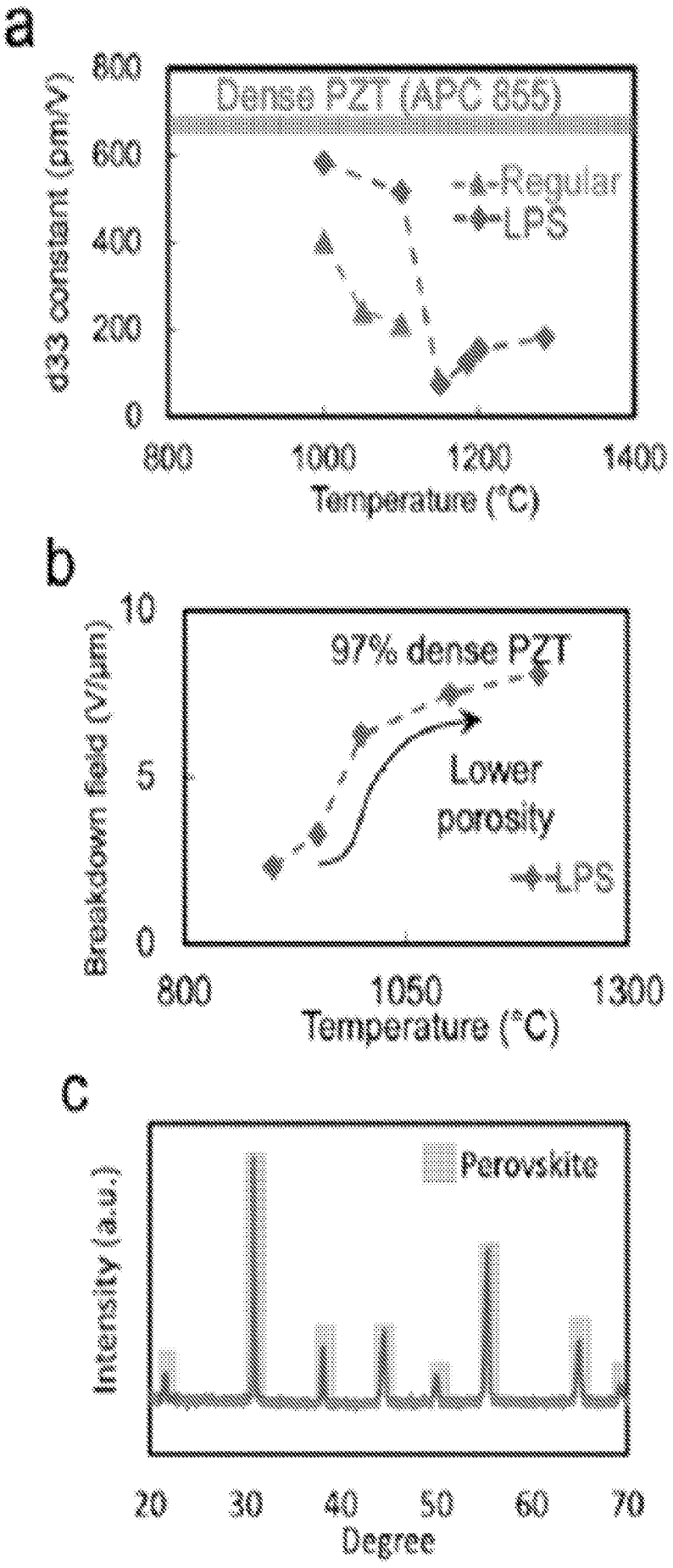
a
Dense PZT (APC 855)
Regular
LPS
d33 constant (pm/V)
800
600
400
200
0
800
1000
1200
1400
Temperature (°C)
b
97% dense PZT
Lower porosity
LPS
Breakdown field (V/μm)
10
5
0
800
1050
1300
Temperature (°C)
c
Perovskite
Intensity (a.u.)
20
30
40
50
60
70
Degree

Fig. 12

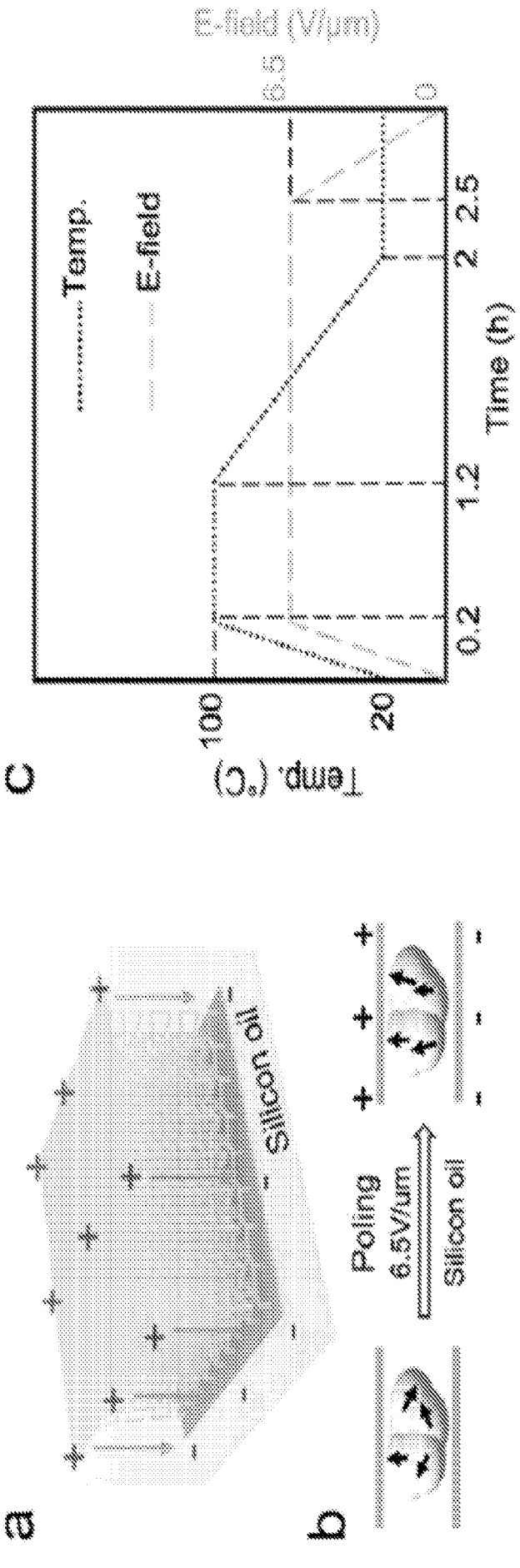
c
Temp. (°C)
100
20
E-field (V/μm)
6.5
0
Temp.
E-field
0.2
1.2
2
2.5
Time (h)
a
Silicon oil
b
Poling
6.5V/um
Silicon oil

Fig. 13

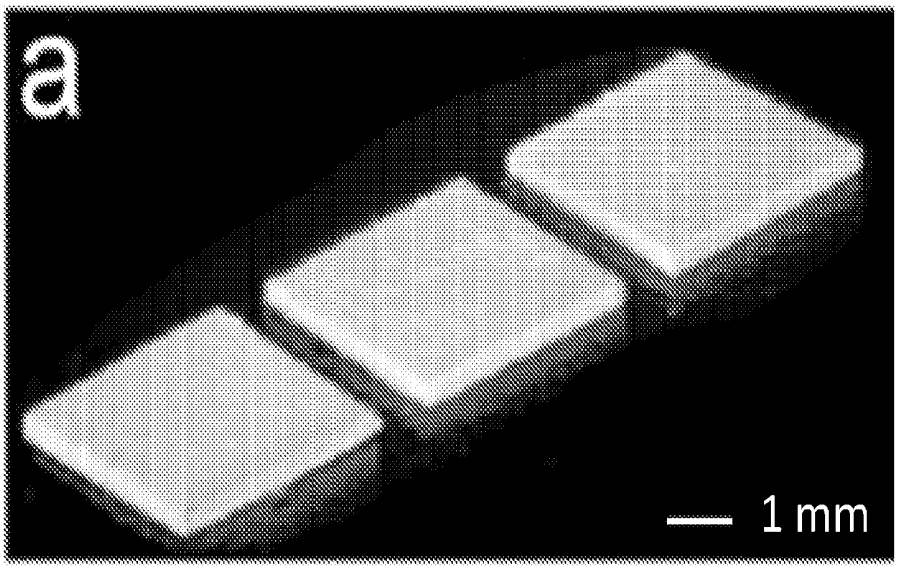
a
1 mm

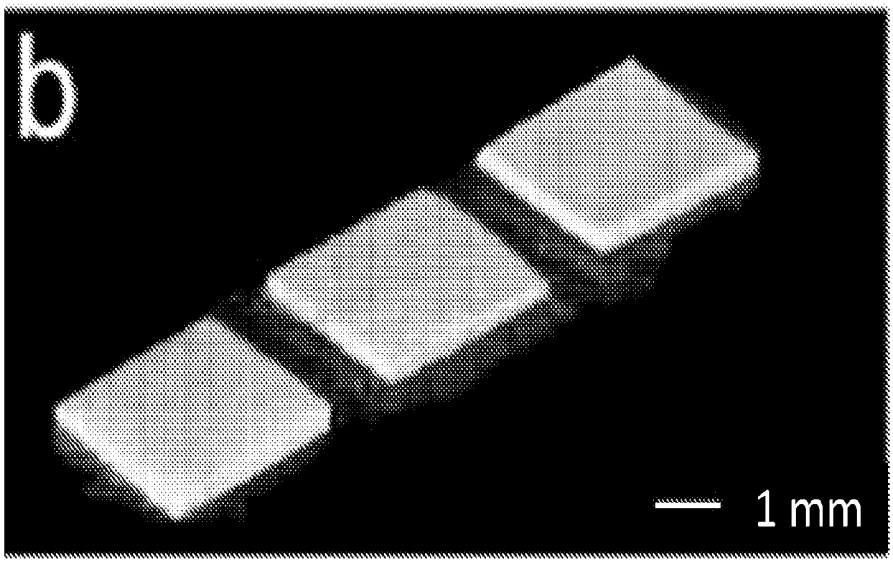
b
1 mm

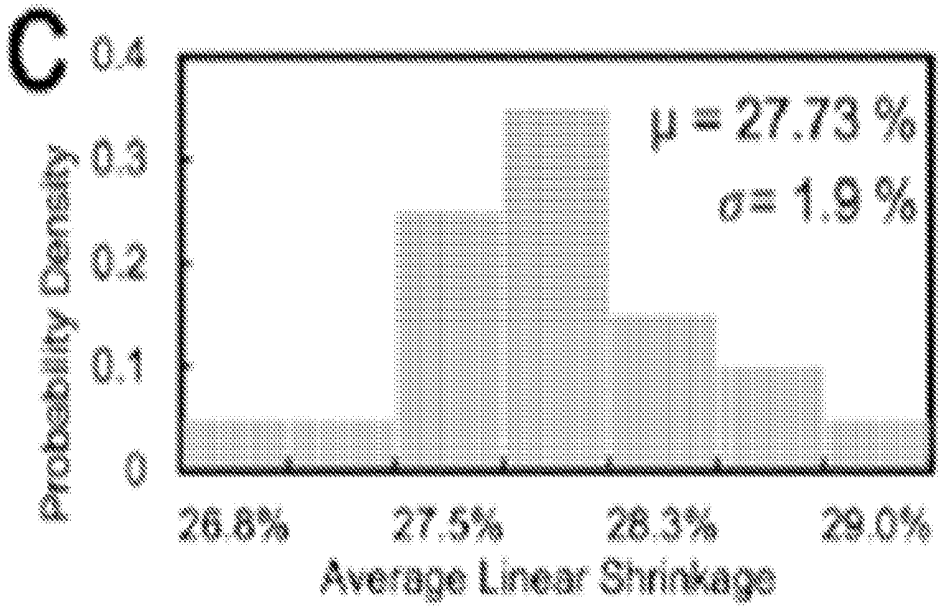
C
0.4
0.3
0.2
0.1
0
Probability Density
μ = 27.73 %
σ = 1.9 %
26.8%
27.5%
28.3%
29.0%
Average Linear Shrinkage

Fig. 14 (cont.)

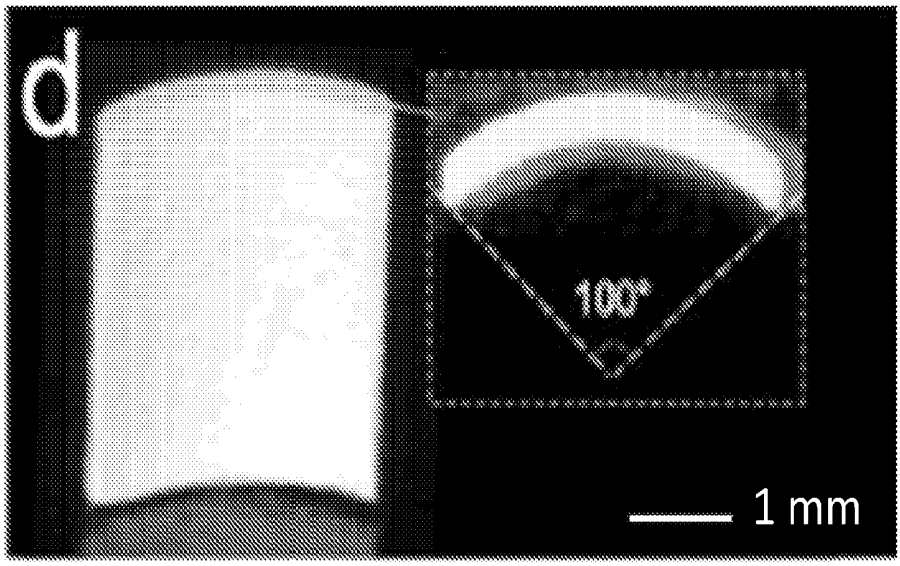
d
100°
1 mm

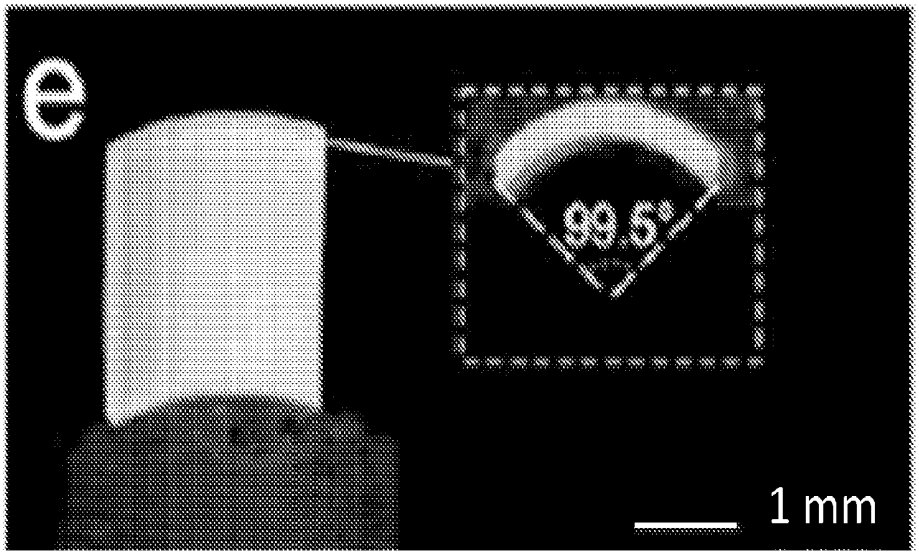
e
99.5°
1 mm

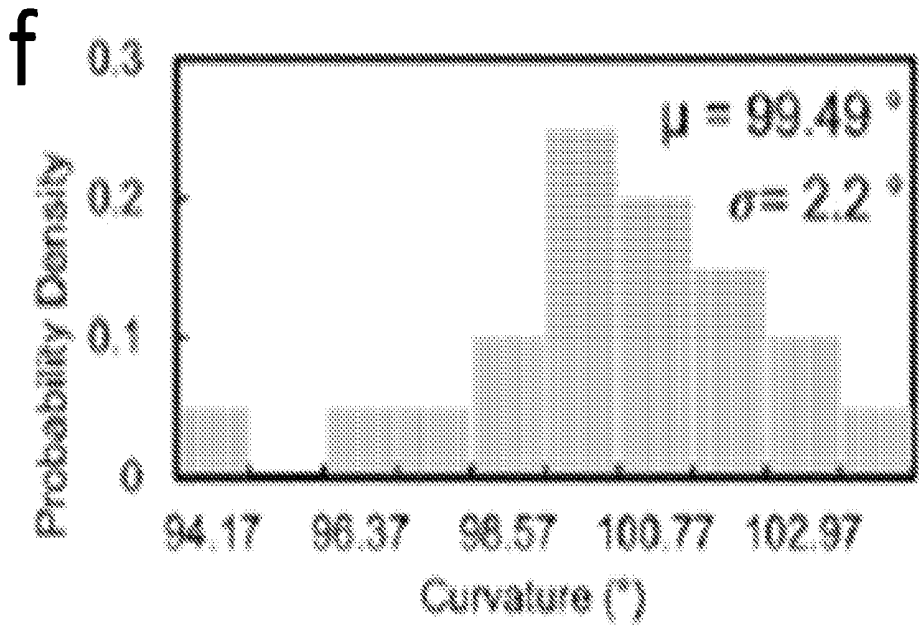
f
0.3
0.2
0.1
0
Probability Density
μ = 99.49 °
σ = 2.2 °
94.17
96.37
98.57
100.77
102.97
Curvature (°)

Fig. 14 (cont.)

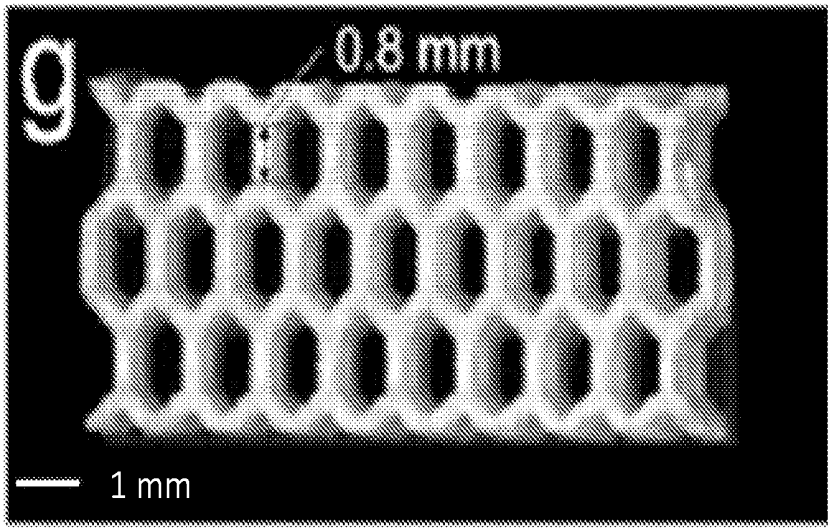
g
0.8 mm
1 mm

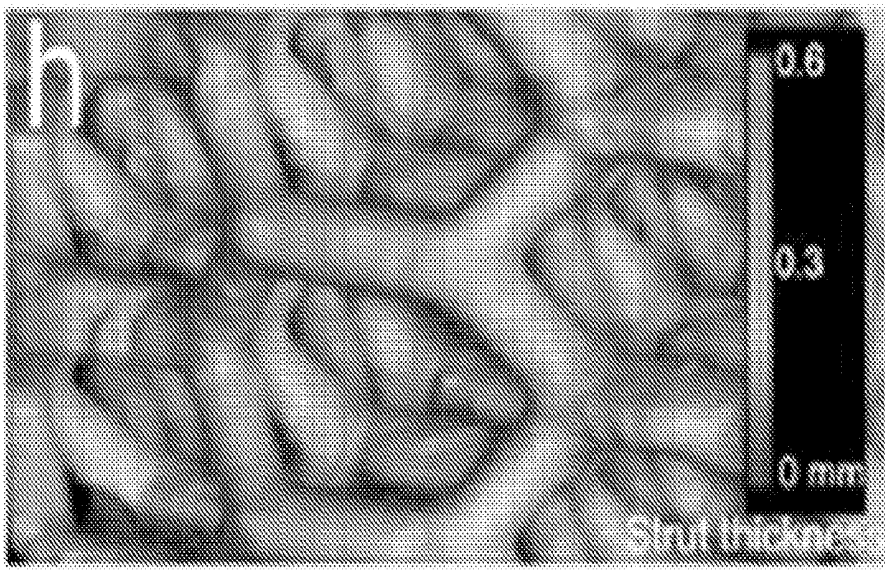
h
0.6
0.3
0 mm
Strut Thickness

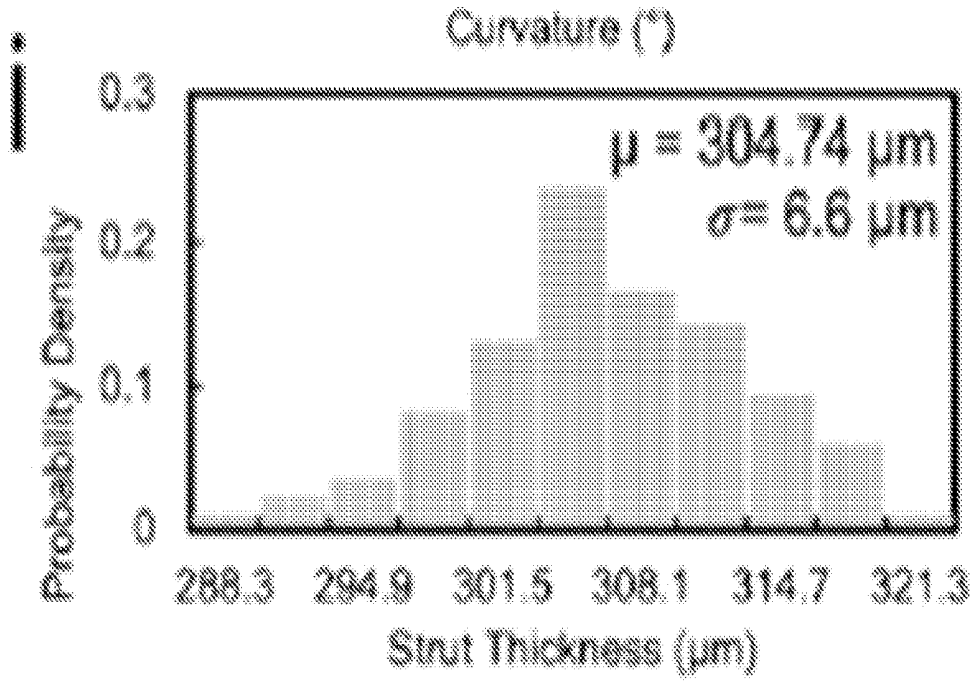
i
Curvature (°)
μ = 304.74 μm
σ = 6.6 μm
Probability Density
0.3
0.2
0.1
0
288.3
294.9
301.5
308.1
314.7
321.3
Strut Thickness (μm)

Fig. 14 (cont.)

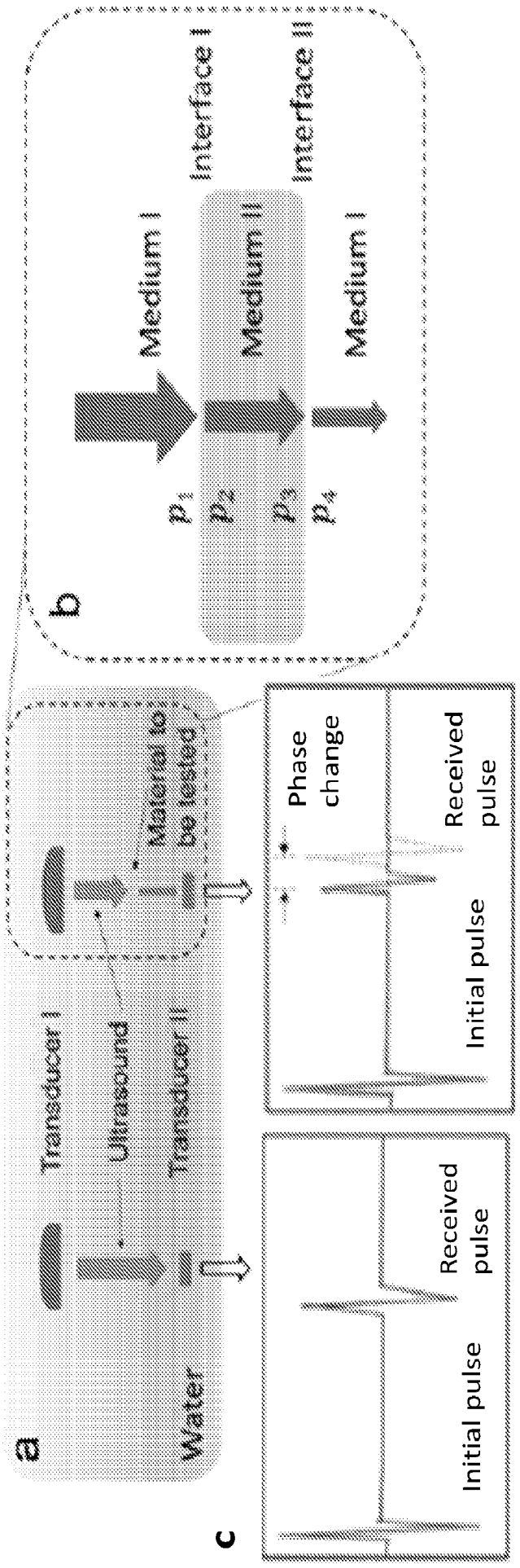
a
Water
Transducer I
Ultrasound
Transducer II
Material to be tested
b
Medium I
Medium II
Medium I
Interface I
Interface II
$p_1$
$p_2$
$p_3$
$p_4$
c
Initial pulse
Received pulse
Initial pulse
Phase change
Received pulse

Fig. 15

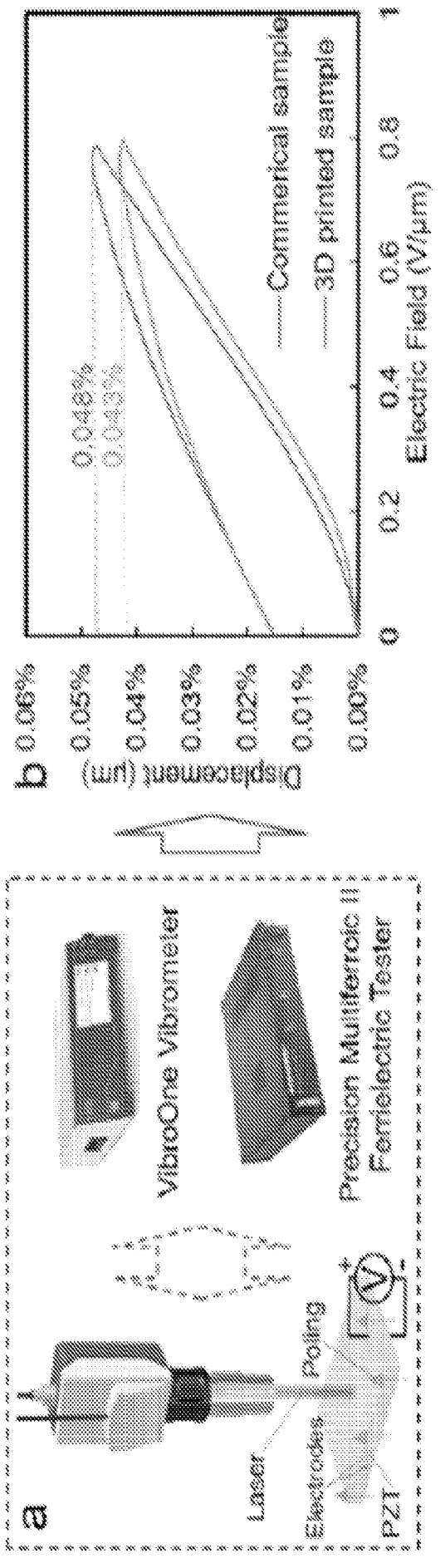
a
Laser
Electrodes
PZT
Poling
VibroOne Vibrometer
Precision Multiferroic II
Ferroelectric Tester
b
Displacement (μm)
0.06%
0.05%
0.04%
0.03%
0.02%
0.01%
0.00%
0
0.2
0.4
0.6
0.8
1
Electric Field (V/μm)
0.046%
0.043%
Commerical sample
3D printed sample

Fig. 16

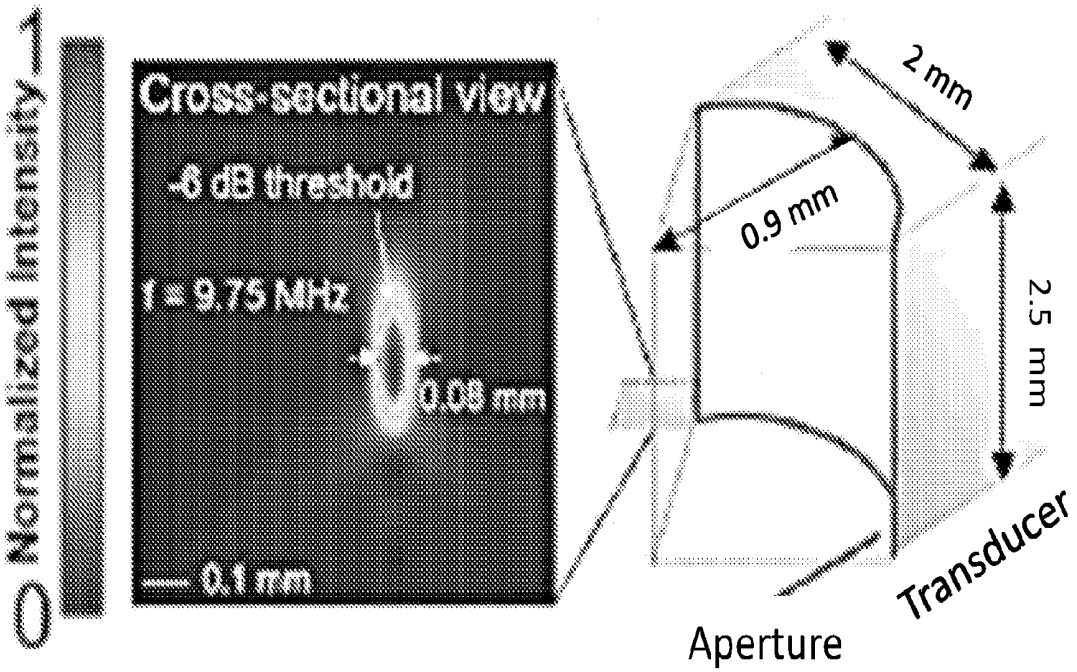


Fig. 17A

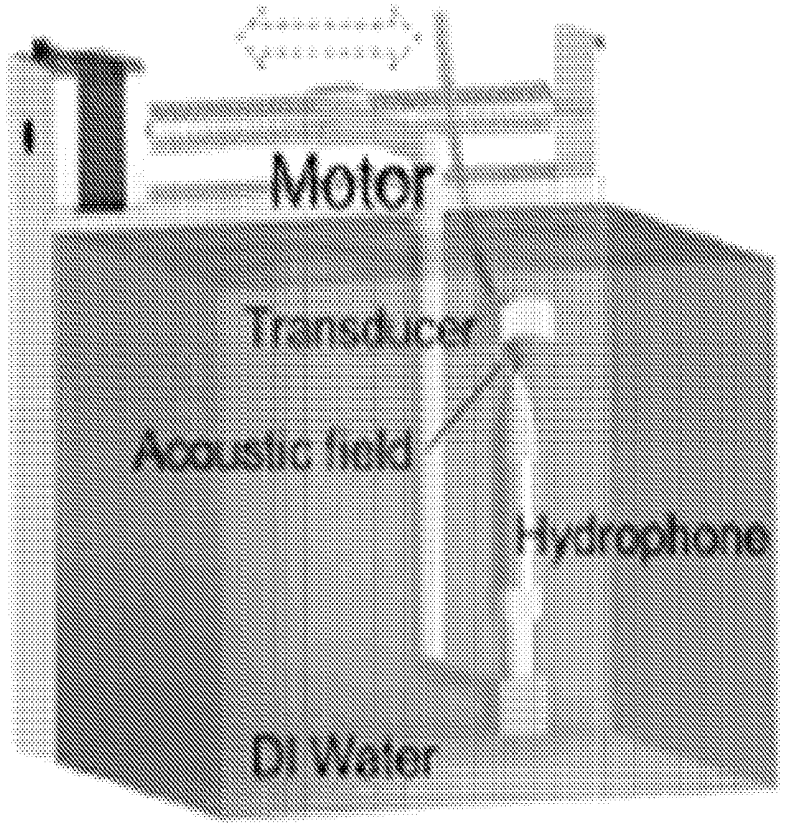


Fig. 17B

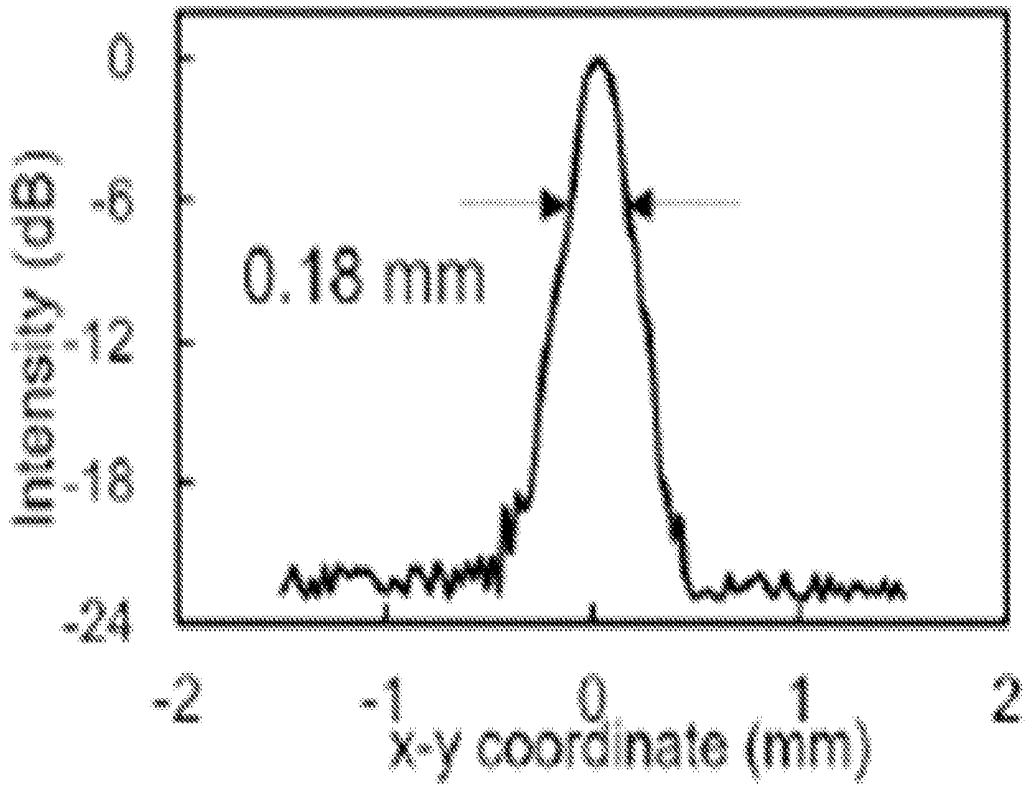


Fig. 17C

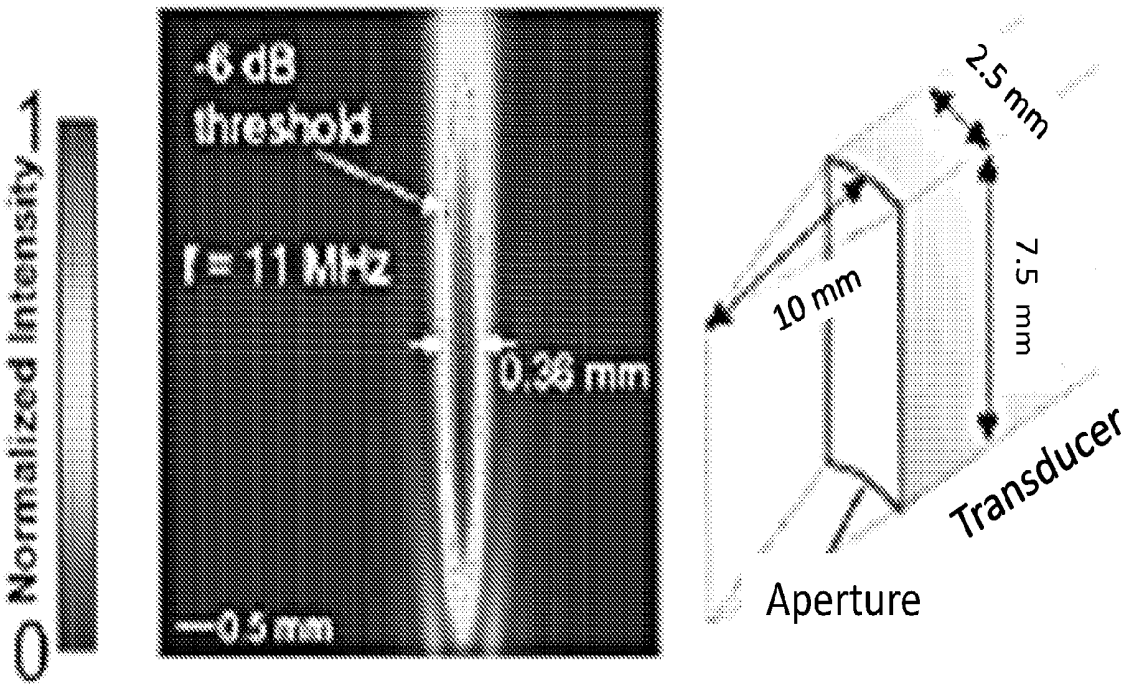


Fig. 17D

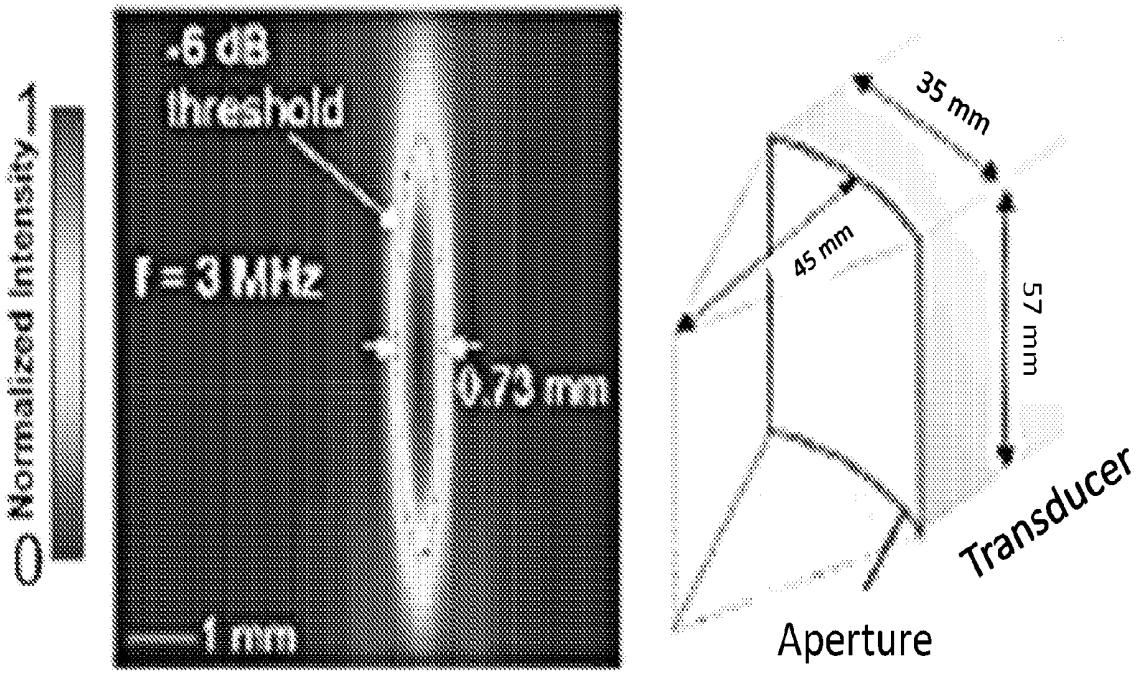


Fig. 17E

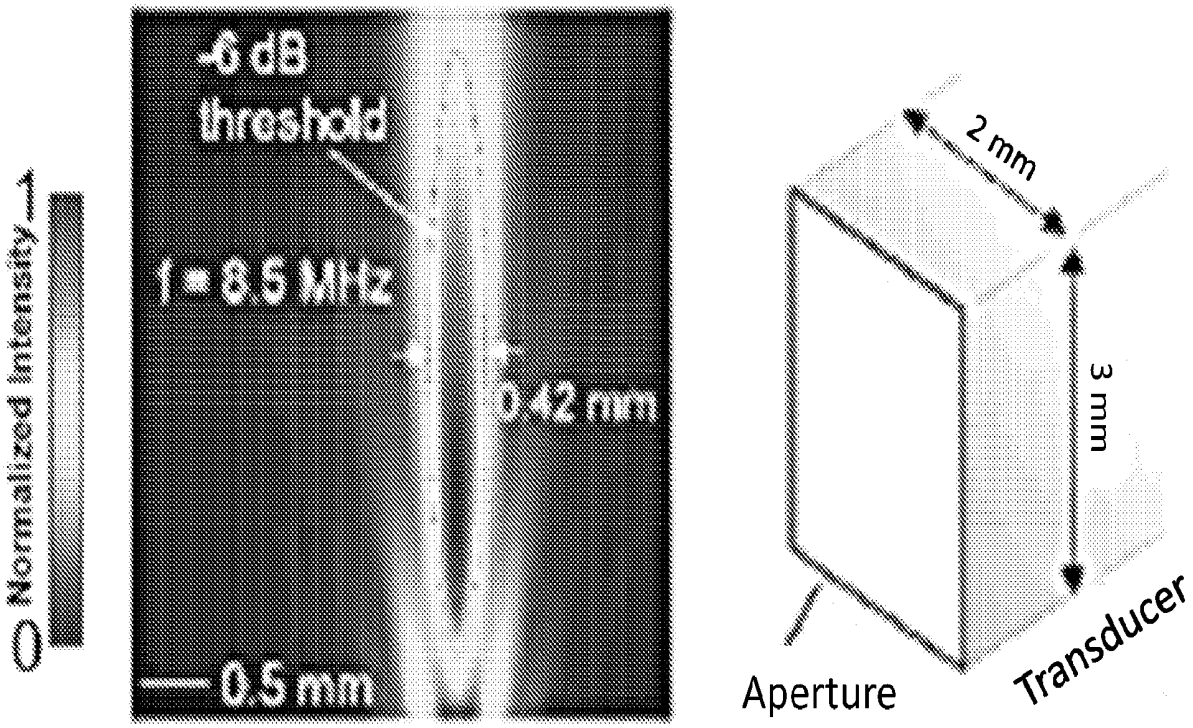


Fig. 17F

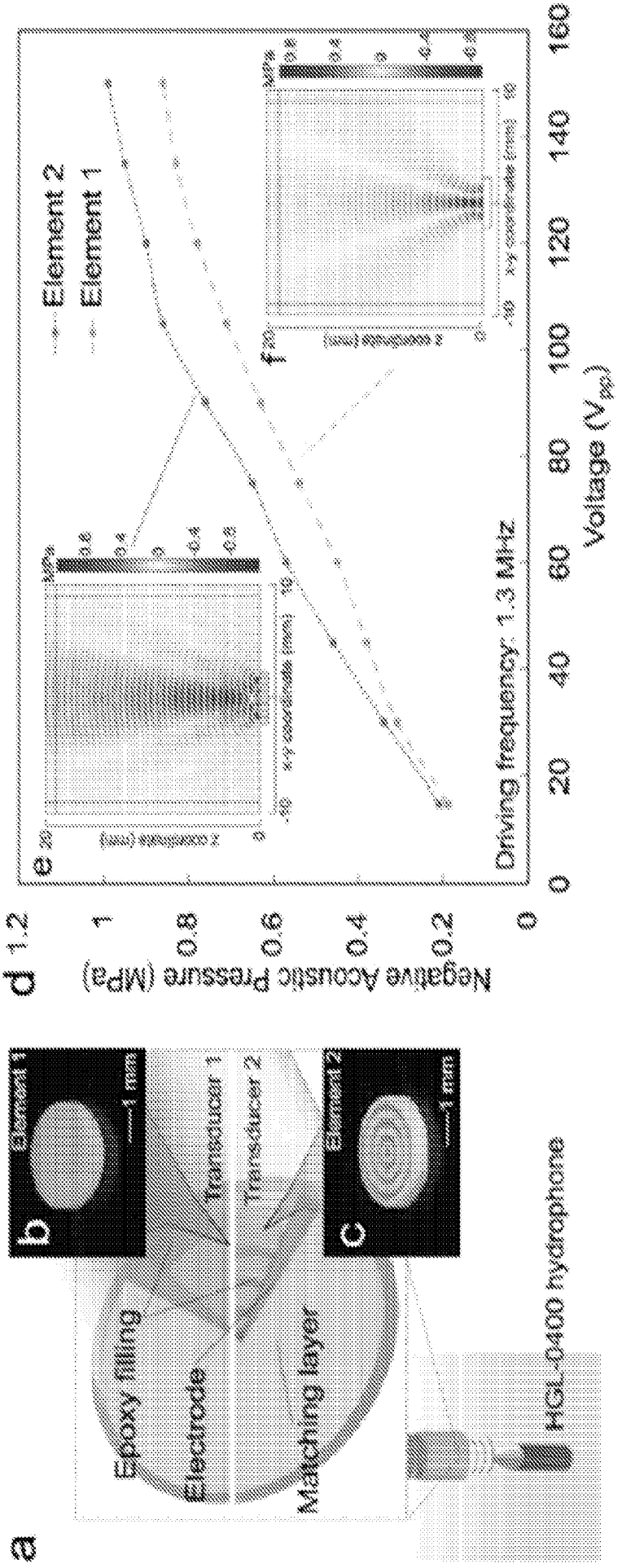
a
b
Element 1
1 mm
c
Element 2
1 mm
Epoxy filling
Electrode
Transducer 1
Transducer 2
Matching layer
HGL-0400 hydrophone
d
Negative Acoustic Pressure (MPa)
Voltage ($V_{pp}$)
Element 2
Element 1
Driving frequency: 1.3 MHz
e
f

Fig. 18

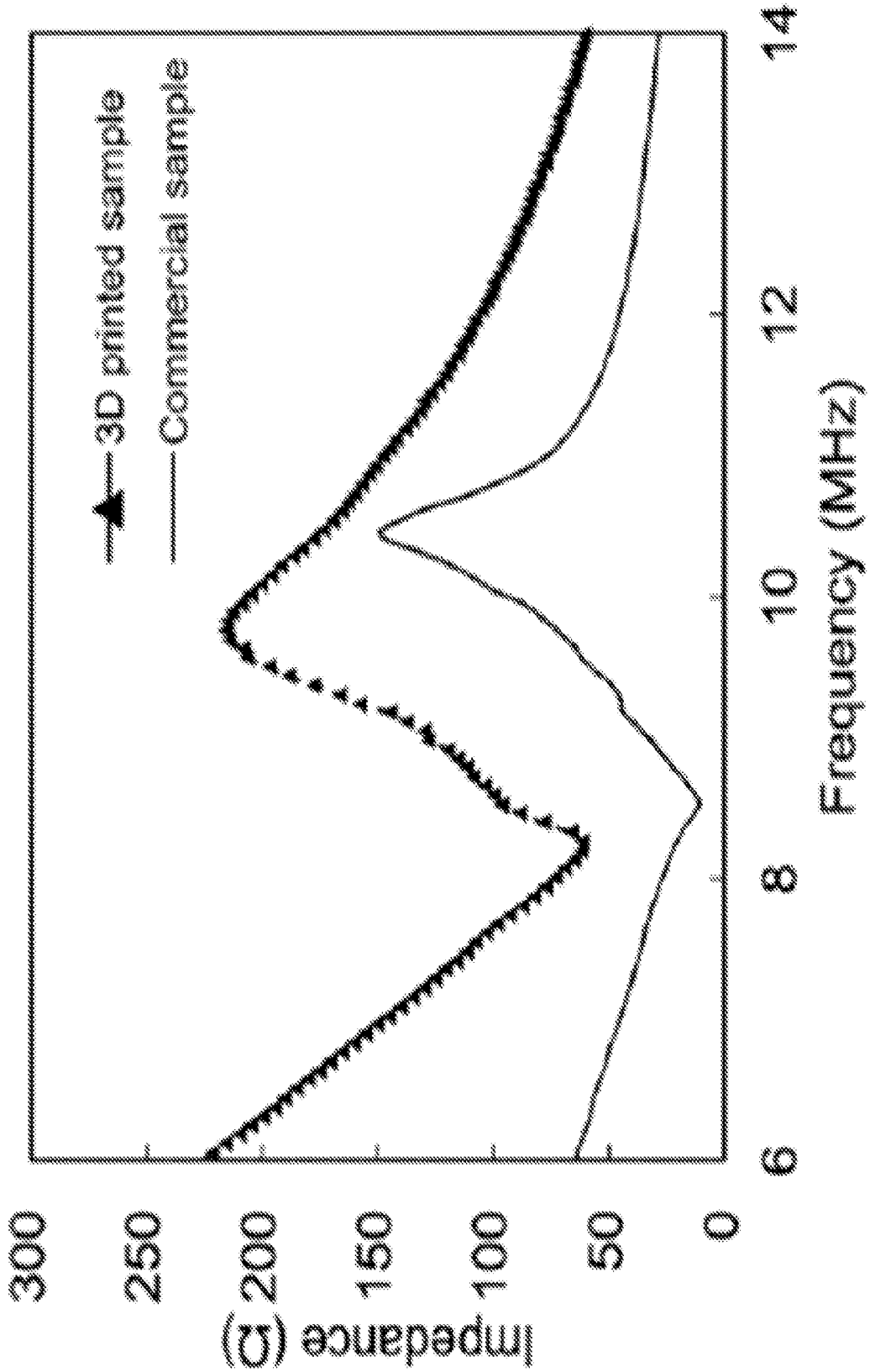
3D printed sample
Commercial sample
Impedance (Ω)
300
250
200
150
100
50
0
6
8
10
12
14
Frequency (MHz)

Fig. 19

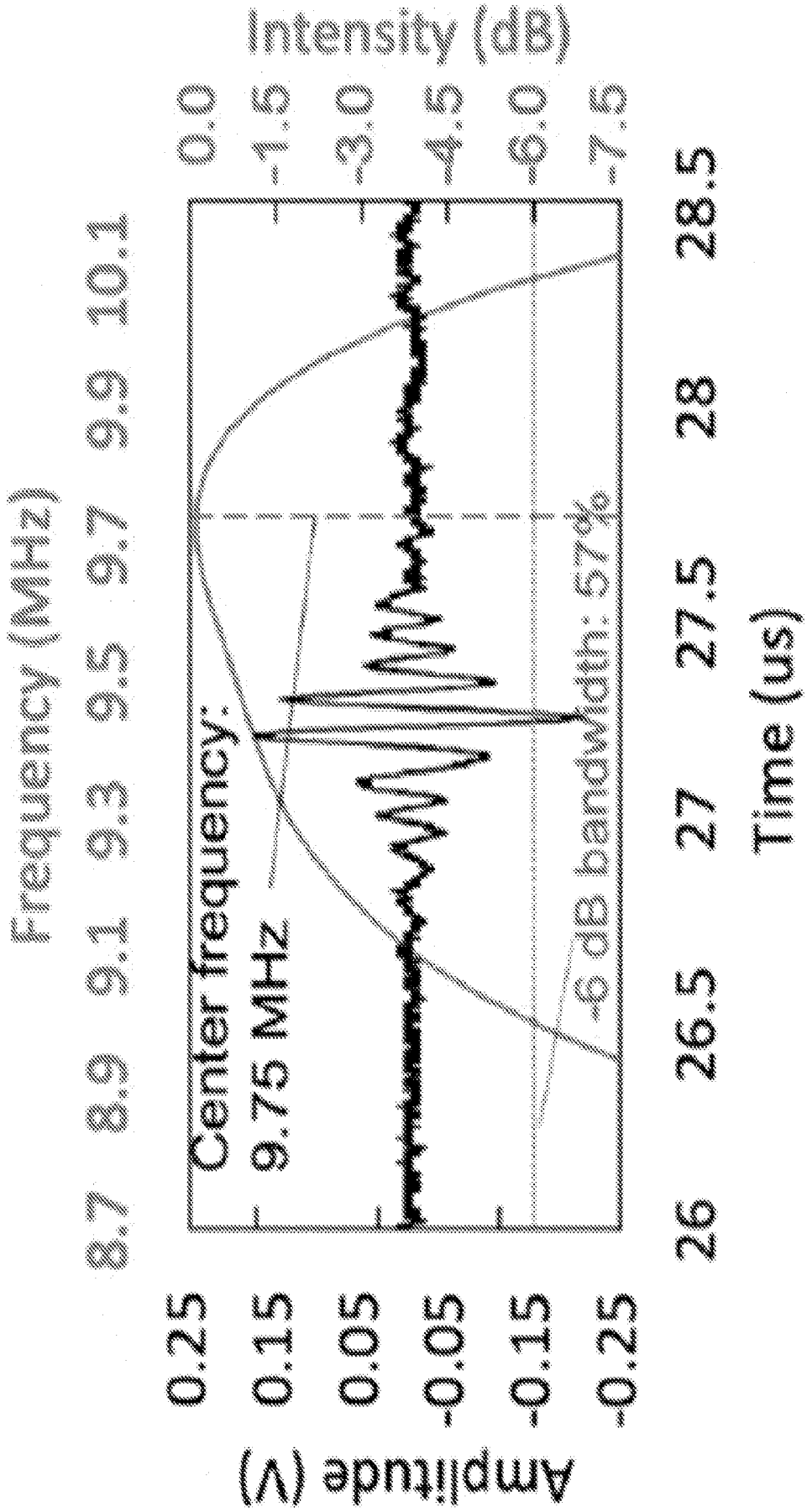
Intensity (dB)
0.0
-1.5
-3.0
-4.5
-6.0
-7.5
Frequency (MHz)
8.7
8.9
9.1
9.3
9.5
9.7
9.9
10.1
Center frequency:
9.75 MHz
-6 dB bandWidth: 67%
Time (us)
26
26.5
27
27.5
28
28.5
Amplitude (V)
0.25
0.15
0.05
-0.05
-0.15
-0.25

Fig. 20

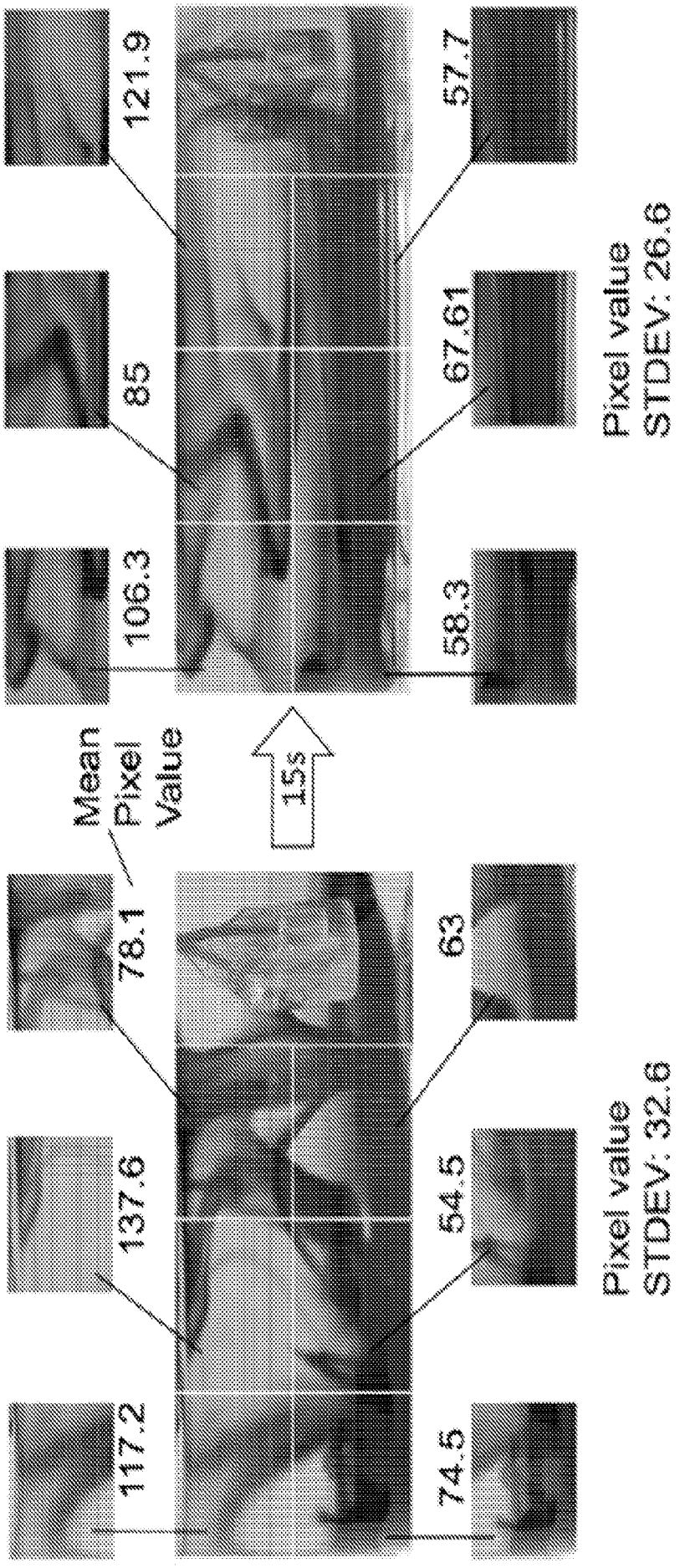
Mean Pixel Value
15s
78.1
137.6
117.2
63
54.5
74.5
Pixel value STDEV: 32.6
106.3
85
121.9
58.3
67.61
57.7
Pixel value STDEV: 26.6

Fig. 21

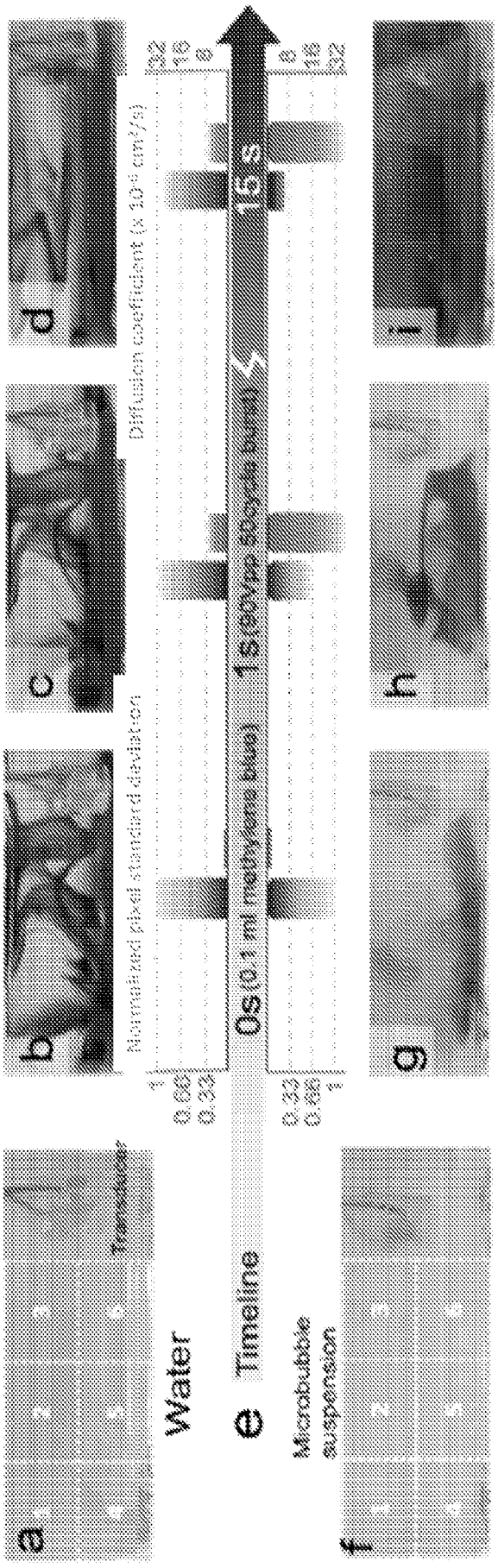
a
Transducer
Water
e Timeline
Microbubble suspension
f
b
c
d
g
h
i
Normalized pixel standard deviation
1
0.66
0.33
0.33
0.66
1
0s (0.1 ml methylene blue)
15 (60vpp, 50cycle burst)
15 s
Diffusion coefficient (x 10⁻⁶ cm²/s)
32
16
8
8
16
32

Fig. 22

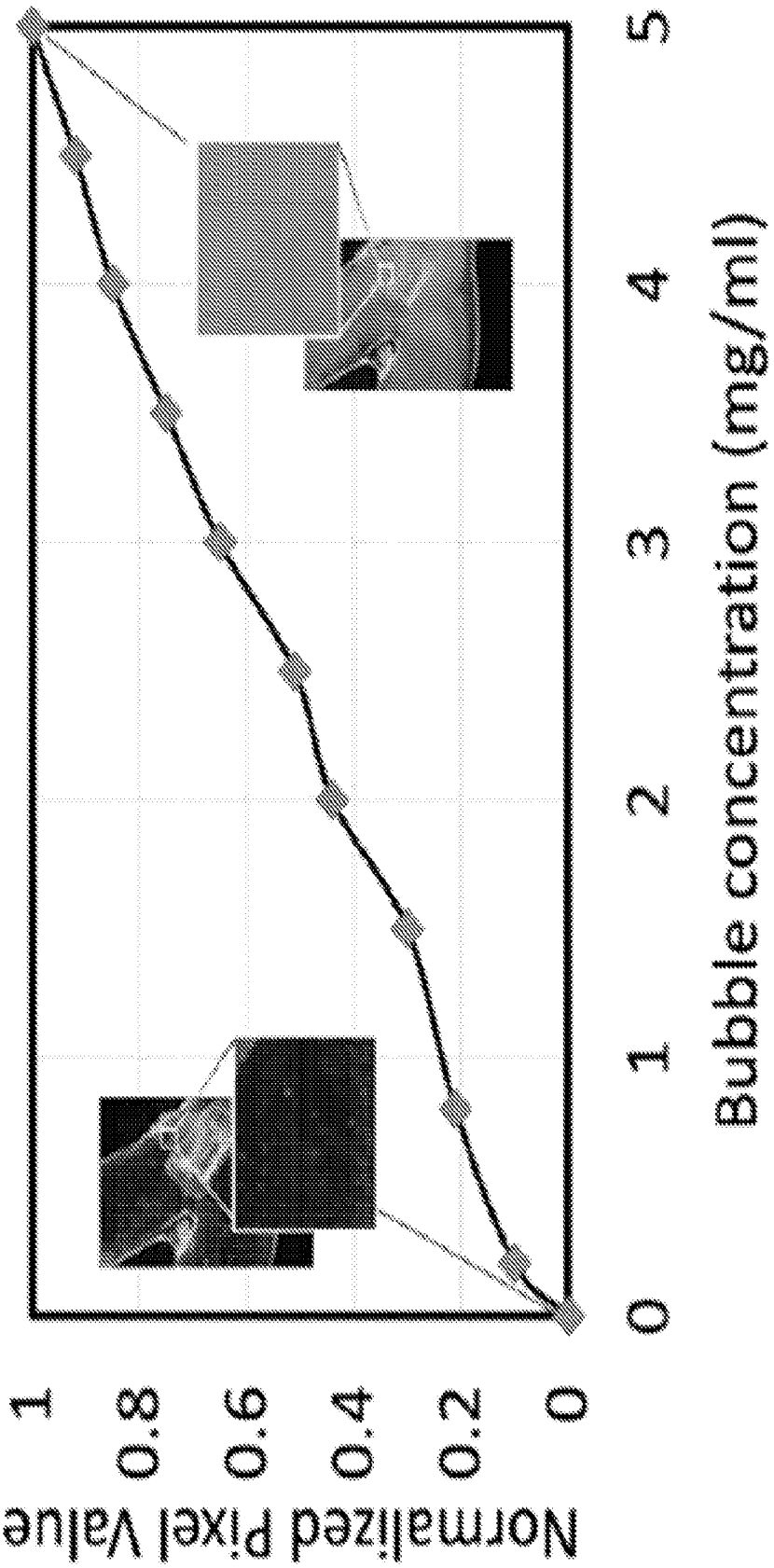
Normalized Pixel Value
0
0.2
0.4
0.6
0.8
1
0
1
2
3
4
5
Bubble concentration (mg/ml)

Fig. 23

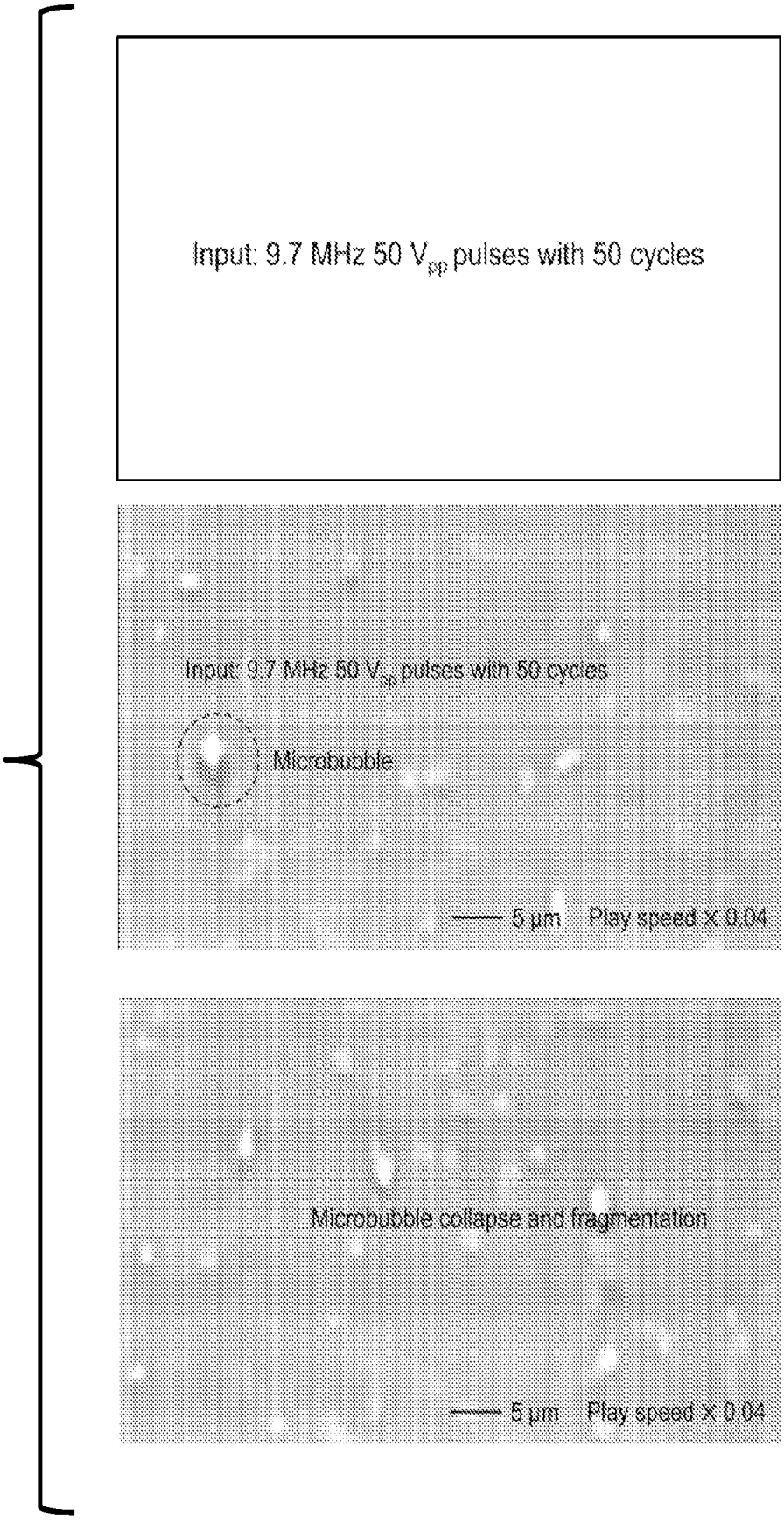
Input: 9.7 MHz 50 $V_{pp}$ pulses with 50 cycles
Input: 9.7 MHz 50 $V_{pp}$ pulses with 50 cycles
Microbubble
5 µm
Play speed x 0.04
Microbubble collapse and fragmentation
5 µm
Play speed x 0.04

Fig. 24A

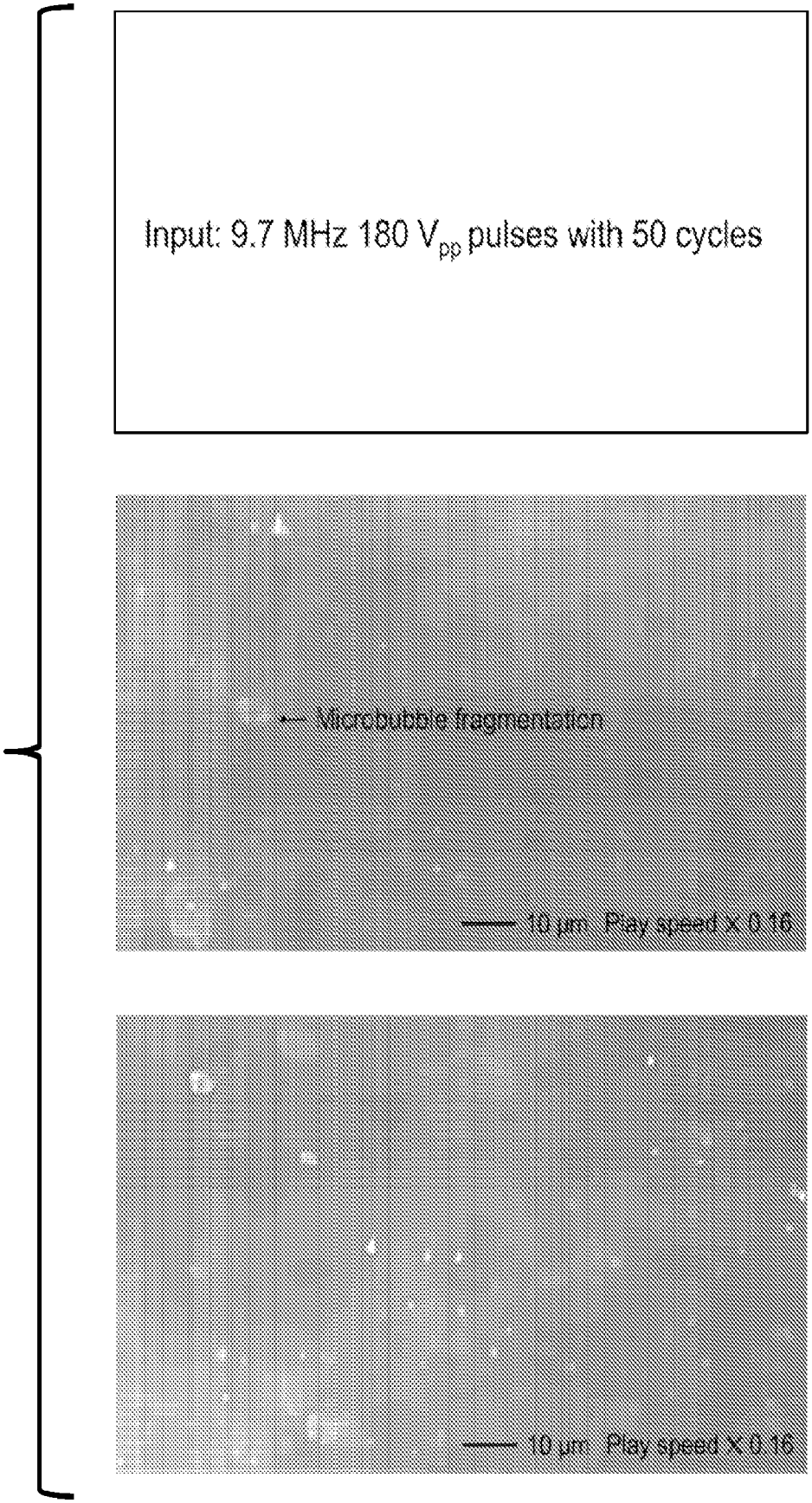
Input: 9.7 MHz 180 $V_{pp}$ pulses with 50 cycles
← Microbubble fragmentation
10 µm Play speed x 0.16
10 µm Play speed x 0.16

Fig. 24B

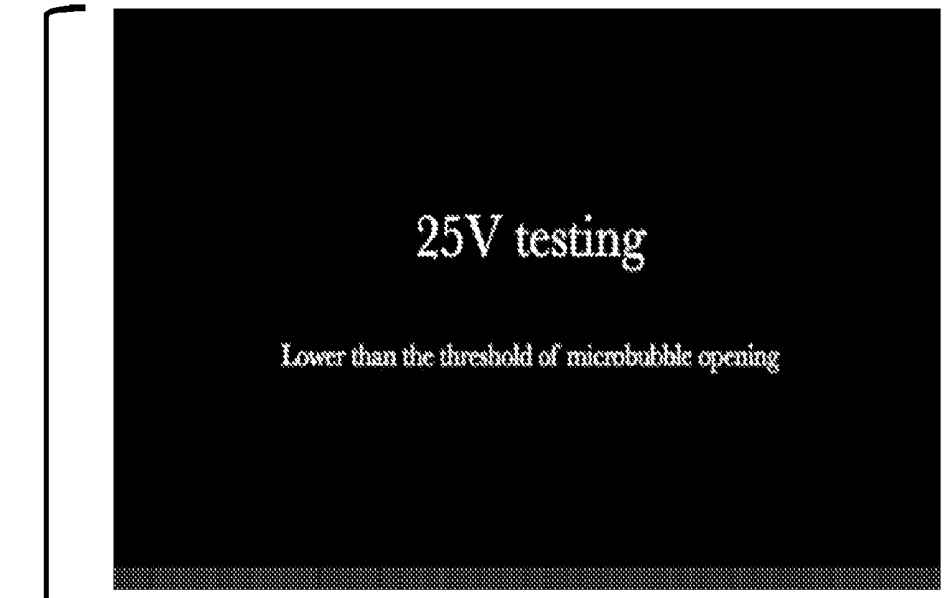


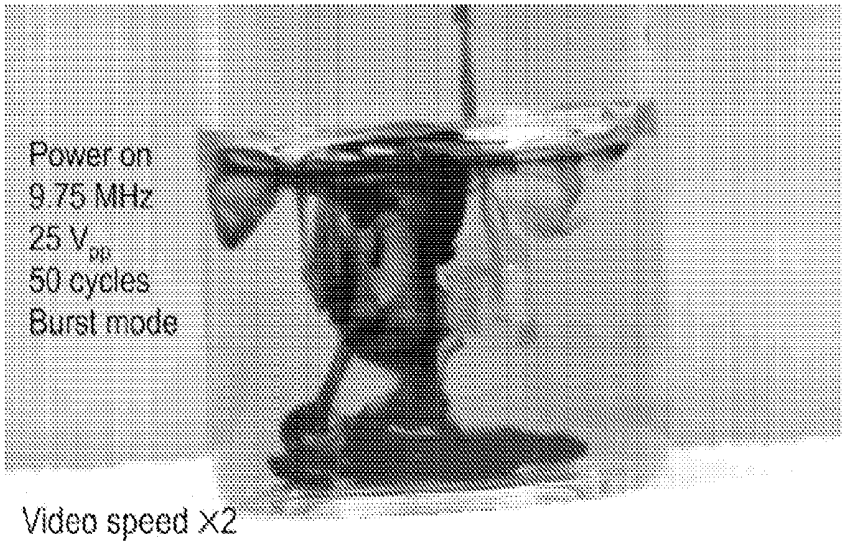


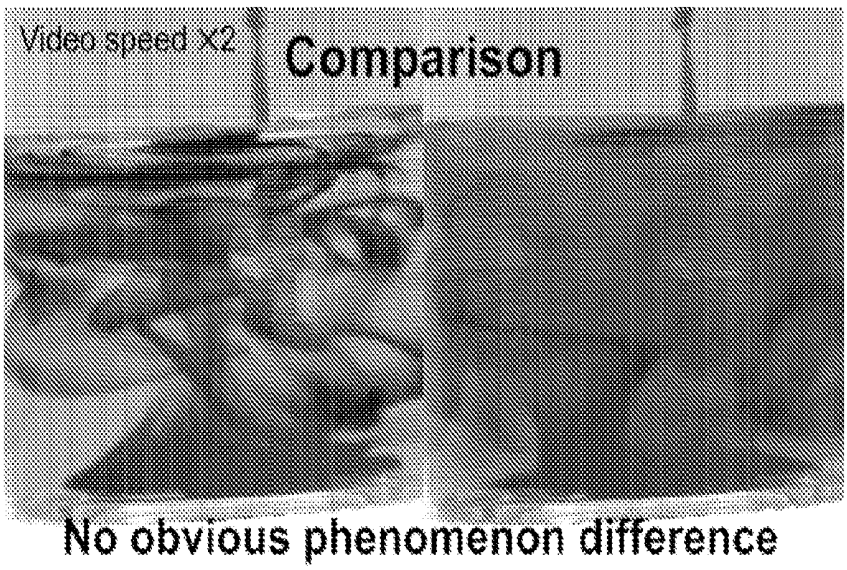


No obvious phenomenon difference

Fig. 25A

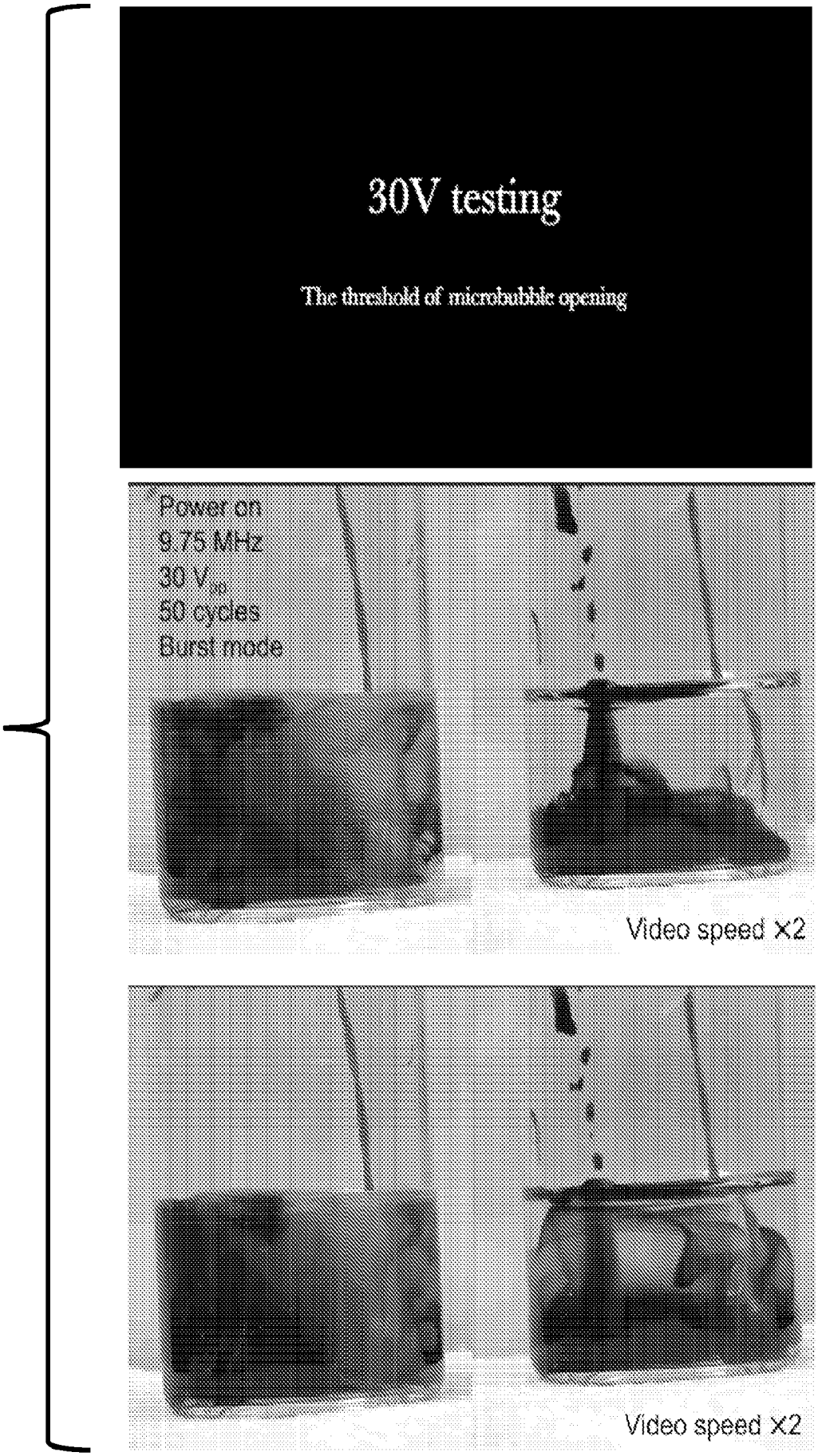
30V testing
The threshold of microbubble opening
Power on
9.75 MHz
30 $V_{pp}$
50 cycles
Burst mode
Video speed ×2
Video speed ×2

Fig. 25B

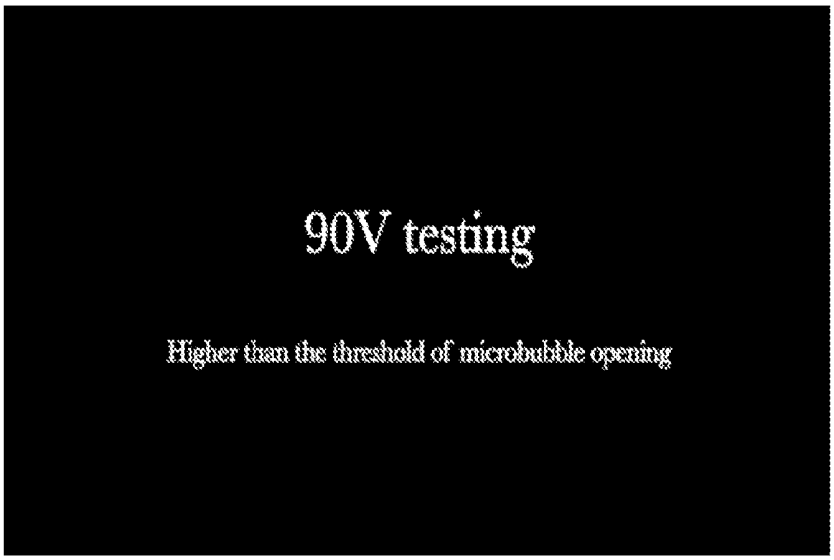
90V testing
Higher than the threshold of microbubble opening

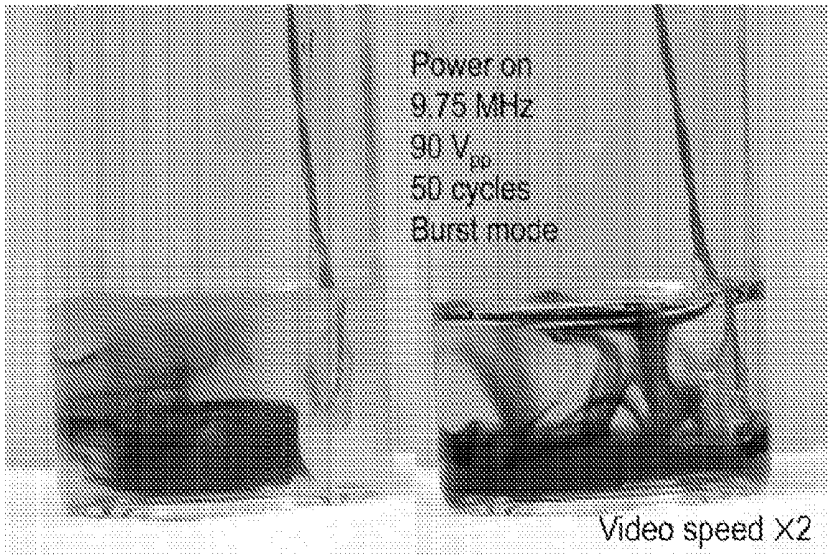
Power on
9.75 MHz
90 $V_{pp}$
50 cycles
Burst mode
Video speed X2

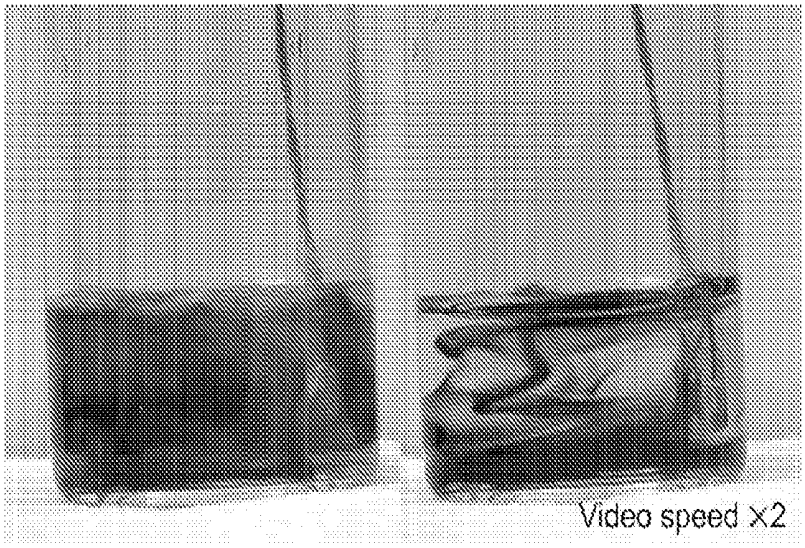
Video speed X2

Fig. 25C

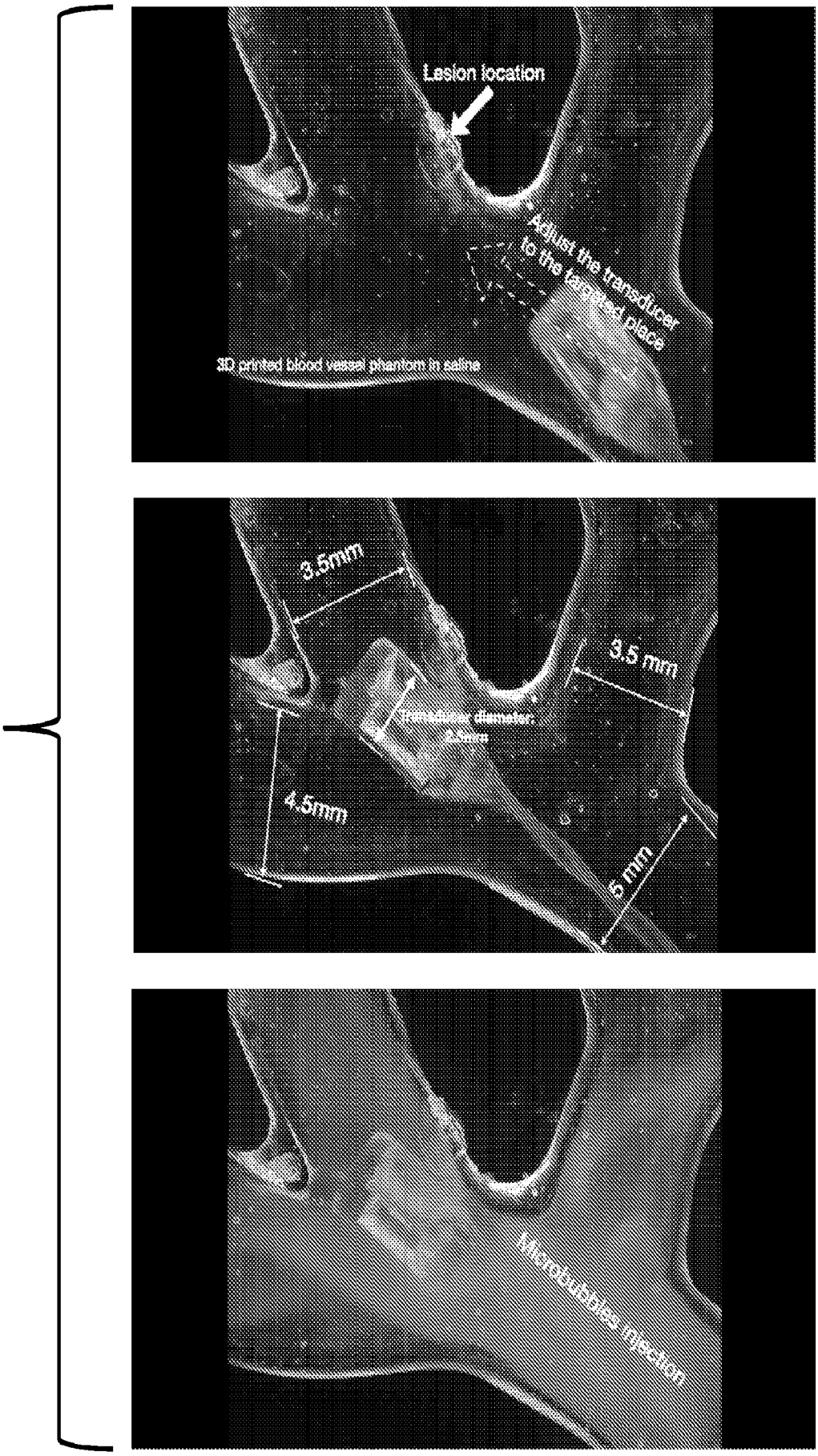
Lesion location
Adjust the transducer to the targeted place
3D printed blood vessel phantom in saline
3.5mm
3.5 mm
4.5mm
5 mm
Microbubbles injection

Fig. 26A

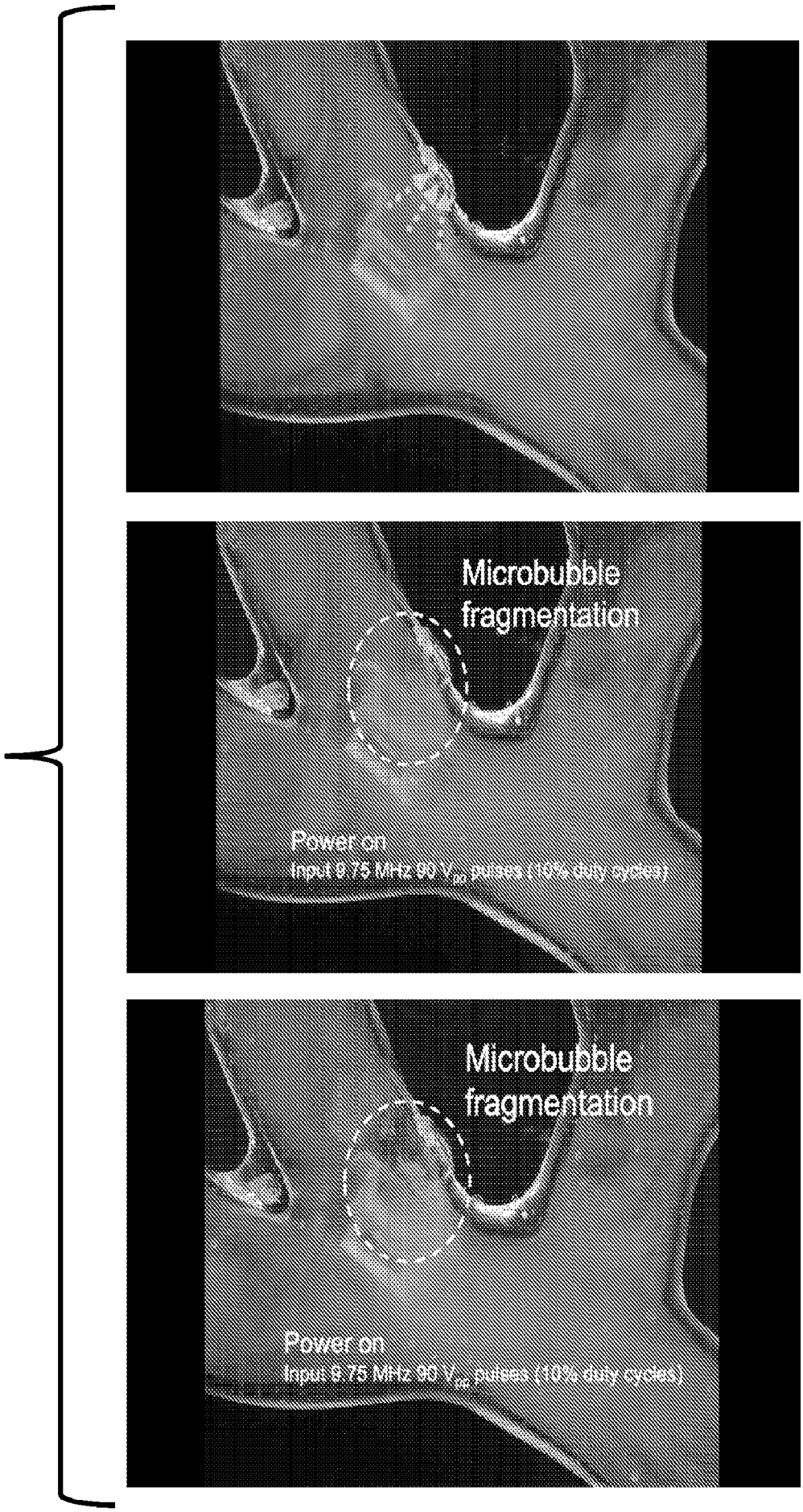
Microbubble fragmentation
Power on
Input 0.75 MHz 90 $V_{pp}$ pulses (10% duty cycles)
Microbubble fragmentation
Power on
Input 0.75 MHz 90 $V_{pp}$ pulses (10% duty cycles)

Fig. 26B

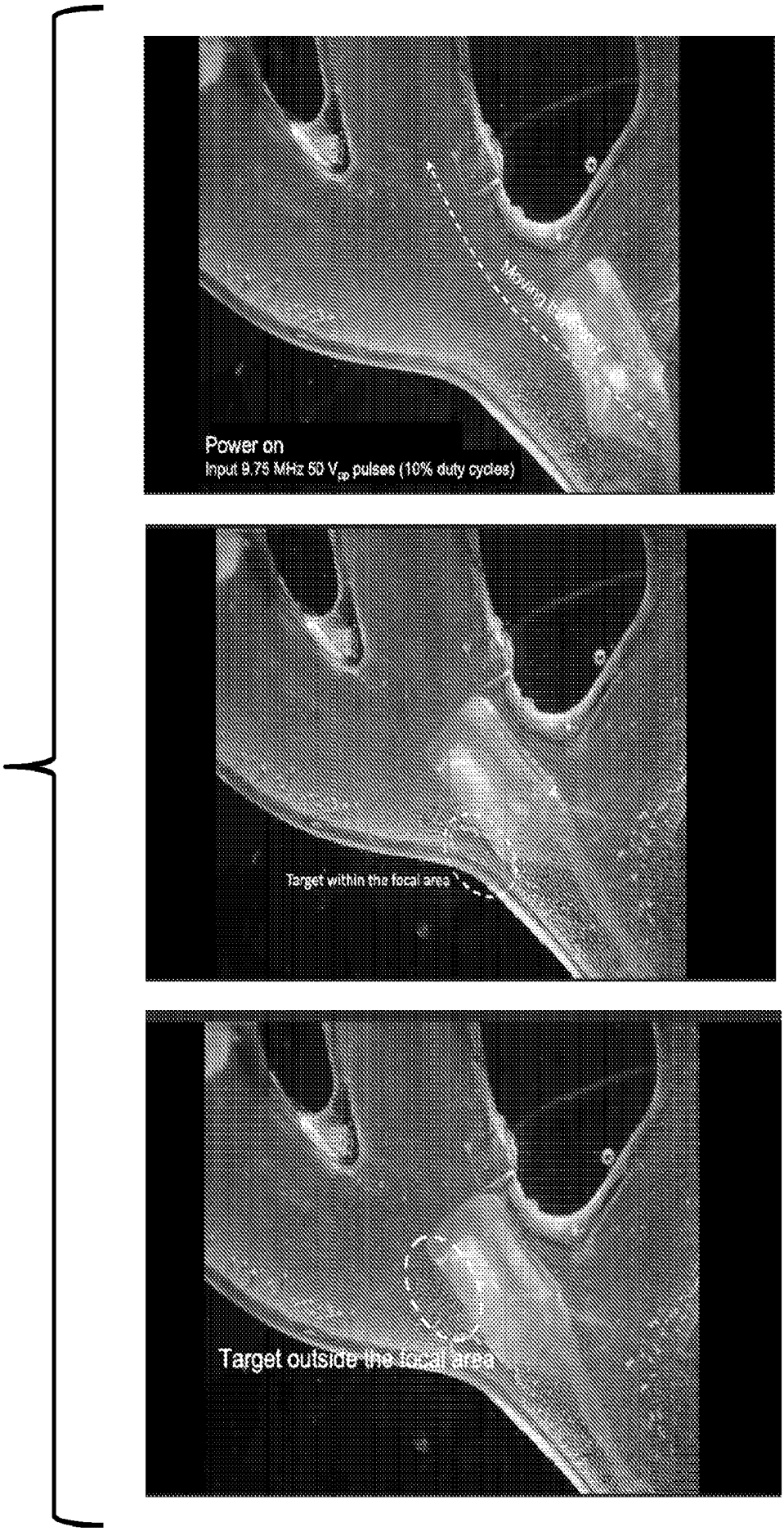
Power on
Input 9.75 MHz 50 $V_{pp}$ pulses (10% duty cycles)
Target within the focal area
Target outside the focal area

Fig. 27A

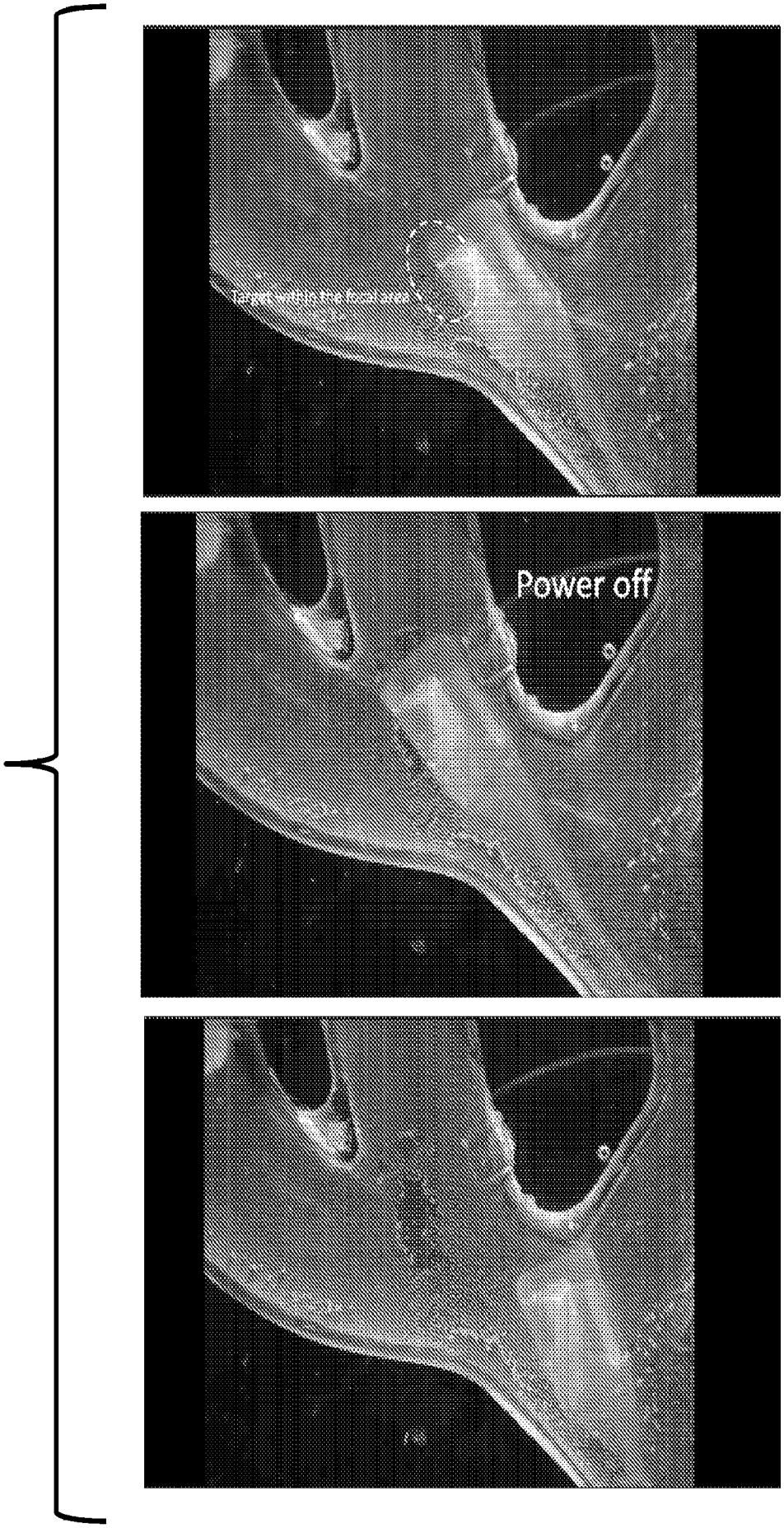


Fig. 27B